MOBILE VELOCITY ESTIMATION IN MULTIPATH FADING CHANNELS

by

Bin Zhou

A thesis submitted to the
Department of Electrical and Computer Engineering
in conformity with the requirements
for the degree of Master of Science (Eng.)

Queen's University
Kingston, Ontario, Canada
June 1999

National Library of Canada
Acquisitions and Bibliographic Services
395 Wellington Street
Ottawa ON K1A 0N4
Canada

Bibliothèque nationale du Canada
Acquisitions et services bibliographiques
395, rue Wellington
Ottawa ON K1A 0N4
Canada

Your file Votre référence

Our file Notre référence

0-612-42710-2

Canada

Abstract

As prior knowlodge of mobile velocity has been found useful in many applications of mobile communications, it is necessary to estimate the mobile velocity at the mobile station (MS) based on the received fading signal. Rice *et al.* have derived a continuous-time fading signal model, which can be used to obtain estimates of mobile velocity. The main emphasis of this thesis is on the development of level crossing rate (LCR) and autocorrelation function (ACF) methods for estimating mobile velocity using the discrete-time received fading signal corrupted by the additive noise. While our results show that both methods produce close estimates to actual mobile velocity, the ACF method has superior performance in low SNR conditions.

We then apply the estimated mobile velocity to the problem of tracking moving mobiles by employing a Kalman filter. By adding the mobile velocity measurements into the mobile motion tracking model, we found, through the simulation results, that the performance of the system can be improved significantly when the mobile velocity is relatively large.

Acknowledgements

I would like to thank my supervisor Dr. Steven Blostein for his financial support and technical advice. Many thanks to Mr. Lin Zhao and Dr. Dajun Cheng, who gave me lots of suggestions when I ran into problems. I am grateful to Mr. David Young for letting me use his fading signal generator program, which is the fundation of my simulations. Thanks also go to my colleagues in IPCL lab, I had a great time with them during my studying period. Finally, I would like to thank my family for their encouragement and supporting me in my decisions.

Contents

List of Tables

List of Figures

Chapter 1

Introduction

Motivation

Mobile velocity is an important parameter in a mobile communication system. There exist a variety of real-world applications that can use the mobile velocity to improve their performance. For example, handoff requests from rapidly moving mobiles in microcellular networks must be processed quickly. Otherwise, excessive dropped calls will occur. Velocity-adaptive handoff algorithms can solve this problem. They are known to be robust to the severe propagation environments that are typical of urban microcellular networks [2, 19, 20, 40].

In a mobile communication system, the signal received by the mobile station always consists of multiple components from different directions and with different delays, due to the reflection, scattering and diffraction of the incoming waves by the objects in the immediate vicinity of the mobile. If there are small changes in the differential delays, large variations in the amplitude and phase of the received signal will occur. This is called multipath fading. The fading rate depends on the mobile velocity. The faster the mobile, the larger the fading rate. Therefore, statistical characterization of the fading signal model is fundamental to mobile velocity estimation. Rice *et al.* developed a continuous-time fading signal model [1, 7, 22, 26, 31, 32, 39]. Some mobile velocity estimation techniques have been developed based on Rice's model [33, 38].

The focus of this thesis is on the development of a discrete-time fading signal model and corresponding mobile velocity estimation techniques.

Contributions

The main contribution of this thesis is the derivation of a discrete-time fading signal model and level crossing rate (LCR) and autocorrelation function (ACF) estimation techniques for mobile velocity using a discrete-time fading signal corrupted by additive noise. Through the use of simulations, we show that both estimators can produce accurate estimates of mobile velocity. We then apply the mobile velocity estimators to the mobile position tracking application. We will find that, by adding velocity measurements, the performance of mobile motion tracking is improved.

Thesis Outline

The following chapters examine various aspects of mobile velocity estimation in multipath fading channels. Chapter 2 introduces the modelling of multipath fading signals and discusses the previous work on mobile velocity estimation using continuous-time received fading signals. The discrete-time fading signal model is presented in Chapter 3, and this chapter studies the derivation of a level crossing rate (LCR) estimation technique as well. In Chapter 4, we present another estimation technique of mobile velocity, autocorrelation function (ACF) estimation. Chapter 5 applies mobile velocity estimation to mobile motion tracking. We then present the conclusions in Chapter 6, where suggestions for future research are also given.

Chapter 2

Background

2.1 Mobile Radio Propagation

A mobile radio system typically consists of a set of base stations (BSs) whose antennas are usually placed well above local terrain. Therefore, the BSs are relatively independent of local scatterers. Most of the time, there hardly exists a line-of-sight (LOS) path between the BS and mobile station (MS) antennas, because there are always many natural and man-made objects in the immediate vicinity of the MS. After the consequences of reflection, diffraction, and scattering the transmitted waves, which are approximately planar at large distances, from the BS arrive at the MS from many different directions and with different delays, as shown in Figure 2.1. This property is called multipath propagation. The multiple plane waves combine vectorially at the MS antenna to produce a composite received signal.

Since the carrier wavelength used in recent mobile radio systems is relatively small, small changes in the differential delays introduced by the moving MS will cause large changes in the phases of the arriving plane waves. These phase differences cause constructive and destructive addition of the arriving plane waves which causes large variations in the envelope amplitude and phase of the composite received signal at the MS end. Since the MS is moving through space, the spatial variations in the envelope and phase of the composite received signal manifest themselves as time variations. This phenomenon is called envelope fading.

In the urban area a MS is usually surrounded by local scatterers, so that there

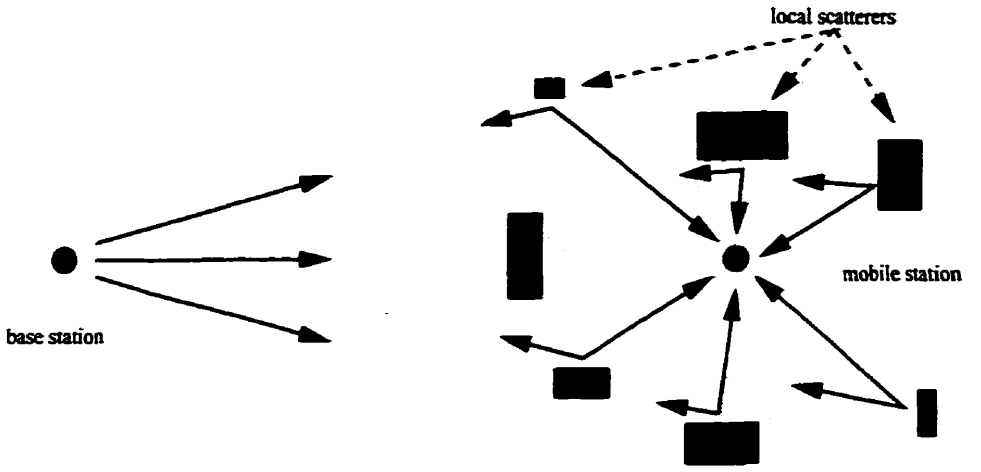

Figure 2.1: Typical radio propagation in mobile radio system.

exists no direct LOS path between the BS and the MS. All plane waves arrive at the MS from all directions with nearly equal probability. Therefore, isotropic scattering is a reasonable modelling assumption [6] and Rayleigh distributed envelope fading is assumed. While in the suburban area, there sometimes exists a LOS path between the MS and BS, and at other times there is no LOS component. The received signal will still experience fading. However, the scattering is usually non-isotropic and the envelope fading has a Ricean distribution.

2.2 Continuous-Time Received Signal Model

As stated in the previous section, the signal received by the MS antenna is made up a number of horizontally travelling plane waves with random amplitudes and angles of arrival for different locations. The phases of the waves are uniformly distributed over $[-\pi, \pi]$. The amplitudes and phases are assumed to be statistically independent.

Figure 2.2 depicts a horizontal x-y plane with a MS moving along the x-axis with velocity v. The MS motion introduces a Doppler shift, or frequency variation, into

the n^{th} incident plane wave, given by

$$f_{d,n}(t) = f_m \cos\theta_n(t) \tag{2.1}$$

where $f_m = v/\lambda_c$ and λ_c is the wavelength of the arriving plane wave, is called maximum Doppler frequency, and $\theta_n(t)$ is the incident angle of the n^{th} wave.

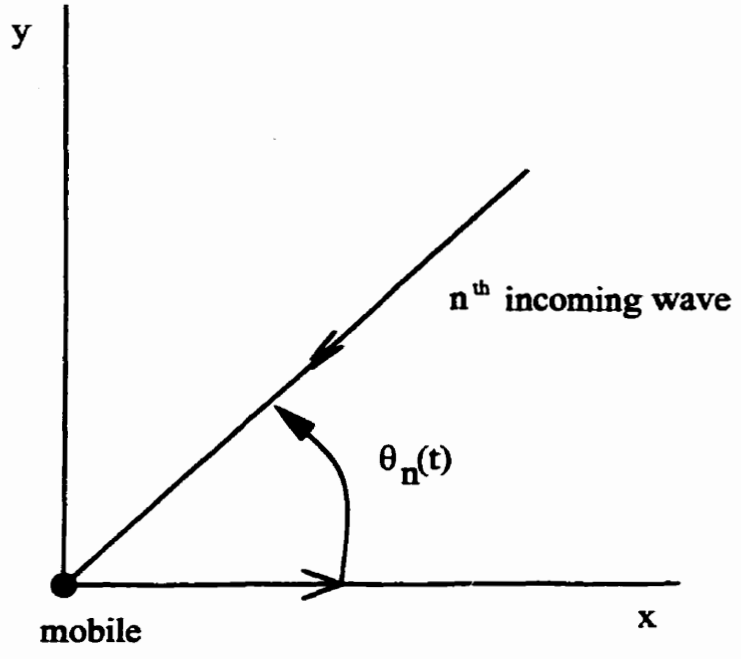

Figure 2.2: A typical component wave incident on the MS receiver

Assuming that the transmitted signal is vertically polarized, the composite received signal can be written as

$$r(t) = \sum_{n=1}^{N} \alpha_n(t) \cos(2\pi f_c t + 2\pi f_{d,n}(t)t + \phi_n(t)) \tag{2.2}$$

where f_c is the carrier frequency, $\alpha_n(t)$ is the amplitude of the n^{th} wave, and $\phi_n(t)$ is the phase angle uniformly distributed over $[-\pi, \pi]$.

Following Rice [31] [32], we can express bandpass signal $r(t)$ in quadrature form

$$r(t) = r_I(t) \cos 2\pi f_c t - r_Q(t) \sin 2\pi f_c t \tag{2.3}$$

where

$$r_I(t) = \sum_{n=1}^{N} \alpha_n(t) \cos(2\pi f_{d,n}(t)t + \phi_n(t)) \tag{2.4}$$

$$r_Q(t) = \sum_{n=1}^{N} \alpha_n(t) \sin(2\pi f_{d,n}(t)t + \phi_n(t)) \tag{2.5}$$

are in-phase and quadrature components of $r(t)$, respectively. According to the Central Limit Theorem, for large N, the quadrature components $r_I(t)$ and $r_Q(t)$ can be approximated as independent Gaussian processes. Furthermore, we can assume that these random processes are wide sense stationary, with constant parameters $f_{d,n}(t) = f_{d,n}$, $\alpha_n(t) = \alpha_n$, $\phi_n(t) = \phi_n$, and assume that the received signal $r(t)$ is wide sense stationary. Therefore, Equations (2.2)–(2.5) can be rewritten as

$$r(t) = \sum_{n=1}^{N} \alpha_n \cos\left[2\pi(f_c + f_{d,n})t + \phi_n\right] \tag{2.6}$$

$$= r_I(t) \cos 2\pi f_c t - r_Q(t) \sin 2\pi f_c t \tag{2.7}$$

and

$$r_I(t) = \sum_{n=1}^{N} \alpha_n \cos(2\pi f_{d,n}t + \phi_n) \tag{2.8}$$

$$r_Q(t) = \sum_{n=1}^{N} \alpha_n \sin(2\pi f_{d,n}t + \phi_n) \tag{2.9}$$

2.2.1 Received Signal Envelope Distribution

We denote r_I and r_Q the random variables corresponding to $r_I(t)$ and $r_Q(t)$ for fixed t, each having zero mean and equal variance:

$$\sigma_{r_I}^2 = \sigma_{r_Q}^2 = \frac{1}{2} \sum_{n=1}^{N} E\{\alpha_n^2\} = \sigma^2 \tag{2.10}$$

if there exists no LOS component between the BS and MS. By using a bivariate transformation, the received signal envelope $z(t) = \sqrt{r_I^2(t) + r_Q^2(t)}$ has a Rayleigh distribution at any time t, i.e.,

$$p_z(x) = \frac{x}{\sigma^2} \exp\left\{-\frac{x^2}{2\sigma^2}\right\} \quad (x \geq 0) \tag{2.11}$$

This type of fading is called Rayleigh fading.

If there is a LOS path or a specular component from a strong (fixed) local scatterer, the amplitude of one incoming plane wave, α_0, is significantly larger than other α_n. Then, r_I and r_Q have non-zero mean and the received signal envelope has a Ricean distribution at any time t, i.e.,

$$p_z(x) = \frac{x}{\sigma^2} \exp\left\{-\frac{x^2+s^2}{2\sigma^2}\right\} I_0\left(\frac{xs}{\sigma^2}\right) \quad (x \geq 0) \tag{2.12}$$

where

$$s^2 = \alpha_0^2 \cos^2 \phi_0 + \alpha_0^2 \sin^2 \phi_0 = \alpha_0^2 \tag{2.13}$$

is the non-centrality parameter and $I_0(x)$ is the zero-order modified Bessel function of the first kind. This type of fading is called Ricean fading.

2.2.2 Received Signal Correlation and Spectrum

The autocorrelation function of $r(t)$ is

$$\begin{aligned} \phi_{rr}(\tau) &= E\{r(t)r(t+\tau)\} \\ &= E\{r_I(t)r_I(t+\tau)\}\cos 2\pi f_c\tau - E\{r_Q(t)r_I(t+\tau)\}\sin 2\pi f_c\tau \\ &= \phi_{r_Ir_I}(\tau)\cos 2\pi f_c\tau - \phi_{r_Qr_I}(\tau)\sin 2\pi f_c\tau \end{aligned} \tag{2.14}$$

Note that in Equation (2.14)

$$\phi_{r_Ir_I}(\tau) = \phi_{r_Qr_Q}(\tau) \tag{2.15}$$

$$\phi_{r_Ir_Q}(\tau) = -\phi_{r_Qr_I}(\tau) \tag{2.16}$$

The autocorrelation function $\phi_{r_Ir_I}(\tau)$ can be obtained from Equations (2.8), (2.10), and (2.1),

$$\begin{aligned} \phi_{r_Ir_I}(\tau) &= E\{r_I(t)r_I(t+\tau)\} \\ &= \left[\frac{1}{2}\sum_{n=1}^{N} E\{\alpha_n^2\}\right] E\{\cos 2\pi f_{d,n}\tau\} \\ &= \frac{\Omega_p}{2} E_\theta\{\cos(2\pi f_m \tau \cos\theta)\} \end{aligned} \tag{2.17}$$

where

$$\frac{\Omega_p}{2} = E\{r_I^2(t)\} = E\{r_Q^2(t)\} = \frac{1}{2}E\{\alpha_n^2\} \tag{2.18}$$

is the total average received power from all multipath components.

Likewise, the crosscorrelation function $\phi_{r_I r_Q}(\tau)$ is

$$\begin{aligned}\phi_{r_I r_Q}(\tau) &= E\{r_I(t) r_Q(t+\tau)\} \\ &= \frac{\Omega_p}{2} E_\theta\{\sin(2\pi f_m \tau \cos\theta)\}\end{aligned} \tag{2.19}$$

In Rayleigh distributed fading channels, Equation (2.17) becomes

$$\begin{aligned}\phi_{r_I r_I}(\tau) &= \frac{\Omega_p}{2}\frac{1}{2\pi}\int_{-\pi}^{\pi} \cos(2\pi f_m \tau \cos\theta) d\theta \\ &= \frac{\Omega_p}{2} J_0(2\pi f_m \tau)\end{aligned} \tag{2.20}$$

where $J_0(x)$ is the zero-order Bessel function of the first kind. Likewise, Equation (2.19) becomes

$$\begin{aligned}\phi_{r_I r_Q}(\tau) &= \frac{\Omega_p}{2}\frac{1}{2\pi}\int_{-\pi}^{\pi} \sin(2\pi f_m \tau \cos\theta) d\theta \\ &= 0\end{aligned} \tag{2.21}$$

The power spectral density (PSD) of $r_I(t)$ and $r_Q(t)$ is the Fourier transform of $\phi_{r_I r_I}(\tau)$ or $\phi_{r_Q r_Q}(\tau)$, respectively, i.e.,

$$\begin{aligned}S_{r_I r_I}(f) &= \mathcal{F}\{\phi_{r_I r_I}(\tau)\} \\ &= \begin{cases} \frac{\Omega_p}{4\pi f_m}\frac{1}{\sqrt{1-(f/f_m)^2}} & |f| \le f_m \\ 0 & \text{otherwise} \end{cases}\end{aligned} \tag{2.22}$$

The PSD of the bandpass received signal $r(t)$ can be expressed in terms of the quadrature components as

$$\begin{aligned}S_{rr}(f) &= \frac{1}{2}[S_{r_I r_I}(f-f_c) + S_{r_I r_I}(-f-f_c)] \\ &= \begin{cases} \frac{3\Omega_p}{4\pi f_m}\frac{1}{\sqrt{1-(\frac{|f-f_c|}{f_m})^2}} & |f-f_c| \le f_m \\ 0 & \text{otherwise} \end{cases}\end{aligned} \tag{2.23}$$

The normalized PSD $S_{rr}(f)/(3\Omega_p/4\pi f_m)$ is plotted against the normalized difference $(f-f_c)/f_m$ in Figure 2.3. Notice that $S_{rr}(f)$ is limited to the range of frequencies $|f-f_c| \le f_m$ or twice the maximum Doppler frequency.

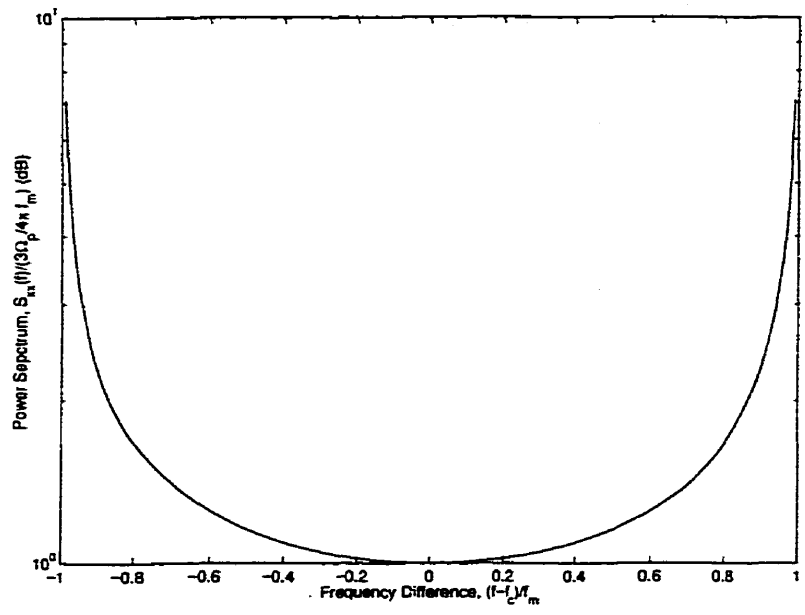

Figure 2.3: PSD of the received signal for a Rayleigh distributed fading channel

2.3 Previous Work on Mobile Velocity Estimation

2.3.1 Level Crossing Rate Estimators

From [38], the envelope level crossing rate (LCR) is defined as the average number of positive-going crossings per second that a signal makes of a predetermined level R. Likewise, the zero crossing rate (ZCR) is defined as the average number of positive going zero crossings that a signal makes per second.

Assuming the fading model in Equation (2.3), Rice has derived the envelope LCR with respect to the level R as [32]

$$\begin{aligned} \text{LCR} &= \int_0^\infty \dot{r} p(R,\dot{r}) d\dot{r} = \frac{R(2\pi)^{-3/2}}{\sqrt{\mathcal{B} b_0}} \int_{-\pi}^{\pi} d\psi \int_0^\infty \dot{r} d\dot{r} \\ &\quad \exp\left\{ -\frac{1}{2\mathcal{B} b_0} \left[\mathcal{B}(R^2 - 2Rs\cos\psi + s^2) + (b_0\dot{r} + b_1 s \sin\psi)^2 \right] \right\} \end{aligned} \tag{2.24}$$

and ZCR of $r_I(t) - m_I$ (or $r_Q(t) - m_Q$) as

$$\text{ZCR} = \frac{1}{\pi}\sqrt{\frac{b_2}{b_0}} \tag{2.25}$$

where m_I, m_Q are the means of $r_I(t)$, $r_Q(t)$, respectively; $p(R,\dot{r})$ is the joint probability density function of the envelope r (evaluated at $r = R$) and the slope of the envelope $\dot{r}$, and $\mathcal{B} = b_0 b_2 - b_1^2$, where for integers $n \geq 0$,

$$b_n = (2\pi)^n \frac{\sigma^2}{\pi} \int_{-f_m}^{f_m} \frac{f^n}{\sqrt{f_m^2 - f^2}} df \tag{2.26}$$

with $b_0 = \sigma^2$, and f_m is the maximum Doppler frequency. Therefore, by using Equation (2.26), Equations (2.24) and (2.25) become, respectively,

$$\text{LCR} = (v/\lambda_c)\sqrt{2\pi(K+1)}\rho e^{-K-(K+1)\rho^2} I_0\left(2\rho\sqrt{K(K+1)}\right) \tag{2.27}$$

and

$$\text{ZCR} = \sqrt{2}v/\lambda_c \tag{2.28}$$

where $\rho = R/R_{\text{rms}}$, where $R_{\text{rms}} = \sqrt{\Omega_p}$ is the rms signal level, K is the Ricean factor and $I_0(x)$ is the zero-order modified Bessel function of the first kind.

From [38], the LCR around $\rho = 1$ is roughly independent of K, and ZCR is not affected by K. Therefore, the steps for using the LCR (or ZCR) of the envelope (or $r_I(t)$ or $r_Q(t)$), for velocity estimation are [38]:

1. Determine R_{rms} (or m_I or m_Q),
2. Estimate the number of crossings per second $\hat{L}_{R_{\text{rms}}}$ (or $\hat{L}_{\text{ZCR}}$), and
3. Use Equation (2.27) to solve for v, with $\rho = 1$ and $K = 0$ (or Equation (2.28) for ZCR).

2.3.2 Covariance Approximation Methods

Holzman and Sampath have proposed a velocity estimator that relies on an estimate of the autocovariance function of received faded samples, which we denote as $r[i]$ [19] [33]. With this method, referred to as the covariance method (COV), the statistic,

$$V = \frac{1}{N}\sum_{k=1}^{N}(r[k+\tau] - r[k])^2 \tag{2.29}$$

is calculated. If N is large and ergodicity applies, then the time average V can be replaced by the sample mean

$$E\{V\} = 2\mu_{rr}(0) - 2\mu_{rr}(\tau) \tag{2.30}$$

where $\mu_{rr}(\tau)$ denotes the autocovariance of $r[k]$. Assuming squared-envelope samples and that the channel is characterized by isotropic scattering, $\mu_{rr}(\tau)$ is written as [1]

$$\mu_{rr}(\tau) = \left(\frac{\Omega_p}{K+1}\right)^2 \left[J_0^2(2\pi\tau/\lambda_c) + 2K J_0(2\pi\tau/\lambda_c)\cos(2\pi\tau\cos\theta)/\lambda_c)\right] \tag{2.31}$$

Substituting Equation (2.31) into (2.30),

$$\bar{V} = E\{V\} = 2\left(\frac{\Omega_p}{K+1}\right)^2 \left[(1+2K) - (J_0^2(2\pi\tau/\lambda_c) + 2K J_0(2\pi\tau/\lambda_c)\cos(2\pi\tau\cos\theta)/\lambda_c))\right] \tag{2.32}$$

which is dependent of K and θ. If $\mu_{rr}(0)$ is known exactly, then the bias with respect to K can be eliminated for small τ by the normalization [33]

$$\frac{\bar{V}}{\mu_{rr}(0)} \approx (2\pi v\tau_t/\lambda_c)^2 \frac{1+2K+K\cos(2\theta)}{(1+2K)} \tag{2.33}$$

so that the estimated mobile velocity $\hat{v}_{\mathrm{COV}}$ is written as [33]

$$\hat{v}_{\mathrm{COV}} \approx \frac{\lambda_c}{2\pi\tau_t}\sqrt{\frac{\bar{V}}{\mu_{rr}(0)}} \tag{2.34}$$

where τ_t is the sample spacing in seconds/sample.

2.4 Laboratory Simulation of Fading Signals

It is desirable to use actual fading signals recorded at a MS antenna. However, at the present time we do not have this opportunity. Therefore, fading signal simulators are of interest that are derived from theoretical principles.

2.4.1 Filtered Gaussian Noise

The simplest fading signal simulator is to use low-pass filtered white Gaussian noises as shown in Figure 2.4. If the Gaussian noise sources have zero-mean, this method produces a Rayleigh fading signal; otherwise a Ricean signal is produced.

The two different noise sources must have the same PSD to produce a fading process that is stationary. The main limitation of this approach is that only rational forms of the fading spectra can be produced, which is accomplished by using a high order pole-zero filter. However, using an infinite impulse response (IIR) filter has stability problems [8].

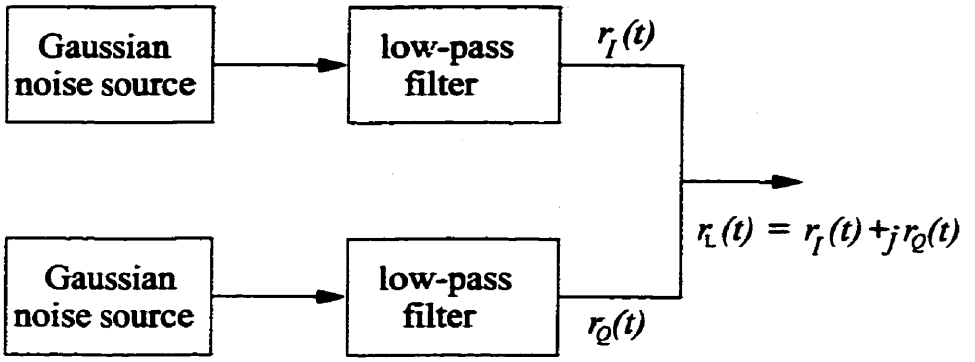

Figure 2.4: Fading simulator that uses low-pass filtered white Gaussian noise. The output signal $r_L(t)$ is the low-pass signal equivalent to the desired bandpass signal.

2.4.2 Jakes' Method

Jakes has introduced a different fading simulator. Assuming that all processes are wide sense stationary with equal strength multipath components (i.e., $\alpha_n = 1$) where each of the N components are uniformly distributed in angle (i.e., $\theta_n = (2\pi n)/N$, $n = 1, 2, \cdots, N$), Jakes proposed that the in-phase and quadrature components be [22]

$$r_I(t) = 2\sum_{n=1}^{M} \cos\beta_n \cos\omega_n t + \sqrt{2}\cos\alpha\cos\omega_m t \tag{2.35}$$

$$r_Q(t) = 2\sum_{n=1}^{M} \sin\beta_n \cos\omega_n t + \sqrt{2}\sin\alpha\cos\omega_m t \tag{2.36}$$

where

$$\begin{aligned} M &= \frac{1}{2}\left(\frac{N}{2} - 1\right) \\ \alpha &= \frac{\pi}{4} \\ \beta_n &= \frac{\pi n}{N} \\ \omega_n &= \omega_m \cos\frac{2\pi n}{N} \end{aligned}$$

and

$$\omega_m = 2\pi v/\lambda_c \tag{2.37}$$

The Jakes' fading simulator is constructed as shown in Figure 2.5.

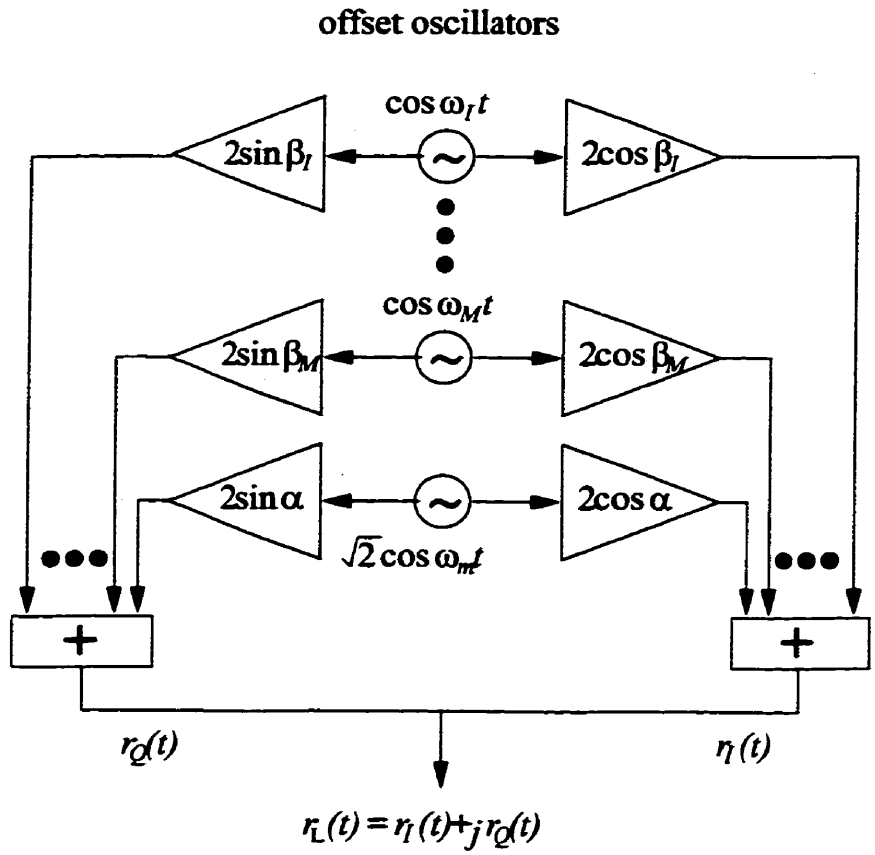

Figure 2.5: Jakes' fading simulator

2.4.3 Inverse Discrete Fourier Transform Rayleigh Fading Simulator

Smith introduced a Rayleigh fading simulator using inverse discrete Fourier transform of uncorrelated Gaussian processes [35]. To generate a desired Rayleigh fading sequence, a complex sequence $\{X[k]\}, k = 0, 1, \cdots\cdots, N-1$ is formed by adding in quadrature two uncorrelated sequences of Gaussian processes, that is

$$X[k] = F[k]A[k] - jF[k]B[k] \tag{2.38}$$

where $\{F[k]\}$ are filter coefficients, $\{A[k]\}$ and $\{B[k]\}$ are i.i.d., $N(0, \sigma^2)$ and $\{A[k]\}$ and $\{B[k]\}$ are independent of all k.

Taking the inverse DFT of $X[k]$, we have

$$x[n] = \frac{1}{N}\sum_{k=0}^{N-1} X[k]e^{j\frac{2\pi kn}{N}} \quad n = 0, 1, \cdots, N-1 \tag{2.39}$$

The real and imaginary parts of $\{x[n]\}$, $\{x_R[n]\}$ and $\{x_R[n]\}$ are

$$\begin{aligned} x_R[n] &= \frac{1}{N}\sum_{k=0}^{N-1} F[k]A[k]\cos\frac{2\pi kn}{N} \\ &\quad + \frac{1}{N}\sum_{k=0}^{N-1} F[k]B[k]\sin\frac{2\pi kn}{N} \end{aligned} \tag{2.40}$$

$$\begin{aligned} x_I[n] &= \frac{1}{N}\sum_{k=0}^{N-1} F[k]A[k]\sin\frac{2\pi kn}{N} \\ &\quad + \frac{1}{N}\sum_{k=0}^{N-1} F[k]B[k]\cos\frac{2\pi kn}{N} \end{aligned} \tag{2.41}$$

$x_R[n]$ and $x_I[n]$ are composed of a weighted sum of $2N$ jointly Gaussian random variables; therefore they are also Gaussian distributed. In order to approximate $x[n]$ as a Rayleigh fading signal, the filter coefficients $\{F[k]\}$ must be appropriately chosen. Smith chose $\{F[k]\}$ to approximate the spectrum

$$S(f) = \frac{1.5}{\pi f_m\sqrt{1-(f/f_m)^2}} \tag{2.42}$$

where f_m is the maximum Doppler frequency, and this choice of $\{F[k]\}$ corresponds to an approximation of the continuous-time autocorrelation $r(\tau) = J_0(2\pi f_m\tau)$, and models fading due to isotropic scattering.

Smith chose the filter coefficients $\{F[k]\}$ as

$$F_s[k] = \begin{cases} 0 & k = 0 \\ \sqrt{\frac{1}{\sqrt{1-(\frac{k}{Nf_m/f_s})^2}}} & k = 1, 2, \cdots, k_m - 1 \\ \sqrt{\frac{\pi}{2} - \arctan(\frac{k_m-1}{\sqrt{2k_m-1}})} & k = k_m \\ 0 & \text{elsewhere} \end{cases} \tag{2.43}$$

where $k_m = \lfloor f_m/f_p \rfloor$, and $f_p = f_s/N$, f_s is the sampling rate.

Young and Beaulieu modified the IDFT fading simulator by choosing a different

set of filter coefficients $\{F[k]\}$ as [43]

$$F_M[k] = \begin{cases} 0 & k = 0 \\ \frac{1}{\sqrt{2}} F_s[k] & k = 1, 2, \cdots, \frac{N}{2} - 1 \\ F_s[k] & k = \frac{N}{2} \\ \frac{1}{\sqrt{2}} F_s[N-k] & k = \frac{N}{2} + 1, \cdots, N-1 \end{cases} \tag{2.44}$$

to reduce the computation time of the simulator.

Chapter 3

Level Crossing Rate Estimator

3.1 Discrete-Time Propagation Model

3.1.1 Received Signals

From Equation (2.2), the received continuous-time band-pass signal is given by

$$x(t) = \sum_{n=1}^{N} \alpha_n \cos(\Omega_c t + \Omega_n t + \phi_n) \tag{3.1}$$

where Ω_c and Ω_n are the continuous-time carrier frequency and Doppler frequency caused by the n^{th} incoming wave, respectively, and ϕ_n is the phase angle of the n^{th} incoming wave. A band-pass continuous-time signal can be represented uniquely at the sampling rate of $2B \leq F_s < 4B$ samples per second [29], where B is the bandwidth of the continuous-time signal. If we sample $x(t)$ at the rate $F_s = 2B$ samples per second, we have

$$x(k) = \sum_{n=1}^{N} \alpha_n \cos(\omega_c k + \omega_n k + \phi_n) \tag{3.2}$$

where $\omega_c = \Omega_c / F_s$ and $\omega_n = \Omega_n / F_s$ are the discrete-time carrier and Doppler frequencies, respectively.

The in-phase and quadrature components of the received signal can be written, respectively, as

$$r_I(k) = \sum_{n=1}^{N} \alpha_n \cos(\omega_n k + \phi_n) \tag{3.3}$$

$$r_Q(k) = \sum_{n=1}^{N} \alpha_n \sin(\omega_n k + \phi_n) \tag{3.4}$$

The low-pass equivalent signal is given by

$$r(k) = r_I(k) + jr_Q(k) \tag{3.5}$$

3.1.2 Received Signal Correlation and Spectrum

Since these random processes of fading signals are assumed to be wide-sense stationary, their autocorrelation functions can be directly derived from their continuous-time counterparts by sampling at the rate F_s samples per second [27]. From Equations (2.17) and (2.19), we obtain

$$\phi_{r_I r_I}(m) = \frac{\Omega_p}{2} E_\theta\{\cos(2\pi f_m m \cos\theta)\} \tag{3.6}$$

$$\phi_{r_I r_Q}(m) = \frac{\Omega_p}{2} E_\theta\{\sin(2\pi f_m m \cos\theta)\} \tag{3.7}$$

and from Equations (2.15) and (2.16)

$$\phi_{r_Q r_Q}(m) = \phi_{r_I r_I}(m) \tag{3.8}$$

$$\phi_{r_Q r_I}(m) = -\phi_{r_I r_Q}(m) \tag{3.9}$$

The autocorrelation function for the low-pass equivalent signal is

$$\phi_{rr}(m) = \phi_{r_I r_I}(m) + j\phi_{r_I r_Q}(m) \tag{3.10}$$

The power spectral density (PSD) of the discrete-time wide-sense stationary (WSS) random process, $S(f)$, is the discrete Fourier transform of its autocorrelation $\phi(m)$, i.e.,

$$S(f) = \sum_{m=-\infty}^{\infty} \phi(m) e^{-j2\pi fm} \tag{3.11}$$

Using the Poisson summation formula [27], the PSD of a WSS discrete-time process equals the sum of the PSD of the continuous-time process and its displacements.

$$S(\omega) = \frac{1}{T_s} \sum_{n=-\infty}^{\infty} S_c\left(\omega + \frac{2n\pi}{T_s}\right) \tag{3.12}$$

where $S(\omega)$, $S_c(\omega)$ are PSD's of discrete-time and continuous-time processes, respectively, and T_s is the sampling period. For a discrete-time signal to be bandlimited, range of $\omega \in [-B, +B]$ where $B < \pi$, we can find that the PSD of discrete-time

process is identical to the PSD of its continuous-time counterpart, which is the most interesting and useful.

If the propagation channels are Rayleigh distributed, from Equations (2.20) and (2.21), the autocorrelation functions can be written as

$$\phi_{r_I r_I}(m) = \phi_{r_I r_I}(m) = \sigma^2 J_0(2\pi f_m m) \tag{3.13}$$

$$\phi_{r_I r_Q}(m) = -\phi_{r_Q r_I}(m) = 0 \tag{3.14}$$

Using Equations (3.8)–(3.10) and (3.13)–(3.14) and taking the Fourier transform, the power spectral density of the low-pass equivalent signal is given as

$$S_{rr}(f) = S_{r_I r_I}(f) = \frac{\sigma^2}{2\pi f_m} \frac{1}{\sqrt{1-(f/f_m)^2}} \tag{3.15}$$

where $|f| \leq f_m$.

3.1.3 Adjacent Signal Envelope Statistics

In order to find the joint pdf of two adjacent envelope samples $p(z_k, z_{k+1})$, the joint pdf of their in-phase and quadrature components, r_I, r_Q, must be derived first. That is, the pdf, $p(r_I(k), r_Q(k), r_I(k+1), r_Q(k+1))$ should be found. We know, from Section 2.2, that the in-phase and quadrature components are normally distributed due to the Central Limit Theorem. For Rayleigh distributed channels, they have zero mean and common variance σ^2. That is

$$E\{r_I^2(k)\} = E\{r_Q^2(k)\} = \sigma^2 \tag{3.16}$$

From Equations (3.13)–(3.14), the following is derived

$$E\{r_I(k) r_I(k+1)\} = E\{r_Q(k) r_Q(k+1)\} = \sigma^2 J_0(2\pi f_m) \tag{3.17}$$

$$\begin{aligned} E\{r_I(k) r_Q(k)\} &= E\{r_I(k) r_Q(k+1)\} \\ &= E\{r_I(k+1) r_Q(k)\} = E\{r_I(k+1) r_Q(k+1)\} = 0 \end{aligned} \tag{3.18}$$

From Equations (3.16)–(3.18), the covariance matrix of these four components is

$$\Lambda = \begin{bmatrix} \sigma^2 & 0 & \sigma^2 J_0 & 0 \\ 0 & \sigma^2 & 0 & \sigma^2 J_0 \\ \sigma^2 J_0 & 0 & \sigma^2 & 0 \\ 0 & \sigma^2 J_0 & 0 & \sigma^2 \end{bmatrix} \tag{3.19}$$

where the Bessel function $J_0(2\pi f_m)$ is simplified to J_0 for notational convenience. From [9], the joint pdf of these four components is

$$p(I_1, Q_1, I_2, Q_2) = \frac{\exp\left\{-\frac{1}{2\sigma^2(1-J_0^2)}\left[I_1^2 - 2J_0 I_1 I_2 + I_2^2 + Q_1^2 - 2J_0 Q_1 Q_2 + Q_2^2\right]\right\}}{4\pi^2\sigma^4(1-J_0^2)} \tag{3.20}$$

where I_1, I_2, Q_1, and Q_2 denote $r_I(k)$, $r_I(k+1)$, $r_Q(k)$, and $r_Q(k+1)$, respectively. For notational simplicity, we have dropped the dependence on time k due to the wide-sense stationarity assumption.

Second, we transform this joint pdf to the joint pdf of the envelopes and phases of the two adjacent signals, $p(z_1, \theta_1, z_2, \theta_2)$. We define the signal envelope, at time k and $k+1$, as

$$\begin{aligned} z_1 &= \sqrt{I_1^2 + Q_1^2} \\ z_2 &= \sqrt{I_2^2 + Q_2^2} \end{aligned} \tag{3.21}$$

and the phase of a signal, at time k and $k+1$, as

$$\begin{aligned} \theta_1 &= \tan^{-1}\frac{Q_1}{I_1} \\ \theta_2 &= \tan^{-1}\frac{Q_2}{I_2} \end{aligned} \tag{3.22}$$

Therefore,

$$\begin{aligned} I_1 &= z_1\cos\theta_1 \\ Q_1 &= z_1\sin\theta_1 \\ I_2 &= z_2\cos\theta_2 \\ Q_2 &= z_2\sin\theta_2 \end{aligned}$$

The Jacobian of the transformation is

$$J(I_1, Q_1, I_2, Q_2) = \begin{vmatrix} \frac{\partial I_1}{\partial z_1} & \frac{\partial I_1}{\partial \theta_1} & 0 & 0 \\ \frac{\partial Q_1}{\partial z_1} & \frac{\partial Q_1}{\partial \theta_1} & 0 & 0 \\ 0 & 0 & \frac{\partial I_2}{\partial z_2} & \frac{\partial I_2}{\partial \theta_2} \\ 0 & 0 & \frac{\partial Q_2}{\partial z_2} & \frac{\partial Q_2}{\partial \theta_2} \end{vmatrix}^{-1}$$

$$= \left| \begin{array}{cccc} \cos\theta_1 & -z_1\sin\theta_1 & 0 & 0 \\ \sin\theta_1 & z_1\cos\theta_1 & 0 & 0 \\ 0 & 0 & \cos\theta_2 & -z_2\sin\theta_2 \\ 0 & 0 & \sin\theta_2 & z_2\cos\theta_2 \end{array} \right|^{-1}$$

$$= \frac{1}{z_1 z_2} \tag{3.23}$$

where $|A|$ denotes the determinant of matrix A.

Using Equations (3.23) and (3.20), the joint pdf of the envelopes and phases is

$$\begin{aligned} p(z_1, \theta_1, z_2, \theta_2) &= \frac{p(I_1, Q_1, I_2, Q_2)}{J(I_1, Q_1, I_2, Q_2)} \\ &= z_1 z_2 p(z_1\cos\theta_1, z_1\sin\theta_1, z_2\cos\theta_2, z_2\sin\theta_2) \\ &= \frac{z_1 z_2}{4\pi^2\sigma^4(1-J_0^2)} \times \\ &\quad \exp\left\{-\frac{1}{2\sigma^2(1-J_0^2)}\left[z_1^2 + z_2^2 - 2J_0 z_1 z_2\cos(\theta_1-\theta_2)\right]\right\} \end{aligned} \tag{3.24}$$

Finally, as in [31], the joint pdf of two adjacent envelope samples can be found by integrating the joint pdf of envelopes and phases with respect to the two adjacent phases. Integrating (3.24) with respect to θ_1 and θ_2, the pdf of two adjacent envelope samples is given by

$$\begin{aligned} p(z_1, z_2) &= \int_{-\pi}^{\pi}\int_{-\pi}^{\pi} p(z_1, z_2, \theta_1, \theta_2)\, d\theta_1 d\theta_2 \\ &= \frac{z_1 z_2 \exp\left\{-\frac{z_1^2+z_2^2}{2\sigma^2(1-J_0^2)}\right\}}{4\pi^2\sigma^4(1-J_0^2)} \int_{-\pi}^{\pi}\int_{-\pi}^{\pi} \exp\left\{\frac{J_0 z_1 z_2}{\sigma^2(1-J_0^2)}\cos(\theta_1-\theta_2)\right\} d\theta_1 d\theta_2 \\ &= \frac{z_1 z_2 \exp\left\{-\frac{z_1^2+z_2^2}{2\sigma^2(1-J_0^2)}\right\}}{\sigma^4(1-J_0^2)} I_0\left(\frac{z_1 z_2 J_0}{\sigma^2(1-J_0^2)}\right) \end{aligned} \tag{3.25}$$

where $I_0(\cdot)$ is the modified Bessel function of the first kind of zero order.

3.1.4 Effects of Additive Noise

The received bandpass signal in the presence of additive noise is given by

$$y(t) = x(t) + n(t) \tag{3.26}$$

where $n(t)$ is the additive white Gaussian noise (AWGN) with zero mean and constant power spectral density over the entire frequency range. It is mathematically convenient in problems concerned with narrow-band signals in noise to model the additive

noise process as white and to represent the noise in terms of quadrature components. This can be accomplished by postulating that the signal and noise at the receiving terminal have passed through an ideal bandpass filter, having a passband. B_n. that includes the spectrum of the signals but is much wider. Such a filter will introduce negligible, if any, distortion on the signal but it does eliminate the noise frequency components outside of the passband[28].

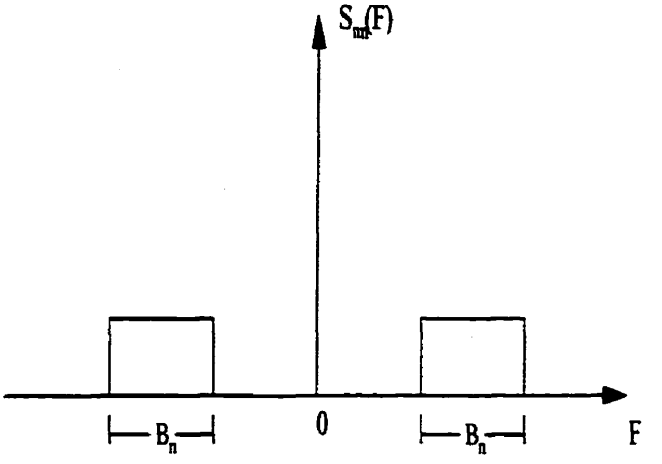

Figure 3.1: Power spectrum density of bandpass white noise

The noise resulting from passing the white noise process through an ideal bandpass filter is termed bandpass white noise and has the power spectral density depicted in Figure 3.1. The power spectral density of the equivalent lowpass noise $n_l(t)$ is given by

$$S_{n_l n_l}(F) = \begin{cases} N_0 & |F| \leq \frac{1}{2}B_n \\ 0 & |F| > \frac{1}{2}B_n \end{cases} \tag{3.27}$$

and its autocorrelation function is

$$\phi_{n_l n_l}(\tau) = N_0 \frac{\sin \pi B_n \tau}{\pi \tau} \tag{3.28}$$

where B_n is the bandwidth of the bandlimited noise. Since the bandlimited noise is a WSS process, we can obtain the autocorrelation function of the discrete-time noise by directly sampling the autocorrelation of the continuous-time bandlimited noise.

which is

$$\phi_{n_l n_l}(m) = N_0 \frac{\sin \pi B_n m T_s}{\pi m T_s} \tag{3.29}$$

where T_s is the sampling rate.

The power spectral density for bandpass white noise is symmetric about $f = 0$, and the autocorrelation functions of quadrature components are given by

$$\phi_{n_I n_I}(m) = \phi_{n_Q n_Q}(m) = \frac{1}{2}\phi_{n_l n_l}(m) \tag{3.30}$$

where $n_I(k)$ and $n_Q(k)$ are the in-phase and quadrature components of the bandpass white noise.

Sometimes the received signal is corrupted by inpulsive noise instead of white noise. Here we adopt the two-term mixture Gaussian noise model [41]. The pdf of this noise has the form

$$f = (1-\epsilon)\mathcal{N}(0, \nu^2) + \epsilon\mathcal{N}(0, \kappa\nu^2) \tag{3.31}$$

with $\nu > 0$, $0 \leq \epsilon \leq 1$, and $\kappa \geq 1$. In Equation (3.31), the $\mathcal{N}(0, \nu^2)$ term represents the nominal background noise, and the $\mathcal{N}(0, \kappa\nu^2)$ term represents the impulsive component, with ϵ is an indicator function, which represents the probability that the impulse occurs. It is assumed that values of the indicator function are independent over time. The variance of this noise is [41]

$$\sigma^2 = (1-\epsilon)\nu^2 + \epsilon\kappa\nu^2 \tag{3.32}$$

By bandpass-filtering with bandwidth B_n and sampling this noise at $1/T_s$ samples per second, we obtain its discrete-time autocorrelation function as

$$\phi_{n_l n_l}(m) = N_0' \frac{\sin \pi B_n m T_s}{\pi m T_s} \tag{3.33}$$

where $N_0' = (1-\epsilon)\nu^2 + \epsilon\kappa\nu^2$.

Adjacent Received Signal Envelope Statistics with Noise

With the presence of additive white noise, the in-phase and quadrature components of the received signal are written as

$$\begin{aligned} y_I(k) &= r_I(k) + n_I(k) \\ y_Q(k) &= r_Q(k) + n_Q(k) \end{aligned} \tag{3.34}$$

where $n_I(k)$ and $n_Q(k)$ are the in-phase and quadrature components of the bandpass white noise, respectively. Therefore,

$$E\{y_I^2(k)\} = E\{y_Q^2(k)\} = \sigma^2 + \frac{1}{2}\sigma_n^2 \tag{3.35}$$

and

$$E\{y_I(k)y_I(k+1)\} = E\{y_Q(k)y_Q(k+1)\} = \sigma^2 J_0(2\pi f_m) + \frac{1}{2}\sigma_n^2 \tag{3.36}$$

$$\begin{aligned} E\{y_I(k)y_Q(k)\} &= E\{y_I(k)y_Q(k+1)\} \\ &= E\{y_I(k+1)y_Q(k)\} = E\{y_I(k+1)y_Q(k+1)\} = 0 \end{aligned} \tag{3.37}$$

where σ_n^2 is the average power of the bandpass noise, which can be equal to $N_0 B_n$ if the noise is white Gaussian noise, or $N_0' B_n$ if the noise is two-term mixture Gaussian noise. From Equations (3.35)–(3.37), the covariance matrix for these four components with noise is given by

$$\Lambda = \begin{bmatrix} \sigma^2 + \frac{1}{2}\sigma_n^2 & 0 & \sigma^2 J_0 + \frac{1}{2}\sigma_n^2 & 0 \\ 0 & \sigma^2 + \frac{1}{2}\sigma_n^2 & 0 & \sigma^2 J_0 + \frac{1}{2}\sigma_n^2 \\ \sigma^2 J_0 + \frac{1}{2}\sigma_n^2 & 0 & \sigma^2 + \frac{1}{2}\sigma_n^2 & 0 \\ 0 & \sigma^2 J_0 + \frac{1}{2}\sigma_n^2 & 0 & \sigma^2 + \frac{1}{2}\sigma_n^2 \end{bmatrix} \tag{3.38}$$

Again, the Bessel function $J_0(2\pi f_m)$ in Equation (3.38) is simplified to J_0 for notational convenience. Similar to the derivation procedure from Equation (3.20) to (3.25), we can obtain the pdf of two adjacent envelope samples written as

$$p(z_1, z_2) = \frac{z_1 z_2 \exp\left\{-\frac{(\sigma^2+\frac{1}{2}\sigma_n^2)(z_1^2+z_2^2)}{2\sigma^2(1-J_0)(\sigma^2+\sigma^2 J_0+\sigma_n^2)}\right\}}{\sigma^2(1-J_0)(\sigma^2+\sigma^2 J_0+\sigma_n^2)} I_0\left(\frac{(\sigma^2 J_0 + \frac{1}{2}\sigma_n^2) z_1 z_2)}{\sigma^2(1-J_0)(\sigma^2+\sigma^2 J_0+\frac{1}{2}\sigma_n^2)}\right) \tag{3.39}$$

3.2 Envelope Level Crossing Rate for Discrete-Time Model

For the discrete-time propagation model introduced in the previous section, a positive level-crossing at time k of envelope $z(k)$ at level A occurs if $z(k-1) \leq A$ and $z(k) > A$. A negative level-crossing at time k of envelope $z(k)$ at level A occurs if $z(k-1) > A$

and $z(k) \leq A$. That is, whenever one of two adjacent samples is lower than A and the other is higher than A, an envelope level crossing is recorded. One must notice that positive and negative crossing directions cannot be mixed when counting the number of level crossings. Since the sample envelopes are random signals, the number of level crossings is a random variable. The level crossing rate over N given samples can be defined as the ratio of the expected number of level crossings to the number of samples. Let X denote the number of level crossings at the specified envelope level A over N given samples, the envelope level crossing rate (LCR) is therefore written as.

$$\text{LCR} = \frac{E\{X\}}{N} \tag{3.40}$$

Let X_k denote the state between two adjacent samples: $X_k = 0$ when there is no level crossing between two adjacent samples, and $X_k = 1$ when there is a level crossing. Therefore,

$$X = \sum_{k=n}^{n+N-1} X_k \tag{3.41}$$

where n denotes an arbitrary starting time and N is the total number of envelope samples processed. Substituting Equation (3.41) into Equation (3.40), we can obtain

$$\begin{aligned} \text{LCR} &= \frac{E\{\sum_{k=n}^{n+N-1} X_k\}}{N} \\ &= \frac{\sum_{k=n}^{n+N-1} E\{X_k\}}{N} \\ &= \frac{\sum_{k=n}^{n+N-1} (0 \times p_0 + 1 \times p_1)}{N} \\ &= \frac{Np_1}{N} \\ &= p_1 \end{aligned} \tag{3.42}$$

where

$$p_0 = P\{X_k = 0\} \tag{3.43}$$

$$p_1 = P\{X_k = 1\} \tag{3.44}$$

denote the probabilities of state 0 and 1, respectively. From the definition of envelope level crossing, Equation (3.42) can be written as

$$\begin{aligned} \text{LCR} &= P\{z_{k-1} \leq A, z_k > A\} \\ &= \int_0^A \int_A^\infty p(z_{k-1}, z_k) dz_{k-1} dz_k \end{aligned} \tag{3.45}$$

where $p(z_{k-1}, z_k)$ is the joint pdf of two ajacent envelope samples. Where it is also assumed that there only one level crossing occurs during the sampling period. In order to find the LCR, we must first evaluate the double integration in Equation (3.45).

With the absence of the additive noise, from Equation (3.25), Equation (3.45) can be written as,

$$\text{LCR} = \int_0^A \int_A^\infty \frac{z_1 z_2 \exp\left\{-\frac{z_1^2+z_2^2}{2\sigma^2(1-J_0^2)}\right\}}{\sigma^4(1-J_0^2)} I_0\left(\frac{z_1 z_2 J_0}{\sigma^2(1-J_0^2)}\right) dz_1 dz_2 \tag{3.46}$$

where z_1 and z_2 denote z_{k-1} and z_k, respectively. Substituting $m^2 = \sigma^2(1-J_0^2)$, $x = z_2/m$, and $\alpha = (z_1 J_0)/m$ into Equation (3.46), we obtain

$$\begin{aligned}
\text{LCR} &= \int_0^A \frac{z_1}{\sigma^2} \exp\left\{-\frac{1}{2}(1-J_0^2)\frac{z_1^2}{m^2}\right\} \left[\int_{A/m}^\infty x \exp\left\{-\frac{1}{2}(x^2+\alpha^2)\right\} I_0(\alpha x) dx\right] dz_1 \\
&= \int_0^A \frac{z_1}{\sigma^2} \exp\left\{-\frac{1}{2}(1-J_0^2)\frac{z_1^2}{m^2}\right\} Q(\alpha, A/m) dz_1 \\
&= \int_0^A \frac{z_1}{\sigma^2} \exp\left\{-\frac{1}{2}(1-J_0^2)\frac{z_1^2}{m^2}\right\} Q\left(\frac{z_1 J_0}{m}, \frac{A}{m}\right) dz_1
\end{aligned} \tag{3.47}$$

where

$$Q(\alpha, \beta) = \int_\beta^\infty x \exp\left\{-\frac{1}{2}(x^2+\alpha^2)\right\} I_0(\alpha x) dx$$

is the Marcum's Q function [17]. Substituting $x = z_1/m$ into Equation (3.47),

$$\text{LCR} = \int_0^{A/m} (1-J_0^2) x \exp\left\{-\frac{1}{2}x^2(1-J_0^2)\right\} Q(J_0 x, A/m) dx \tag{3.48}$$

The Marcum's Q function can be written in terms of the following series [17],

$$Q(\alpha, \beta) = e^{-\frac{1}{2}(\alpha^2+\beta^2)} \sum_{n=0}^\infty \left(\frac{\alpha}{\beta}\right)^n I_n(\alpha\beta) \tag{3.49}$$

Substituting Equation (3.49) into (3.48),

$$\begin{aligned}
\text{LCR} &= (1-J_0^2) e^{-A^2/(2m^2)} \sum_{n=0}^\infty \left(\frac{J_0 m}{A}\right)^n \int_0^{A/m} x^{n+1} e^{-x^2/2} I_n\left(\frac{J_0 A x}{m}\right) dx \\
&= (1-J_0^2) e^{-A^2/(2m^2)} \sum_{n=0}^\infty \left(\frac{J_0 m}{A}\right)^n G
\end{aligned} \tag{3.50}$$

where

$$G = \int_0^{A/m} x^{n+1} e^{-x^2/2} I_n\left(\frac{J_0 A x}{m}\right) dx \tag{3.51}$$

Substituting $v = A/m$ into Equation (3.51), we obtain

$$G = \int_0^v x^{n+1} e^{-x^2/2} I_n(J_0 v x) dx \tag{3.52}$$

Expanding $e^{-x^2/2}$ into series,

$$e^{-x^2/2} = 1 + \left(-\frac{x^2}{2}\right) + \frac{1}{2!}\left(-\frac{x^2}{2}\right)^2 + \cdots + \frac{1}{k!}\left(-\frac{x^2}{2}\right)^k + \cdots \tag{3.53}$$

and substituting Equation (3.53) into (3.52), we obtain,

$$\begin{aligned} G &= \int_0^v x^{n+1} I_n(J_0 v x) dx + \int_0^v x^{n+1} \left(\frac{x^2}{2}\right) I_n(J_0 v x) dx \\ &\quad + \cdots + \int_0^v \frac{1}{k!} x^{n+1} \left(\frac{x^2}{2}\right) I_n(J_0 v x) dx + \cdots \end{aligned} \tag{3.54}$$

The modified Bessel functions have the property [17],

$$\int \alpha^n I_{n-1}(\alpha\beta) d\alpha = \frac{\alpha^n}{\beta} I_n(\alpha\beta) \tag{3.55}$$

Using Equations (3.54) and (3.55), we obtain,

$$\begin{aligned} G &= v^n e^{-v^2/2} \sum_{k=1}^{\infty} J_0^{-k} I_{n+k}(J_0 v^2) \\ &= \left(\frac{A}{m}\right)^n e^{-A^2/2m^2} \sum_{k=1}^{\infty} J_0^{-k} I_{n+k}\left(\frac{J_0 A^2}{m^2}\right) \end{aligned} \tag{3.56}$$

Substituting Equation (3.56) into Equation (3.50), we obtain

$$\begin{aligned} \text{LCR} &= (1 - J_0^2) e^{-A^2/m^2} \sum_{n=0}^{\infty} \sum_{k=1}^{\infty} J_0^{n-k} I_{n+k}\left(\frac{J_0 A^2}{m^2}\right) \\ &= (1 - J_0^2) e^{-A^2/\sigma^2(1-J_0^2)} \sum_{n=0}^{\infty} \sum_{k=1}^{\infty} J_0^{n-k} I_{n+k}\left(\frac{J_0 A^2}{\sigma^2(1-J_0^2)}\right) \\ &= (1 - J_0^2) e^{-2\rho^2/(1-J_0^2)} \sum_{n=0}^{\infty} \sum_{k=1}^{\infty} J_0^{n-k} I_{n+k}\left(\frac{2J_0\rho^2}{1-J_0^2}\right) \end{aligned} \tag{3.57}$$

where $\rho = A/\sqrt{2\sigma^2}$, and $\sqrt{2\sigma^2}$ is the rms value of the signal envelope amplitude.

With the presence of noise, by using the derivation procedure shown from Equations (3.45) to (3.57) and using Equation (3.39), we can obtain the LCR as

$$\begin{aligned} \text{LCR} &= (1 - J_0)(1 + J_0 + \frac{2}{\gamma_s}) e^{-\frac{2(1+\frac{1}{\gamma_s})^2 \rho^2}{(1-J_0)(1+J_0+\frac{2}{\gamma_s})}} \sum_{n=0}^{\infty} \sum_{k=1}^{\infty} \left(\frac{J_0 + \frac{1}{\gamma_s}}{1 + \frac{1}{\gamma_s}}\right)^{n-k} \\ &\quad \times I_{n+k}\left(\frac{2(J_0 + \frac{1}{\gamma_s}(1 + \frac{1}{\gamma_s})\rho^2}{(1 - J_0)(1 + J_0 + \frac{2}{\gamma_s})}\right) \end{aligned} \tag{3.58}$$

where $\gamma_s = (2\sigma^2)/\sigma_n^2$ is the signal-to-noise ratio (SNR).

We can solve for the estimated mobile velocity $\hat{v}$ by using a table-looking method. That is, we calculate LCR values according to various mobile velocities using Equation (3.57) or Equation (3.58) and construct a table, where the number of the summations in these two equations can be set to 30. When we are estimating the mobile velocity, we can look up the calculated table in accordance with the calculated LCR value to obtain the estimate of the mobile velocity.

3.3 Level Crossing Rate Estimation

We have shown that the level crossing rates of the envelope $z(k) = \sqrt{r_I^2(k) + r_Q^2(k)}$ of a received signal in noise are functions of the mobile velocity as discussed in previous sections. The envelope level crossing rate (LCR) is defined as the average number of level-crossings per envelope sample at an envelope amplitude level A, which is predeterminated by received signals.

Therefore, the LCR of the received signals can be used to estimate the mobile velocity. The LCR as the function of mobile velocity is given by Equation (3.57) for the noiseless case, and Equation (3.58) for the case in the presence of additive noise. As long as we are given the LCR for the received signal, we can solve for the maximum Doppler frequency f_m using the equations shown above. Once f_m is calculated, using

$$v = \frac{f_m F_s c}{F_c} \tag{3.59}$$

where F_s is the sampling rate, F_c is the carrier frequency and c is the velocity of light, we can solve for the desired mobile velocity v.

3.3.1 Level Crossing Rate Estimation Procedures

In level crossing rate estimation of mobile velocity, the first step should be bandpass-filtering the received signal in additive noise to get rid of the out-of-band component of the signal. Then we can sample the output of the bandpass filter at F_s samples per second to obtain the discrete-time signal. In order to obtain the LCR, we need to convert the received discrete-time signal into an equivalent lowpass signal and

calculate the LCR at a specified level A over N envelope samples. From the obtained LCR and using Equations (3.57)–(3.59), we can calculate the desired mobile velocity. The procedure is shown in Figure 3.2. Before we go further, we must clarify some issues in parameter determination. We need to know how the bandwidth of the bandpass filter is specified; how to choose the sampling rate F_s; and how many envelope samples should be processed to obtain the LCR.

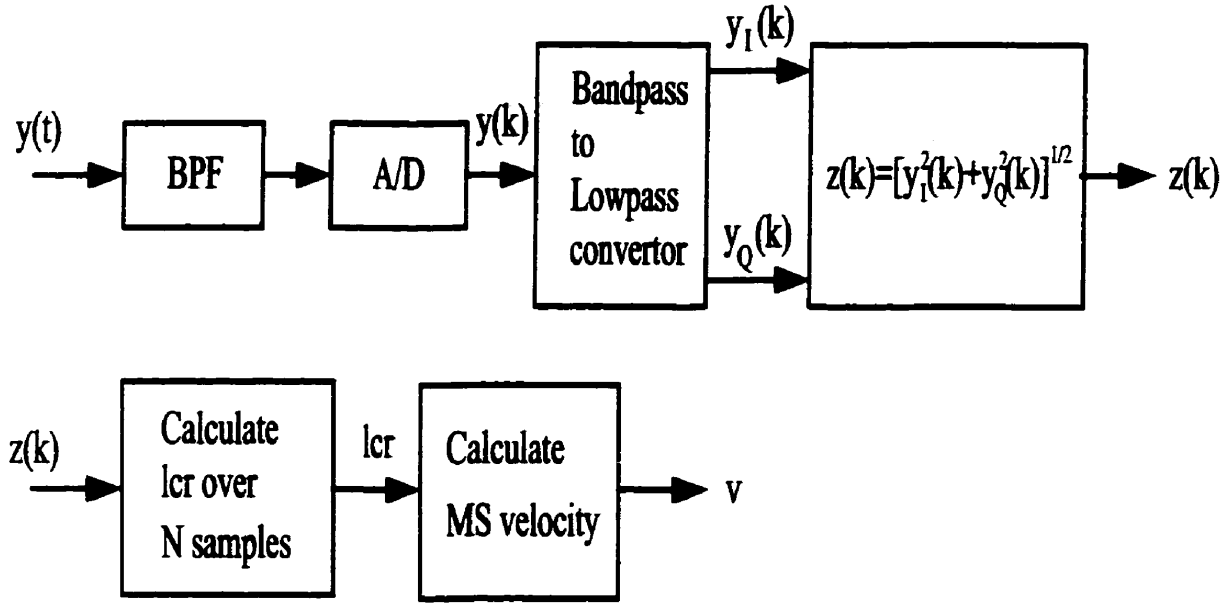

Figure 3.2: Procedure for obtaining LCR

Bandpass Filter Bandwidth B_n

As described in Section 3.1.4, the passband of the bandpass filter must include the spectrum of the signal. For mobile velocity estimation, only the maximum Doppler frequency F_m introduced by the mobile mobility is needed; and from Figure 2.3, we can see that the spectrum of the fading signal is within the range of $(F_c - F_m, F_c + F_m)$, where F_c is the carrier frequency. Therefore, the bandwidth of the bandpass filter B_n should be larger than $2F_m$.

The maximum Doppler frequency F_m depends on the carrier frequency F_c and mobile velocity v, as shown below,

$$F_m = \frac{vF_c}{c} \tag{3.60}$$

where c is the velocity of light. For a specific mobile communication system, the carrier frequency F_c is usually fixed, that is, F_m is mainly affected by the mobile velocity, v. Therefore, as long as we set B_n larger than twice of the maximum value of the expected maximum Doppler frequency for a specific system, useful information will not be eliminated by the bandpass filter.

Sampling Rate F_s

The sampling rate F_s can be theoretically chosen as twice the upper bound of the bandpass signal due to the sampling theorem. In practice, it would be expensive in the case that the upper bound frequency is extremely high. Generally, the carrier frequency in mobile communication systems is very high. For example, about 2 GHz is used for recent personal communications systems. We need to find another sampling method. It would be advantageous to perform a bandpass-to-lowpass conversion, and sample the equivalent lowpass signal [29]. Figure 3.2 is, therefore, modified as in Figure 3.3. The resulting equivalent lowpass signal has a bandwidth $B_n/2$; hence it can be represented uniquely by samples taken at the rate of B_n samples per second for each of the quadrature components. Thus the sampling can be performed on each of the lowpass filter outputs at the rate of B_n samples per second. Therefore, the resulting rate is $2B_n$ samples per second.

In Equations (3.57) and (3.58), we are using $J_0^2(2\pi f_m)$, which is depicted in Figure 3.4. From this figure, we can find that $J_0^2(2\pi f_m)$ descends monotonically from its maximum value until it reaches 0, then it goes upward. This implies that for one unique LCR, we may obtain more than one estimated f_m by using these two equations. To guarantee a unique estimated f_m, we must limit the maximum value of the expected f_m for a specific mobile communication system to be less than 0.3827, which is the smallest positive solution of $J_0^2(2\pi f_m) = 0$. This can be accomplished by choosing a large enough sampling rate. Fortunately, if we set the sampling rate F_s to be at least larger than $2B_n$, which in turn is larger than $4F_m$, the maximum value of the expected maximum Doppler frequency $f_m = F_m/F_s$ is always less than 0.25. Therefore, a unique solution of the estimated f_m is always guaranteed.

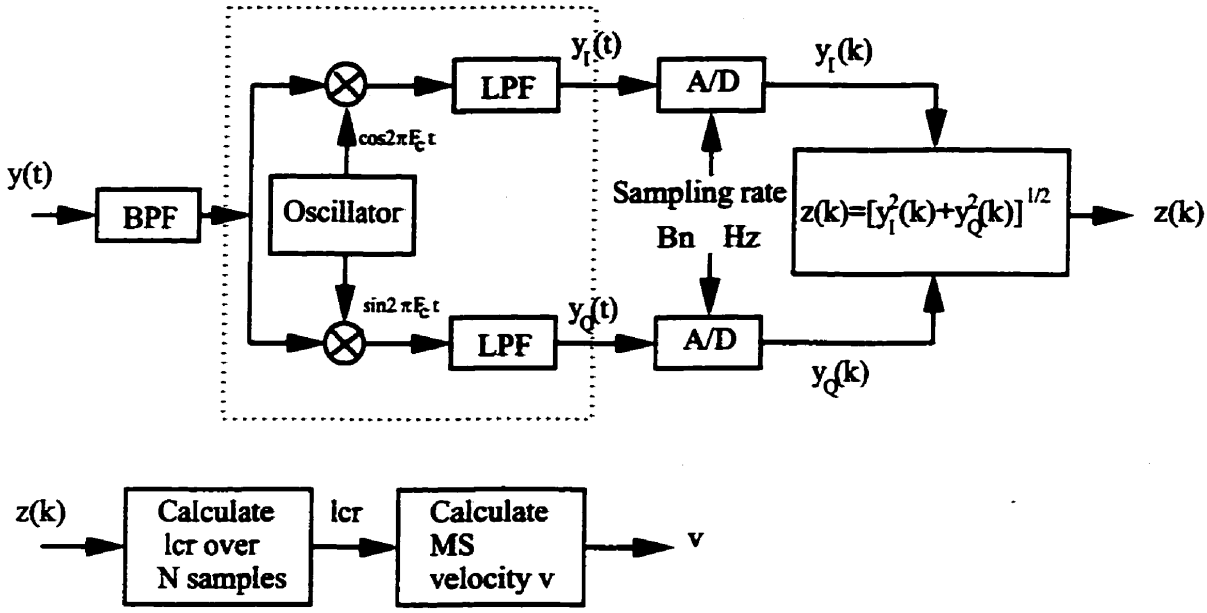

Figure 3.3: Modified procedure for obtaining lcr

Number of Samples N

In order to obtain an accurate estimate of the actual LCR, it is necessary to process a sufficient number of envelope samples. This can be accomplished by determining the confidence interval for the observed LCR. By specifying the desired width of interval, the necessary number of samples can be calculated.

Letting δ_l denote the confidence interval, the observed LCR $\hat{R}_l$ should fall into the range of $(R_l - \delta_l, R_l + \delta_l)$, where R_l represents the actual LCR. If the received fading signal samples are independent, and Gaussian distributed, the interval boundary δ_l can be calculated from the observed values as [10]

$$\delta_l = Q\sqrt{\frac{\hat{R}_l(1-\hat{R}_l)}{N}} \tag{3.61}$$

where N is the total number of samples to be processed and the value of Q depends on $\delta_l/\hat{R}_l$ as shown in Table 3.1.

As we know, the received fading signal samples are correlated, and not Gaussian distributed. Therefore, the interval boundary of the received fading signal samples are different from the one shown in Equation (3.61). However, for the sake of simplicity, we still use Equation (3.61) to calculate the confidence interval and determine the

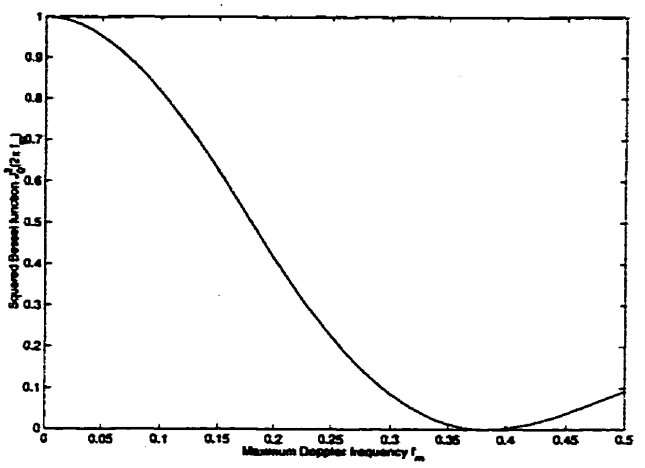

Figure 3.4: Squared Bessel function

necessary number of samples processed.

$\delta_l/\hat{R}_l$	10%	5%	1%
Q	1.65	1.96	2.58

Table 3.1: Standard deviation multipliers for various confidence intervals

Solving for N from Equation (3.61),

$$N = \frac{Q^2 \hat{R}_l (1 - \hat{R}_l)}{\delta_l^2} \tag{3.62}$$

By specifying δ_l, we can calculate the desired number of samples processed. Table 3.2 shows numbers of samples corresponding to various observed LCR, where δ_l is specified as $0.1\hat{R}_l$.

Algorithm Summary

The algorithm for estimation of mobile velocity using LCR method is summarized as below,

- Design a bandpass filter with bandwidth B_n. In all experiments, a Butterworth filter is used with upper cutoff frequency $F_{cu} = F_c + B_n/2$, lower cutoff frequency $F_{cl} = F_c - B_n/2$, upper stopband frequency $F_{su} = F_{cu} + B_n/4$, lower stopband

$\hat{R}_l$	0.1	0.01	0.001
δ_l	0.01	0.001	0.0001
N	2.4×10^3	2.69×10^4	2.72×10^5

Table 3.2: Total number of samples for various observed LCR

frequency $F_{sl} = F_{cl} - B_n/4$, and 60 dB stopband attenuation, where F_c is the carrier frequency,

- Bandpass-filter the received fading signal through the bandpass filter,
- Convert the bandpass received signal into its lowpass equivalent signal,
- Sample the lowpass equivalent signal at the sampling rate of F_s samples per second,
- Calculate the LCR at a specified level A over N envelope samples, and
- Calculate the desired mobile velocity from the obtained LCR using Equations (3.57) or (3.58) and (3.59).

3.3.2 Implementation and Simulation Results

In the previous section, we have introduced a new algorithm and procedure of LCR estimation of mobile velocity, as well as the parameter specifications for the LCR velocity estimator. We will represent the detailed simulation procedure and results in this section.

Before we describe the results in detail, we have to first specify the parameters for velocity estimation. As we have described in the previous section, both the bandwidth of the bandpass filter B_n and the sampling rate F_s depend on the maximum value of the expected Doppler frequency F_m, which in turn depends on the maximum expected mobile velocity v_{max} and the carrier frequency F_c. If the mobile stations are automobiles, it is reasonable to assume that the maximum expected velocity v_{max} is 200 km/h. Assuming that the carrier frequency is 2 GHz, we can, therefore,

calculate the other parameters using the methods described in previous section. These parameters are shown in Table 3.3. The curve of LCR against mobile velocity v is depicted in Figure 3.5, using Equations (3.57) and (3.59).

F_c	v_{max}	$F_{m,max}$	B_n	F_s	$f_{m,max}$
2 GHz	200 km/h	370.4 Hz	800 Hz	1600 Hz	0.2315

Table 3.3: Parameters for simulation system

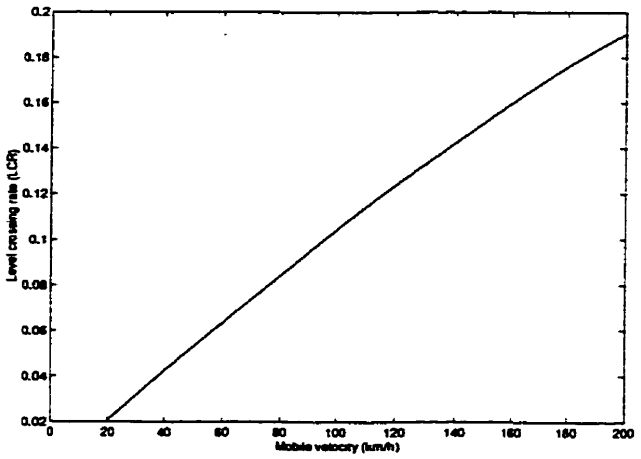

Figure 3.5: Level crossing rate against vehicle speed v

The final parameter to be specified is the total number of samples processed. In an urban area, the vehicle speed usually ranges from 20 to 70 km/h. This corresponds to a maximum Doppler frequency f_m, within the range of $(0.02316, 0.08103)$, using parameters shown in Table 3.3 and Equation (3.60). From Figure 3.5 or using Equations (3.57), we obtain that the range of LCR is within $(0.0141, 0.1038)$. Using Equation (3.62) and setting the confidence interval to be 10% of observed LCR, we can calculate the total number of samples processed N to be within the range of $(2.4 \times 10^3, 2.69 \times 10^4)$. To assure the accuracy of simulation, we choose the upper bound 2.69×10^4 as the total number of samples processed, which corresponds to a vehicle speed of 20 km/h.

Now that we have specified all the parameters used in the LCR method of mobile velocity estimation, we simulate the implementation of this estimator. As described

in the previous section, we need to bandpass-filter the input fading signal, sample the output of the bandpass filter, calculate the LCR at a specified envelope amplitude level, then calculate the desired mobile velocity using Equations (3.59) and (3.57) or (3.58).

Ideally, we would like to test the estimator on real data with known mobile velocity. Since we do not have the real fading signal, we generate a fading signal using a fading signal generator described in Section 2.4. For the sake of simplicity, we use Young and Beaulieu's generator. First, we generate a sequence of fading signal samples according to a specific vehicle speed. Since, from Section 2.4.3, the generated signal is already discrete-time, we do not have to implement the sampling procedure. Second, we count the number of positive crossings through a specific envelope level over N envelope samples and calculate the LCR. Finally, we calculate the estimated vehicle speed using Equations (3.57) to (3.59) and the given LCR. If the estimated vehicle speed is close to the one specified to generate the fading signal, the LCR estimation method for the mobile velocity is justified.

In order to simulate the implementation of the LCR method in the presence of noise, we also need to generate a bandlimited noise sequence with bandwidth B_n, and add it onto the generated fading signal. We can find that Equation (3.58) tends to Equation (3.57) when the SNR tends to infinity. In high SNR conditions, we can, therefore, use Equation (3.57) to solve for the LCR in the presence of noise. Since the fading signal and additive noise are generated by computer, Monte-Carlo trials are used to smooth the fluctuation.

The procedure is shown in Figure 3.6 and sumarized below,

- Generate a fading signal using Young and Beaulieu's generator according to a specific vehicle speed,

- Generate bandlimited noise with bandwidth B_n according to a SNR value and add it onto the generated fading signal to form the received signal at the mobile station,

- Count positive crossings through a specified envelope level over N envelope samples and calculate the LCR, and

- Calculate estimated vehicle speed using Equations (3.57) and (3.59),
- Repeat the above steps until the total number of Monte-Carlo trials is reached and calculate the average vehicle speeds obtained from the trails.

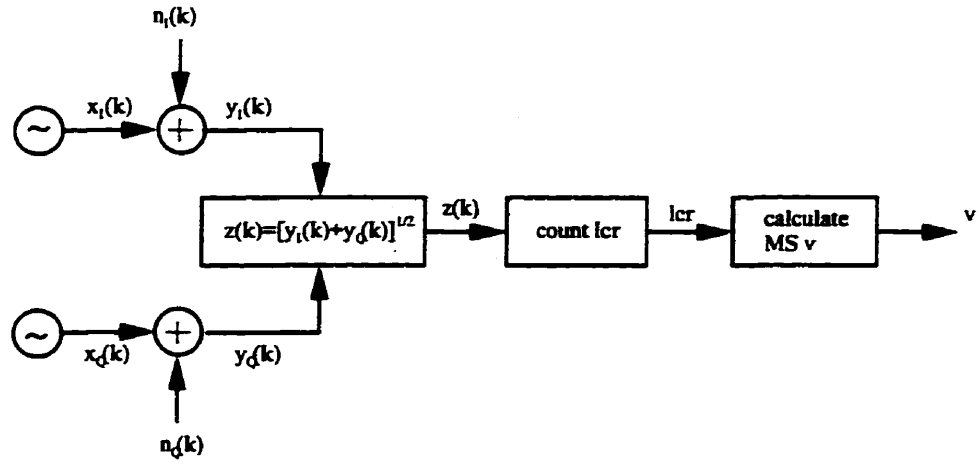

Figure 3.6: Simulation procedure for LCR mobile velocity estimation

Simulation Results without Noise

Simulating the LCR estimation method of mobile velocity using a received fading signal that is not corrupted by noise is relatively straightforward. Assuming that the maximum vehicle speed is 200 km/h, the carrier frequency is 2 GHz, then the maximum expected value of the maximum Doppler frequency is 370.4 Hz. Following the previous section, we can set the sampling rate to be 1600 Hz. Letting the input to the fading signal generator corresponds to the desired vehicle speed, we can obtain the output of the generator is a sequence of discrete-time fading signal samples, where the number of samples to be processed is set to 2.69×10^4. Simply following the estimation procedure described in Figure 3.6, we can obtain the simulation results, using Equations (3.59) and (3.57), where $\rho = 1$, and the number of terms of both sumations is set to be 30. The number of Monte-Carlo trials is set to be 30. Table 3.4 and Figure 3.8 show the simulation results corresponding to various actual vehicle speeds. Figure 3.7 shows the theoretical results and simulation results of LCR against vehicle speed.

v (km/h)	20	30	40	50	60	70	80
$\hat{v}$ (km/h)	20.71	30.53	40.59	50.39	60.15	69.40	78.96
v (km/h)	90	100	110	120	130	140	150
$\hat{v}$ (km/h)	87.05	95.20	102.01	108.82	115.54	120.37	125.92
v (km/h)	160	170	180	190	200		
$\hat{v}$ (km/h)	128.63	133.36	136.72	139.97	142.09		

Table 3.4: LCR estimation results without noise, maximum vehicle speed: 200 km/h, sampling rate: 1600 Hz, Monte-Carlo trials: 30

From Figure 3.7, we can find that the estimated LCR obtained from the sequence of generated fading signals are significantly lower than the theoretical LCR value when the real vehicle speed exceeds 100 km/h. This could result in underestimation of vehicle speed, which is shown in Table 3.4 and Figure 3.8. The possible reason for this problem could be a low sampling rate. Since the fading depends on vehicle speed, the faster the vehicle, the larger the fading rate. If the sampling rate is not large enough, level crossings would be missed by the sampling of the received analog signal. We were using a sampling rate of 1600 Hz. The simulation results, using a sampling rate of 3200 Hz, are shown in Table 3.5 and Figure 3.9. From the table and figure, we can find that when we increase the sampling rate, the estimates of vehicle speeds are closer to the actual values. Therefore, the sampling rate used in the LCR estimator is dependent on vehicle speed. The faster the vehicle, the larger the required sampling rate. In a practical system, we can set a threshold of the mobile speed due to the carrier frequency and maximum expected mobile speed. If the estimated vehicle speed crosses this threshold, we must increase the sampling rate and re-estimate the vehicle speed to obtain more accuracy.

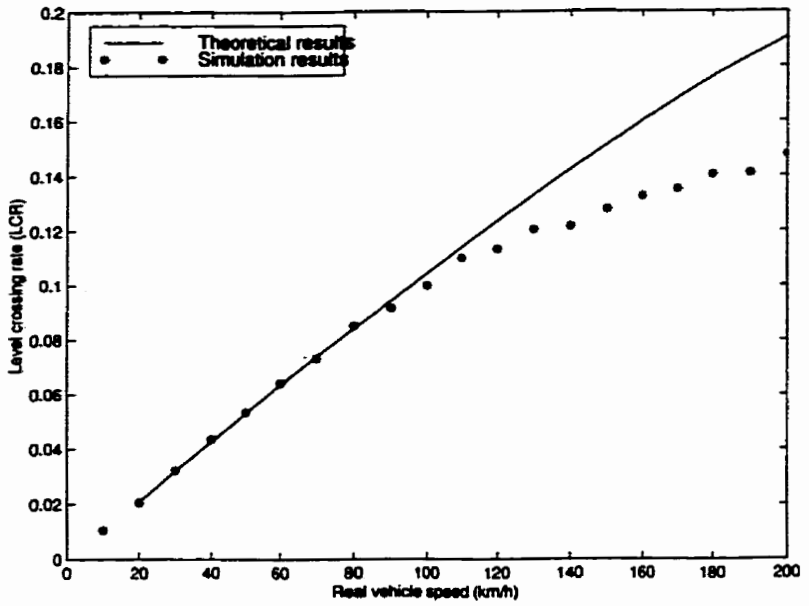

Figure 3.7: Level crossing rate against vehicle speed without noise, maximum vehicle speed: 200 km/h, sampling rate: 1600 Hz, Monte-Carlo trials: 30

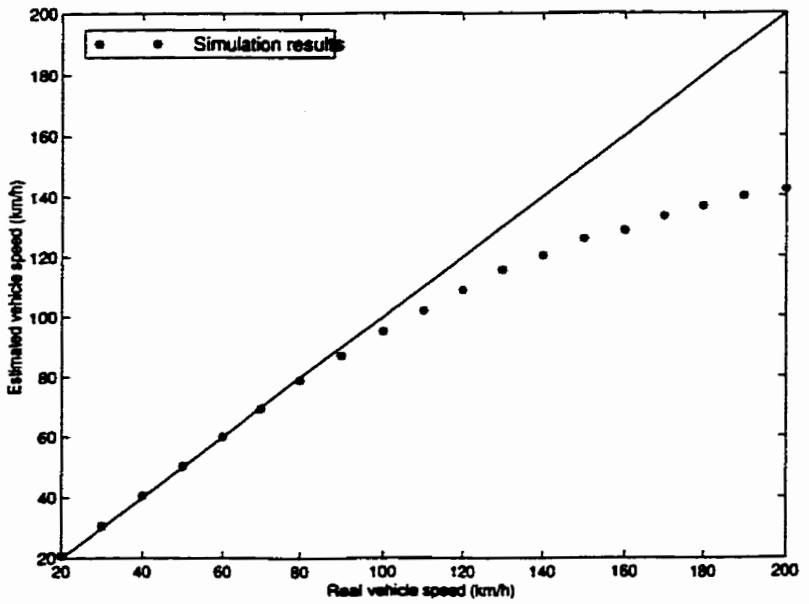

Figure 3.8: LCR estimation results without noise, maximum vehicle speed: 200 km/h, sampling rate: 1600 Hz, Monte-Carlo trials: 30

v (km/h)	100	110	120	130	140	150
$\hat{v}$ (km/h)	100.17	110.32	119.13	129.68	138.67	147.04
v (km/h)	160	170	180	190	200	
$\hat{v}$ (km/h)	157.41	165.67	173.40	181.88	190.67	

Table 3.5: LCR estimation results without noise, maximum vehicle speed: 200 km/h, sampling rate: 3200 Hz, Monte-Carlo trails: 30

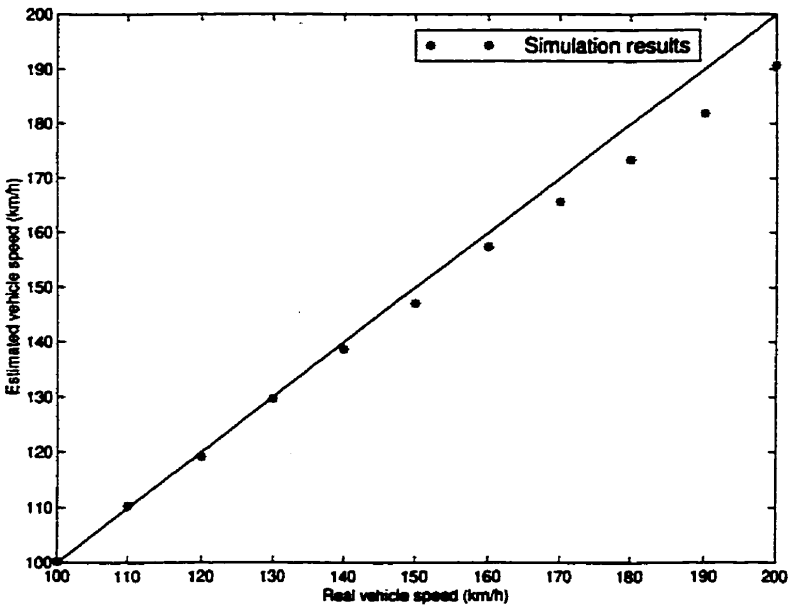

Figure 3.9: LCR estimation results without noise, maximum vehicle speed: 200 km/h, sampling rate 3200 Hz, Monte-Carlo trials: 30

Simulation Results in Additive White Gaussian Noise

We now simulate the LCR estimation system of the mobile speed with received fading signal corrupted by additive white Gaussian noise. Equations (3.58) and (3.59) will be used. In practical estimation system, however, since we do not exactly know the signal-to-noise ratio, therefore, the use of Equation (3.58) is inconvenient. It will be advantageous to use Equation (3.57) in the noisy case. This would imply that the use of Equation (3.57) is robust in the estimation of mobile speed using received fading signal regardless of additive noise. We will demonstrate the robustness by using this equation in simulation of mobile speed in presence of additive noise.

Assuming that the maximum vehicle speed is 200 km/h, the carrier frequency is 2 GHz, then the maximum expected value of the maximum Doppler frequency is 370.4 Hz. Following the previous section, the bandwidth of the bandpass filter could be set to be 800 Hz, then the sampling rate could be set to be 1600 Hz for the vehicle speeds lower than 100 km/h, and 3200 Hz for the vehicle speeds of 100 km/h and above. Letting the input to the fading signal generator correspond to the actual vehicle speed, we can obtain the output of the generator is a sequence of discrete-time fading signal samples, where the number of samples processed is set to be 2.69×10^4.

Simply following the estimation procedure described in Figure 3.6,we can obtain the simulation results, using Equations (3.59) and (3.57), where $\rho = 1$, and the number of the terms of the sumations is set to be 30. The signal-to-noise ratio for each speed is varied from 5 to 50 dB. The simulation results are shown in Figures 3.10 to 3.15. From these figures, we can observe that the estimated vehicle speeds are close to the actual values. When the signal-to-noise ratio exceeds 30 dB, the simulation results become quite accurate. Then, we can conclude that the robustness of Equation (3.57) in the presence of additive white Gaussian noise is justified in SNR's of at least 30 dB.

Simulation Results in Impulsive Noise

In the previous section, we have demostrated that the LCR mobile speed estimator is robust in the presence of additive Gaussian noise. However, as described in Section 3.1.4, impulsive noise is sometimes encountered in practical application of mobile

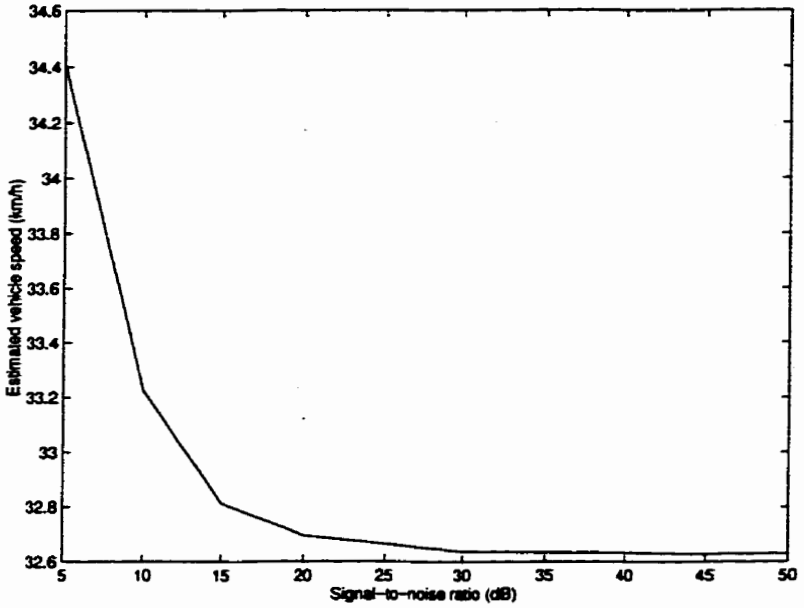

Figure 3.10: Simulation results of actual vehicle speed of 30 km/h in presence of additive Gaussian noise

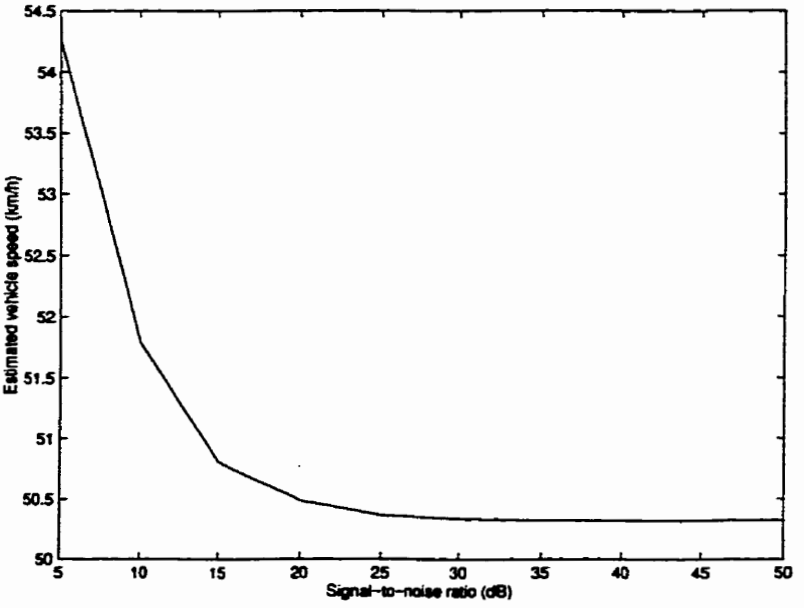

Figure 3.11: Simulation results of actual vehicle speed of 50 km/h in presence of additive Gaussian noise

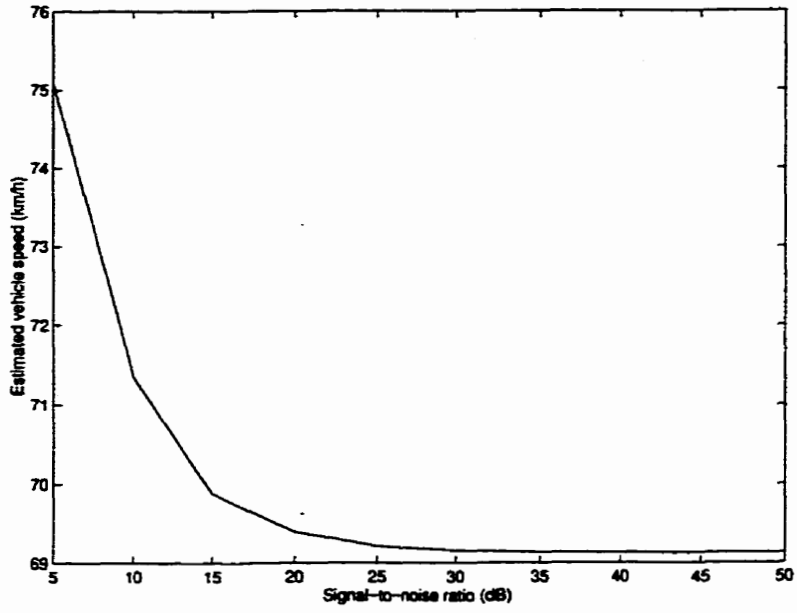

Figure 3.12: Simulation results of actual vehicle speed of 70 km/h in presence of additive Gaussian noise

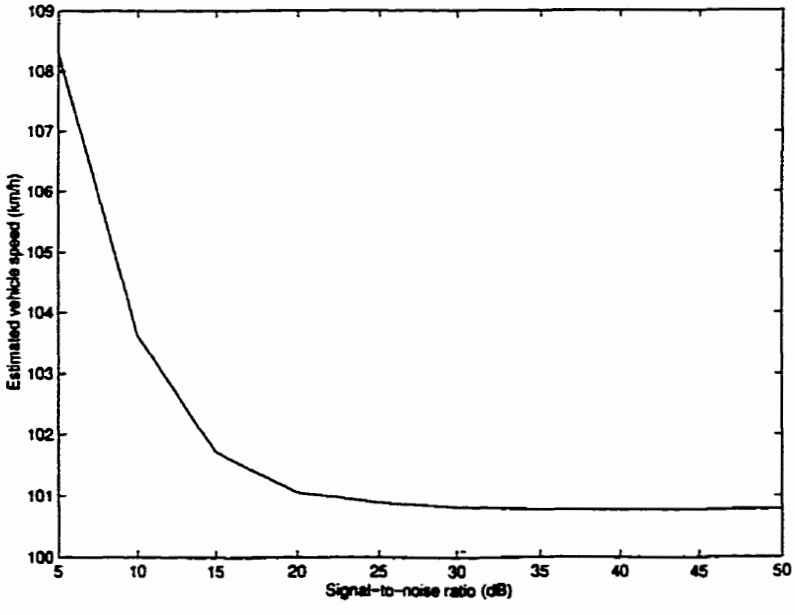

Figure 3.13: Simulation results of actual vehicle speed of 100 km/h in presence of additive Gaussian noise

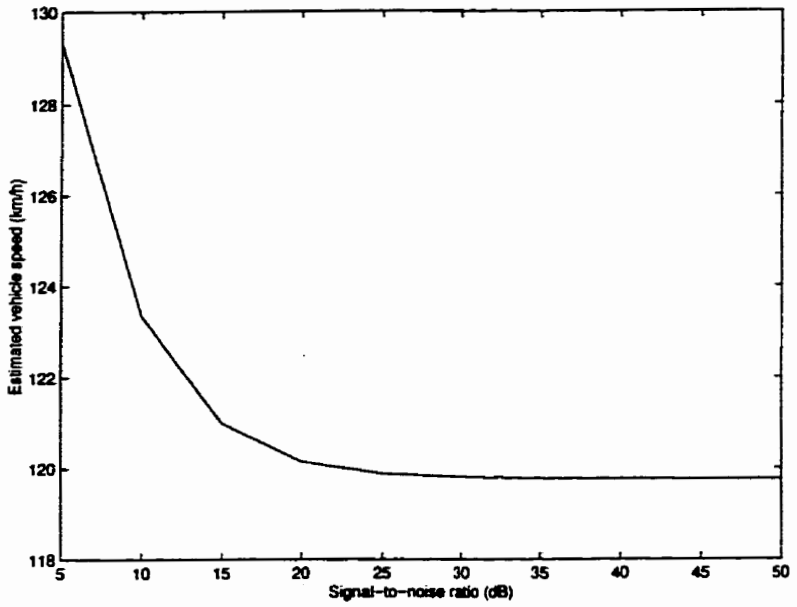

Figure 3.14: Simulation results of actual vehicle speed of 120 km/h in presence of additive Gaussian noise

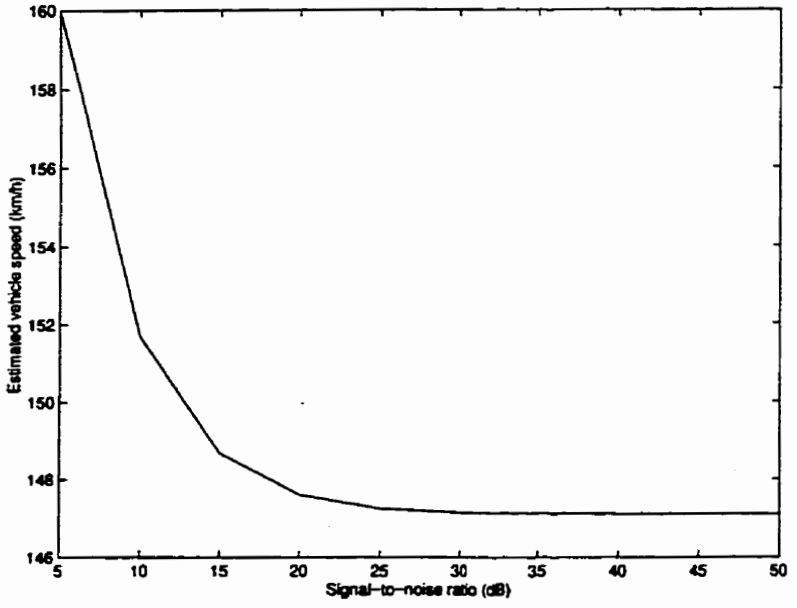

Figure 3.15: Simulation results of actual vehicle speed of 150 km/h in presence of additive Gaussian noise

communication systems. Therefore, in this section, we will simulate the LCR mobile speed estimator in the presence of impulsive noise. Here we use the two-term mixture Gaussian noise to represent impulsive noise as described in Section 3.1.4.

Assuming that the maximum vehicle speed is 200 km/h, the carrier frequency is 2 GHz, then the maximum expected value of the maximum Doppler frequency is 370.4 Hz. Following the previous section, the bandwidth of the bandpass filter is set to be 800 Hz, then the sampling rate could be set to be 1600 Hz for the vehicle speeds lower than 100 km/h, and 3200 Hz for the vehicle speeds of 100 km/h and above. Letting the input to the fading signal generator correspond to the actual vehicle speed, we obtain at the output of the generator, a sequence of discrete-time fading signal samples, where the number of samples processed is set to be 2.69×10^4.

Simply following the estimation procedure described in Figure 3.6, we obtain the simulation results, using Equations (3.59) and (3.57), where $\rho = 1$, and the number of the terms of the sumations is set to be 30. The signal-to-noise ratio for each speed is varied from 5 to 50 dB, $\epsilon = 0.01$, and $\kappa = 100$. The simulation results are shown in Figures 3.16 to 3.21. The simulation results are close to the actual mobile speeds. Then, robustness of Equation (3.57) in the presence of two-term mixture Gaussian noise is justified.

3.4 Summary

We have derived the LCR mothod of the mobile velocity estimation and shown the implementation procedure and simulation results of the LCR estimator in this chapter. The simulation results show that the estimates of the mobile velocity are close to the actual values, in the presence of white additive noise or two-term mixture Gaussian noise. However, the sampling rate used in the LCR estimator depends on the vehicle speed. In a practical system, a threshold may be set to adjust the sampling rate. When the estimated mobile velocity exceeds the threshold, the sampling rate should be increased and the mobile velocity should be re-estimated.

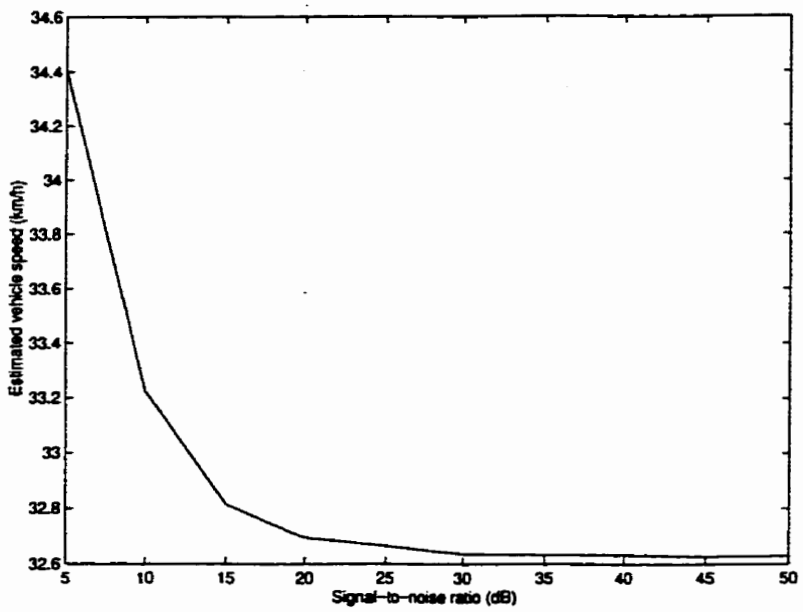

Figure 3.16: Simulation results of actual vehicle speed of 30 km/h in presence of two-term mixture Gaussian noise

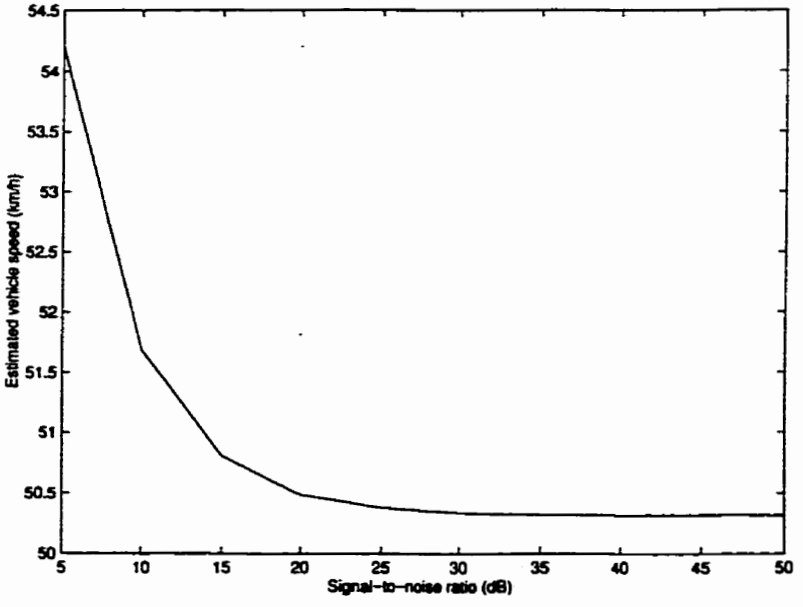

Figure 3.17: Simulation results of actual vehicle speed of 50 km/h in presence of two-term mixture Gaussian noise

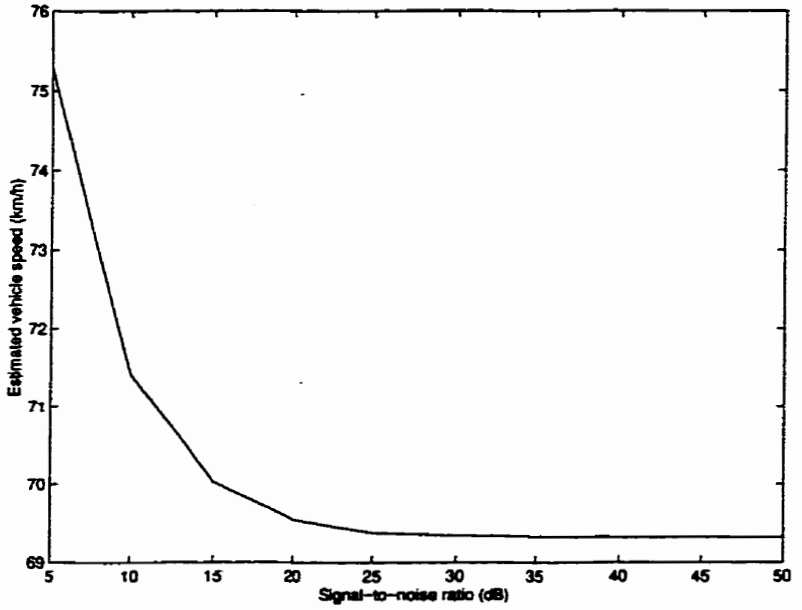

Figure 3.18: Simulation results of actual vehicle speed of 70 km/h in presence of two-term mixture Gaussian noise

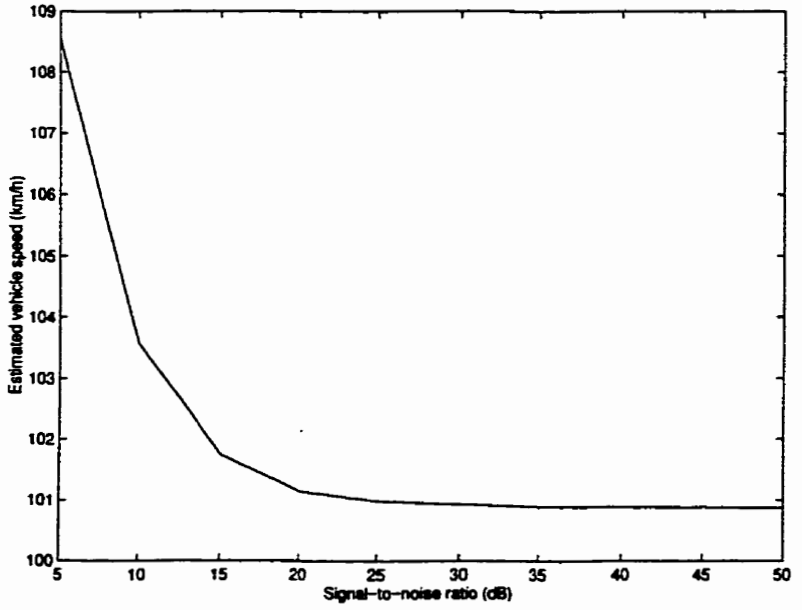

Figure 3.19: Simulation results of actual vehicle speed of 100 km/h in presence of two-term mixture Gaussian noise

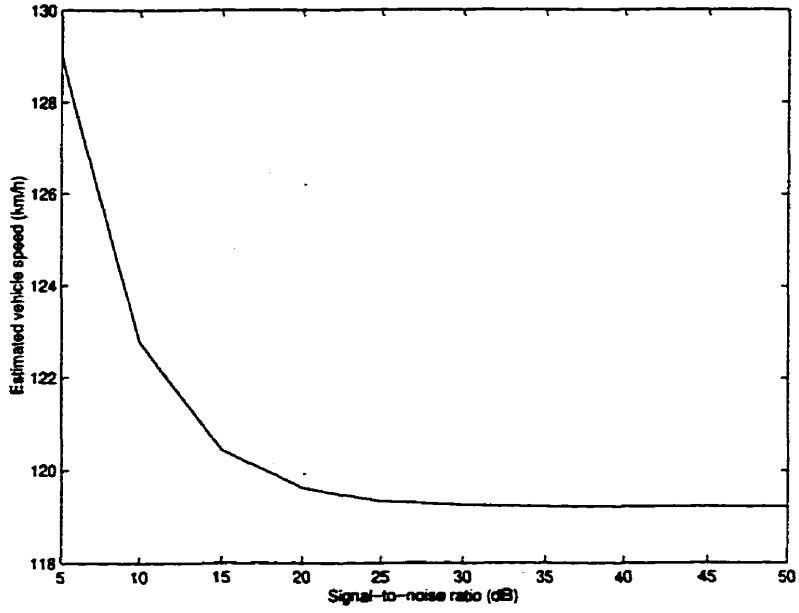

Figure 3.20: Simulation results of actual vehicle speed of 120 km/h in presence of two-term mixture Gaussian noise

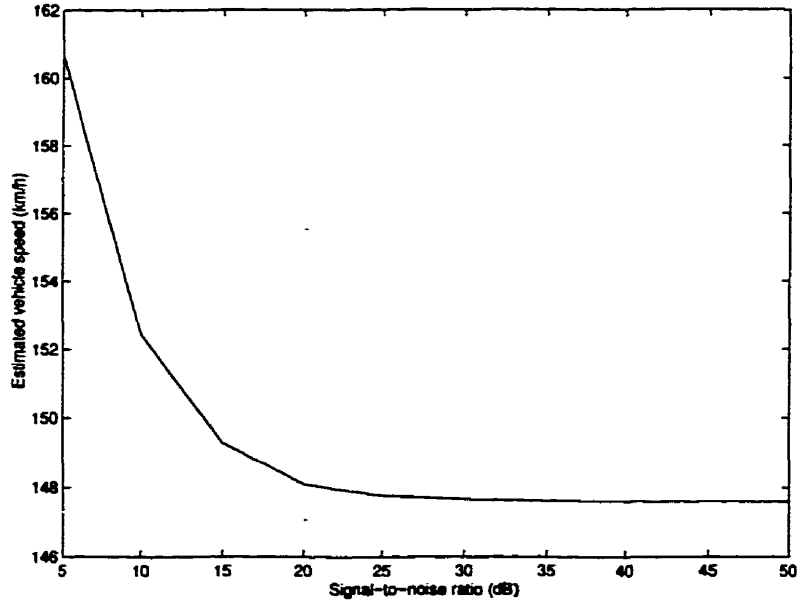

Figure 3.21: Simulation results of actual vehicle speed of 150 km/h in presence of two-term mixture Gaussian noise

Chapter 4

Autocorrelation Function Estimator

We have described the level crossing rate (LCR) method of mobile velocity estimation and shown implemention and simulation results in the previous chapter. From that chapter, we noted that there is a drawback in using the LCR estimator. When the mobile speed is large, it will be underestimated if the sampling rate of the continuous-time received signal is relatively small. That is, the sampling rate must be either larger or cannot be fixed when we are using LCR estimation. In this chapter, we propose a new type of estimator using the autocorrelation function of discrete-time received fading signal with a fixed sampling rate of the continuous-time received signal, which is denoted as autocorrelation function (ACF) estimator for mobile velocity.

In Section 4.1, we describe the algorithm for the new ACF estimator, and we will show implementation and simulation results in Section 4.2.

4.1 ACF Estimator Algorithm

As we have described in Section 3.1.2, the autocorrelation function (ACF) of the in-phase and quadrature components of the discrete-time fading signal is a function of the maximum Doppler frequency, which is proportional to the mobile velocity. Therefore, the ACF is a function of the mobile velocity. From Equations (3.13) and (3.57) or (3.58), we find that the relationship between the ACF of the in-phase or quadrature components of the fading signal and the mobile velocity is much simpler than the relationship between the LCR and the mobile velocity. It is therefore much easier to derive a mobile velocity estimator using the relationship between the ACF

of the in-phase or quadrature components of the fading signal and mobile velocity. We will derive the algorithm without assuming additive noise first, then later present an algorithm suitable in the presence of noise.

4.1.1 ACF Estimator without Noise

From Section 3.1.2, for Rayleigh distributed channels, the autocorrelation function of quadrature components of fading signal is a product of the average envelope power and a Bessel function, of which the maximum Doppler frequency f_m is the variable. That is,

$$\phi_{II}(m) = \sigma^2 J_0(2\pi f_m m) \tag{4.1}$$

where σ^2 is the variance of the quadrature components of the fading signal. $J_0(\cdot)$ is the zero-order Bessel function of the first kind.

Letting m in Equation (4.1) equal 0 and 1, respectively, we obtain

$$\begin{cases} \phi_{II}(0) = \sigma^2 \\ \phi_{II}(1) = \sigma^2 J_0(2\pi f_m) \end{cases} \tag{4.2}$$

Then the ratio $\phi_{II}(1)/\phi_{II}(0)$ can be used to solve for f_m,

$$f_m = \frac{1}{2\pi} J_0^{-1}\left(\frac{\phi_{II}(1)}{\phi_{II}(0)}\right) \tag{4.3}$$

where $J_0^{-1}(\cdot)$ is the inverse function of the zero-order Bessel function of the first kind.

We use the following maximum-likelihood estimators (MLE's) of $\phi_{II}(1)$ and $\phi_{II}(0)$ over N samples for the case of unstructured covariance matrices [25],

$$\begin{aligned} \hat{\phi}_{II}(0) &= \frac{1}{N}\sum_{k=1}^{N} x_I(k)^2 \\ \hat{\phi}_{II}(1) &= \frac{1}{N-1}\sum_{k=1}^{N} x_I(k)x_I(k+1) \end{aligned} \tag{4.4}$$

where $x_I(k)$ is the quadrature component of the received fading signal. Substituting Equation (4.4) into Equation (4.3), we can obtain the estimate of Doppler frequency $\hat{f}_m$. Using invariance [25], we note that $\hat{f}_m$ is also a MLE of the Doppler frequency f_m.

As we know, the maximum Doppler frequency f_m is appropriate to the moblie velocity v we are estimating, it is, therefore, straightforward to obtain the mobile velocity using the relationship formula between these two quantities. Using Equation (3.59), the estimated mobile velocity is derived as

$$\hat{v} = \frac{cF_s}{2\pi F_c} J_0^{-1}\left(\frac{\hat{\phi}_{II}(1)}{\hat{\phi}_{II}(0)}\right) \tag{4.5}$$

4.1.2 ACF Estimator with Noise

In the previous section, we have derived the ideal ACF estimator for mobile velocity in the absence of noise. In fact, the received fading signal is always corrupted by noise in practical mobile communication systems. It is, therefore, necessary to derive an ACF estimator using the received fading signal corrupted by noise.

Being corrupted by noise, the quadrature components of the received fading signal, $y_I(k)$ can be written as

$$y_I(k) = x_I(k) + n_I(k) \tag{4.6}$$

where $n_I(k)$ is the quadrature component of noise. Therefore, the autocorrelation function of the quadrature components of the received signal becomes (see Section 3.1.4)

$$\phi_{II}(m) = \sigma^2 J_0(2\pi f_m m) + \frac{1}{2} N_0 \frac{\sin \pi B_n m T_s}{\pi m T_s} \tag{4.7}$$

for band-limited white Gaussian noise, where N_0 is the power of the noise, B_n is the bandwidth of the noise, T_s is the sampling period.

If the sampling period T_s is small, the second term of Equation (4.7) can be simplified as 0 and $1/2(N_0 B_n)$, when m equals 0 and 1, respectively. Thus, $\phi_{II}(0)$ and $\phi_{II}(1)$ become

$$\begin{aligned} \phi_{II}(0) &= \sigma^2 \\ \phi_{II}(1) &= \sigma^2 J_0(2\pi f_m) + \frac{1}{2}\sigma_n^2 \end{aligned} \tag{4.8}$$

where $\sigma_n^2 = N_0 B_n$. Therefore, Equation (4.3) becomes

$$f_m = \frac{1}{2\pi} J_0^{-1}\left(\frac{\phi_{II}(1)}{\phi_{II}(0)} - \frac{1}{\gamma_s}\right) \tag{4.9}$$

where

$$\gamma_s = \frac{2\sigma^2}{\sigma_n^2} \tag{4.10}$$

is the signal-to-noise ratio (SNR).

If the recevied fading signal is corrupted by two-term mixture Gaussian noise, the autocorrelation function of quadrature components of fading signal is written as (see Section 3.1.4)

$$\begin{aligned} \phi_{II}(m) &= \sigma^2 J_0(2\pi f_m m) + \frac{1}{2}[(1-\epsilon)\nu^2 + \epsilon\kappa\nu^2]\frac{\sin \pi B_n m T_s}{\pi m T_s} \\ &= \sigma^2 J_0(2\pi f_m m) + \frac{1}{2}N_0'\frac{\sin \pi B_n m T_s}{\pi m T_s} \end{aligned} \tag{4.11}$$

where $N_0' = (1-\epsilon)\nu^2 + \epsilon\kappa\nu^2$.

Similarly, when the sampling period is small and letting m equal 0 and 1, we can obtain

$$\begin{aligned} \phi_{II}(0) &= \sigma^2 \\ \phi_{II}(1) &= \sigma^2 J_0(2\pi f_m) + \frac{1}{2}{\sigma_n'}^2 \end{aligned} \tag{4.12}$$

where ${\sigma_n'}^2 = N_0' B_n$. Solve for the maximum Doppler frequency using the ratio of $\phi_{II}(1)/\phi_{II}(0)$,

$$f_m = \frac{1}{2\pi} J_0^{-1}\left(\frac{\phi_{II}(1)}{\phi_{II}(0)} - \frac{1}{\gamma_s'}\right) \tag{4.13}$$

where

$$\gamma_s' = \frac{2\sigma^2}{{\sigma_n'}^2} \tag{4.14}$$

is the signal-to-noise ratio (SNR).

Given the signal-to-noise ratio and using Equation (4.4), where $x_I(k)$ is replaced by $y_I(k)$, we can obtain the MLE of f_m. Then we can solve for the mobile velocity estimate $\hat{v}$

$$\hat{v} = \frac{cF_s}{2\pi F_c} J_0^{-1}\left(\frac{\hat{\phi}_{II}(1)}{\hat{\phi}_{II}(0)} - \frac{1}{\gamma_s}\right) \tag{4.15}$$

where γ_s is either the SNR in Equation (4.10) or in Equation (4.14).

Compared to the ACF method in this chapter, the covariance approximation (COV) method [33] described in Section 2.3.2 uses the squared-envelope of the received fading signal rather than the in-phase or quadrature components. Furthermore,

the COV method assumes that the covariance $\mu_{rr}(0)$ is known exactly for eliminating the bias with respect to K. However, since $\mu_{rr}(0)$ is always unknown, it must be estimated. Therefore, the estimation erorr of $\mu_{rr}(0)$ will introduce more bias to the mobile velocity estimates.

4.2 Implemention and Simulation Results

We have described the algorithms of the ACF estimators for mobile velocity in the previous section. We will deal with implementation and simulation issues for the ACF estimators in this section.

4.2.1 Implementation Procedures

The implementation procedure of the ACF estimator is slightly different from that of the LCR estimator. We deal with the in-phase component of the received fading signal instead of the envelope of the signal. Figure 4.1 shows the implementation procedure of the mobile velocity using the received fading signal with the presence of noise, where the noise could be additive white Gaussian noise or two-term mixture Gaussian noise described earlier. As described in Chapter 3, we need to know how the bandwidth of the bandpass filter is specified; how to choose the sampling rate F_s; and how many signal samples should be performed to obtain the mobile speed.

Bandpass Filter Bandwidth B_n

Assuming that we pass the in-phase or quadrature component of the received signal

$$r(k) = r_I(k) + n_I(k) \tag{4.16}$$

through a lowpass filter with an impulse response $h(k)$ and bandwidth $B_n/2$, we obtain the output $z(k)$. In Equation (4.16), $r_I(k)$ denotes the in-phase or quadrature component of the fading signal and $n_I(k)$ is the in-phase or quadrature component of the additive noise. The variance of $z(k)$ is given by

$$\phi_{zz}(0) = \int_{-B_n/2}^{B_n/2} S_{rr}(f)|H(f)|^2 df \tag{4.17}$$

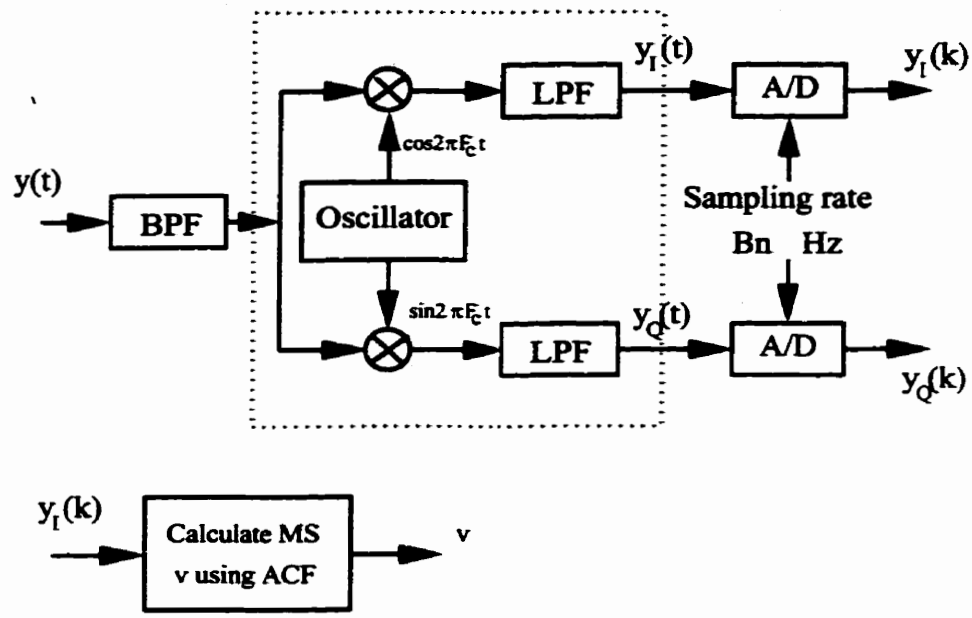

Figure 4.1: Implementation procedure for ACF estimator for mobile velocity

where $S_{rr}(f)$ is the power spectral density of $r(k)$, and $H(f)$ represents the frequency response of the filter. It can be shown that if $H(f)$ is an ideal lowpass filter, the variance of $z(k)$ becomes

$$\phi_{zz}(0) = \begin{cases} \phi_{r_I r_I}(0) + \frac{1}{2} N_0 B_n, & B_n/2 > F_m \\ \phi_{r_I r_I}(0) - 2\int_{B_n/2}^{F_m} S_{rr}(f)df + \frac{1}{2} N_0 B_n, & B_n/2 < F_m \end{cases} \tag{4.18}$$

where N_0 is the variance of noise.

We obtain the correlation of two adjacent output samples

$$\phi_{zz}(1) = \int_{-B_n/2}^{B_n/2} [N_0 + S_{rr}(f)] \, |H(f)|^2 \cos 2\pi f df \tag{4.19}$$

Again, if $H(f)$ is an ideal lowpass filter, we get

$$\phi_{zz}(1) \simeq \begin{cases} \phi_{r_I r_I}(1), & B_n/2 > F_m \\ \phi_{r_I r_I}(1) - 2\int_{B_n/2}^{F_m} S_{rr}(f)df, & B_n/2 < F_m \end{cases} \tag{4.20}$$

using the approximation

$$\int_{-B_n/2}^{B_n/2} N_0 \cos 2\pi f df \simeq 0 \tag{4.21}$$

From Equations (4.18) and (4.20), we can conclude that we require $B_n/2$ to be larger than F_m for accurate estimation of $\phi_{r_I r_I}(1)$. But we also need $B_n/2$ to be as close

to F_m as possible for accurate estimation of $\phi_{r_I r_I}(0)$. This justifies our choice of $B_n \simeq 2F_m$ as the bandwidth of the bandpass filter.

As in Section 3.3.1, the maximum Doppler frequency F_m depends on the carrier frequency F_c and mobile velocity v. However, the carrier frequency is usually fixed for a practical mobile communication system, the maximum Doppler frequency is mainly affected by the mobile velocity v. Therefore, as long as the bandwidth of the bandpass filter is set to be at least $2F_m$, useful information will not be eliminated by the bandpass filter.

Sampling Rate F_s

From Section 3.3.1, if the sampling rate F_s is set to be at least $2B_n$, which in turn is larger than $4F_m$. This makes the discrete-time maximum Doppler frequency f_m is always less than 0.25 and guarantees the mobile velocity and LCR are one-to-one mapped. This is also true for the ACF estimation. When we limit f_m to be less than 0.25, the autocorrelation function of the received fading signal uniquely corresponds to the mobile velocity.

Number of Samples N

In order to obtain an accurate estimate of the actual f_m, it is necessary to process a sufficient number of signal samples. This can be accomplished by determining the confidence interval for the f_m. By specifying the desired width of interval, the necessary number of samples can be calculated using Equation (3.62).

Implementation Summary

The algorithm for estimation of mobile velocity using ACF method is summarized as below,

- Design a bandpass filter with bandwidth B_n, for example, the Butterworth filter described in Section 3.3.1,
- Bandpass-filter the received fading signal through the bandpass filter,
- Convert the bandpass received signal into its lowpass equivalent signal,

- Sample the lowpass equivalent signal at the sampling rate of F_s samples per second,
- Obtain the MLE's of $\phi_{II}(0)$ and $\phi_{II}(1)$ from N given samples,
- Calculate the desired mobile velocity from the obtained $\hat{\phi}_{II}(0)$ and $\hat{\phi}_{II}(0)$ and Equations (4.5), or Equation (4.15) if we have known the SNR.

4.2.2 Simulation Results

In the previous section, we have introduced the algorithm and implementation precedure of ACF mobile velocity estimator, we will study the detailed simulation procedure and results in this section.

The simulation procedure is slightly different from the implementation procedure shown in Figure 4.1, because we do not have the actual fading signal. The simulation precedure is shown in Figure 4.2, where $x_I(k)$ and $n_I(k)$ are generated in-phase component of fading signal and noise. Here we use Young and Beaulieu's fading signal generator described in Section 2.4.3 to produce a fading signal, whose autocorrelation function matches the autocorrelation function of the actual fading signal very well [43]. Because the output of the generator is already discrete-time, we do not have to implement the sampling procedure.

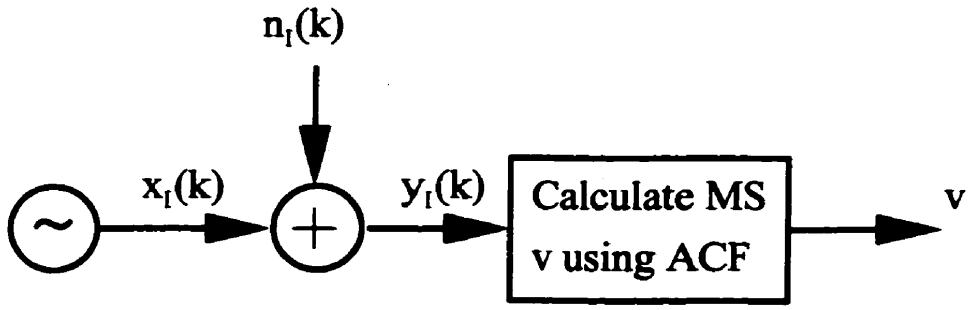

Figure 4.2: Simulation procedure for ACF estimator for mobile velocity

Before doing the simulation, we discuss the specification of the parameters. It is reasonable to assume that the maximum expected velocity v_{max} being 200 km/h if the mobile stations are automobiles. Assuming that the carrier frequency is 2 GHz,

we can obtain the bandwidth of the bandpass filter B_n, the sampling rate F_s, which are shown in Table 3.3. We should also set the total number of samples processed to obtain an accurate estimate of vehicle speed. Assuming that the minimum expected vehicle speed of 10 km/h, the digital maximum Doppler frequency f_m is 0.01158. Using Equation (3.62) and setting the confidence interval to be 10% of estimated f_m, we can calculate the total number of samples processed N is 2.33×10^4. The parameters calculated are shown in Table 4.1.

F_c	B_n	F_s	N
2 GHz	800 Hz	1600 Hz	2.33×10^4

Table 4.1: Parameters of ACF estimator

We will study the simulation results without noise, with additive white Gaussian noise and with two-term mixture Gaussian noise. Since the fading signal and noise are generated by computer, Monte-Carlo trials are used to smooth the fluctuation. The simulation procedure is summarized as below,

- Generate in-phase component of fading signal using Young and Beaulieu's generator according to a specific vehicle speed,
- Generate in-phase component of bandlimited noise with bandwidth B_n according to a SNR value and add it onto the generated fading signal to create the in-phase component of received signal at the mobile station
- Calculate the MLE's of $\phi_{II}(0)$ and $\phi_{II}(1)$ over N samples, and
- Calculate estimated vehicle speed using Equation (4.5),
- Repeat above steps until the total number of Monte-Carlo trials is reached and calculate the average vehicle speeds obtained from the trials.

Simulation Results in the absence of noise

Following the simulation precedure depicted in Figure 4.2, except for the generation of noise, and using parameters in Table 4.1, we obtain the simulation results in the

absence of noise, which are shown in Table 4.2 and Figure 4.3. From the figure and

v km/h	10	20	30	40	50
$\hat{v}$ km/h	10.03	19.89	29.84	39.83	49.82
v km/h	60	70	80	90	100
$\hat{v}$ km/h	59.60	69.46	79.29	88.64	98.41
v km/h	110	120	130	140	150
$\hat{v}$ km/h	107.82	117.19	126.44	135.35	144.31
v km/h	160	170	180	190	200
$\hat{v}$ km/h	153.53	162.27	170.48	178.58	187.18

Table 4.2: ACF estimation results without noise

the table, we can find that the estimated vehicle speeds match the acutal ones very well. All errors introduced are less than 10%. This implies that the correctness of the ACF estimator is justified. Also, the use of a fixed sampling rate simplifies the implementation of the ACF estimator of the mobile speed.

Simulation Results in the presence of AWGN

We have illustrated the simulation results of ACF estimator in the absence of noise and found that the estimates of the mobile velocity are close to the actual values. Now we will deal with issues of simulation in the presence of AWGN. Following the simulation procedure depicted in Figure 4.2 and using the parameters in Table 4.1, and letting the signal-to-noise ratio range from 5 to 50 dB, we obtain the simulation results shown in Figures 4.4 to 4.9, and estimated vehicle speed variances shown in Figure 4.10 to 4.15, where circle-lines represent ACF estimates and star-lines represent LCR estimates. The sampling rates for both methods are 1600 Hz for the case of the mobile speeds are less than 100 km/h, and 3200 Hz for the case of the mobile speeds are larger than 100 km/h.

These figures show that ACF estimates of the mobile speeds obtained from the noisy signal are close to actual values for various SNR's. Then, we can justify the

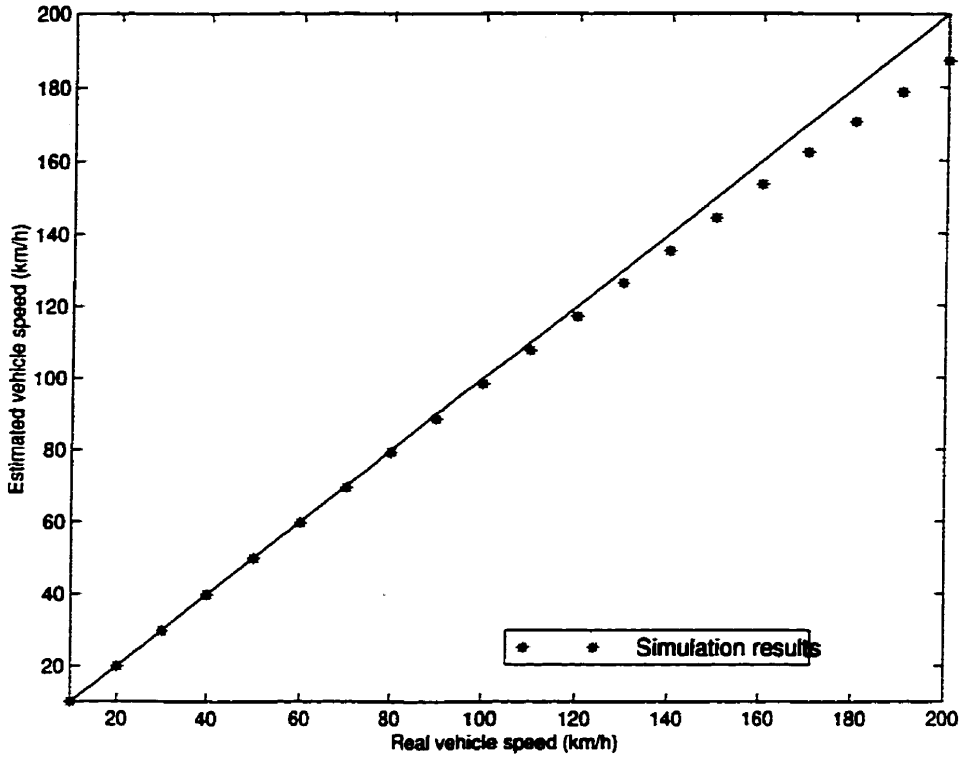

Figure 4.3: ACF estimation results without noise

correctness of ACF estimator in the presence of AWGN. From these figures, especially from the variance figures, we also find that ACF estimates are more accurate than LCR estimates in low SNR conditions. However, when the actual mobile speeds and the SNR are large, LCR estimates are very close to ACF estimates.

Simulation Results in the presence of Impulsive Noise

For a practical mobile communication system, as described in Section 3.1.4, the received fading signal is often corrupted by impulsive noise. Therefore, it is necessary to simulate the ACF estimator in the presence of impulsive noise. Here we use two-term mixture Gaussian noise to represent it. Following the simulation procedure depicted in Figure 4.2 and using the parameters in Table 4.1, and letting the signal-to-noise ratio range from 5 to 50 dB, $\epsilon = 0.01$, and $\kappa = 100$, we obtain the simulation results shown in Figures 4.16 to 4.21, and the estimated vehicle speed variances shown in

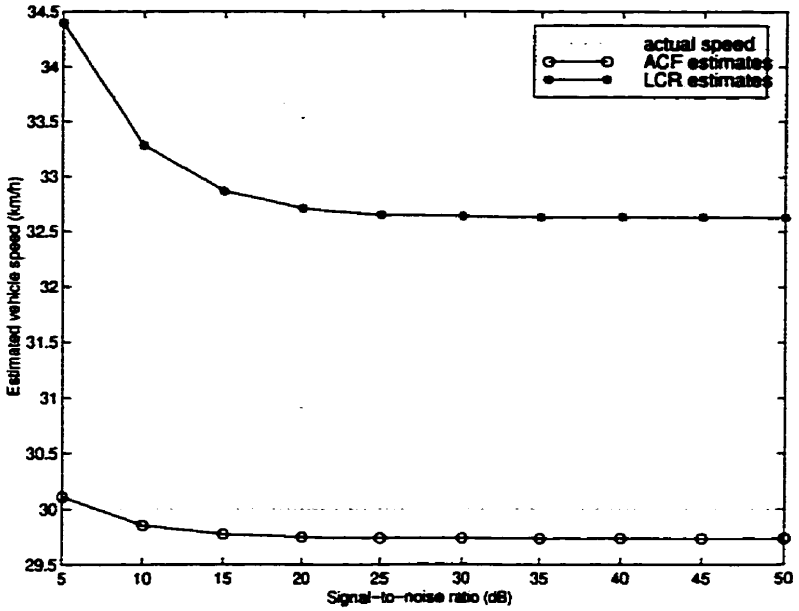

Figure 4.4: Simulation results of actual vehicle speed of 30 km/h in presence of additive Gaussian noise

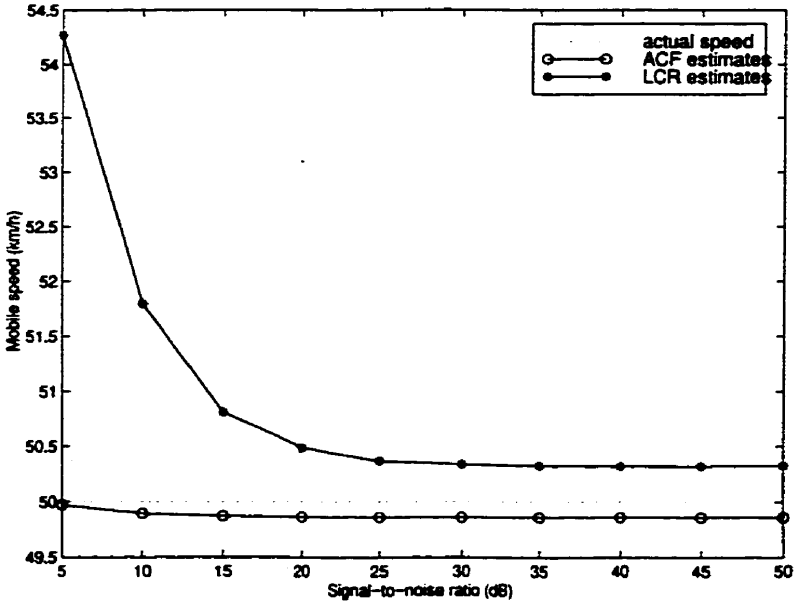

Figure 4.5: Simulation results of actual vehicle speed of 50 km/h in presence of additive Gaussian noise

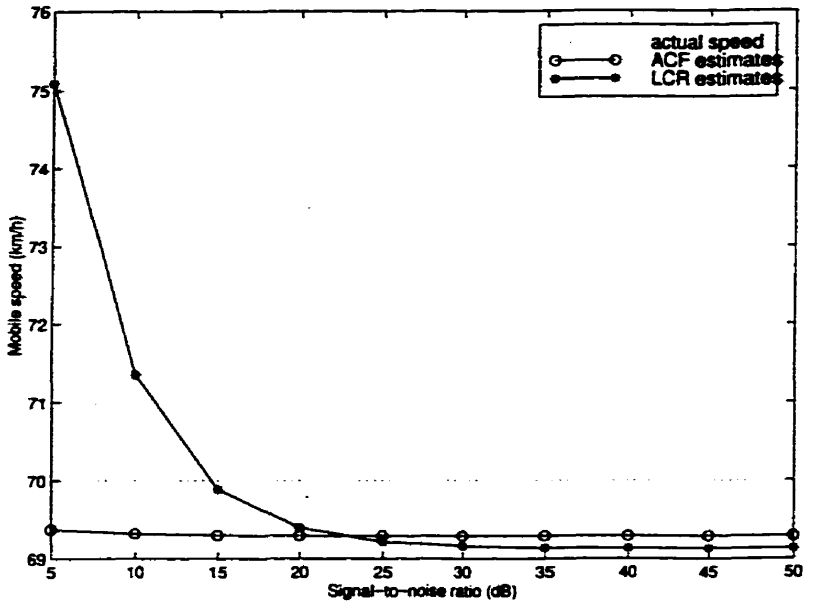

Figure 4.6: Simulation results of actual vehicle speed of 70 km/h in presence of additive Gaussian noise

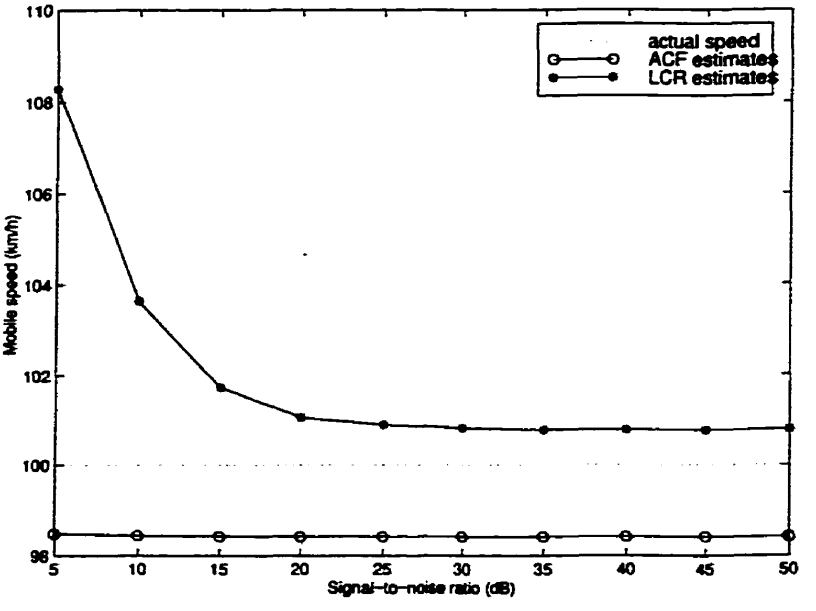

Figure 4.7: Simulation results of actual vehicle speed of 100 km/h in presence of additive Gaussian noise

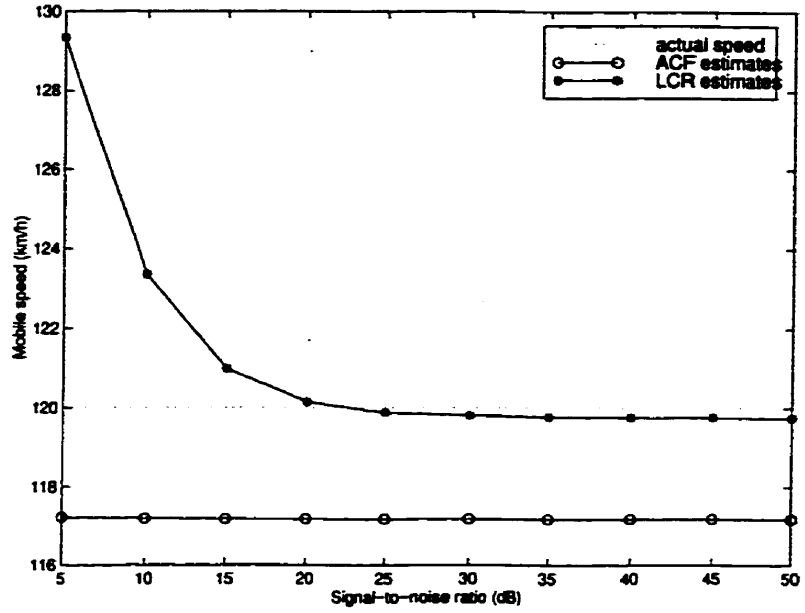

Figure 4.8: Simulation results of actual vehicle speed of 120 km/h in presence of additive Gaussian noise

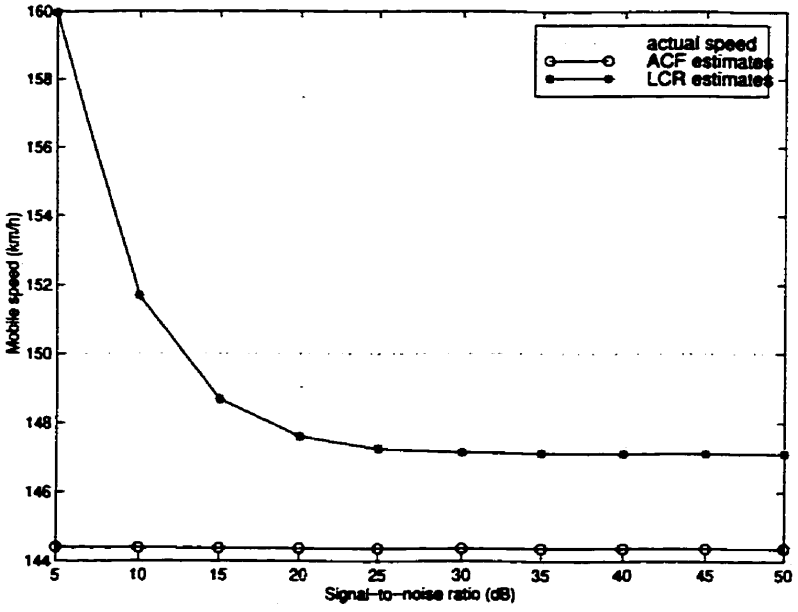

Figure 4.9: Simulation results of actual vehicle speed of 150 km/h in presence of additive Gaussian noise

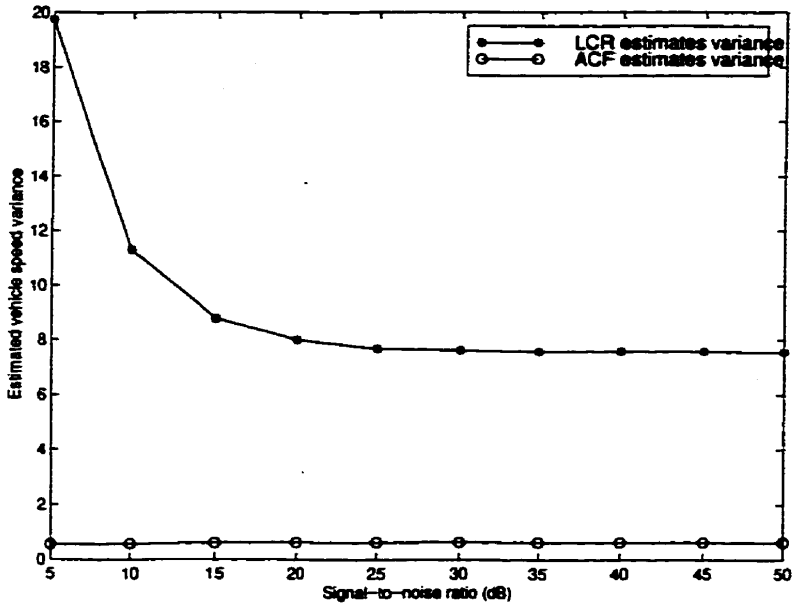

Figure 4.10: Simulation results of actual vehicle speed of 30 km/h in presence of additive Gaussian noise, estimated vehicle speed variance

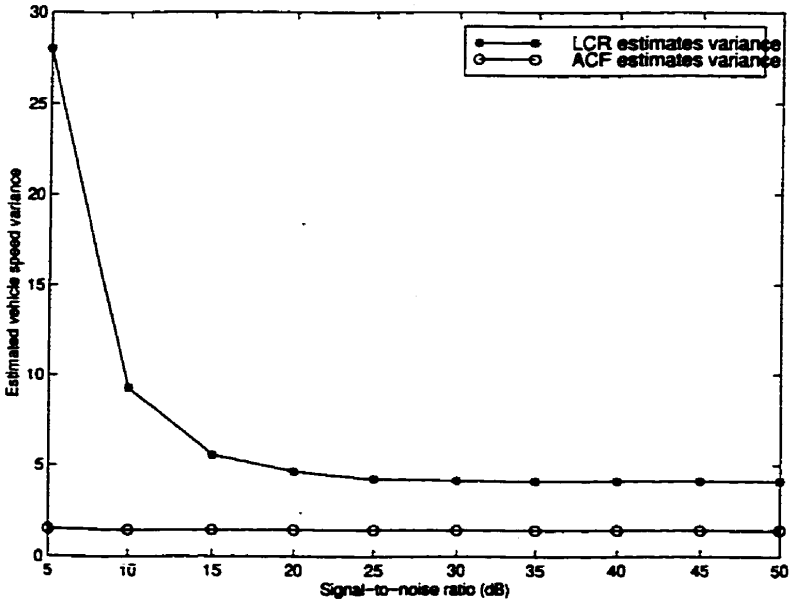

Figure 4.11: Simulation results of actual vehicle speed of 50 km/h in presence of additive Gaussian noise, estimated vehicle speed variance

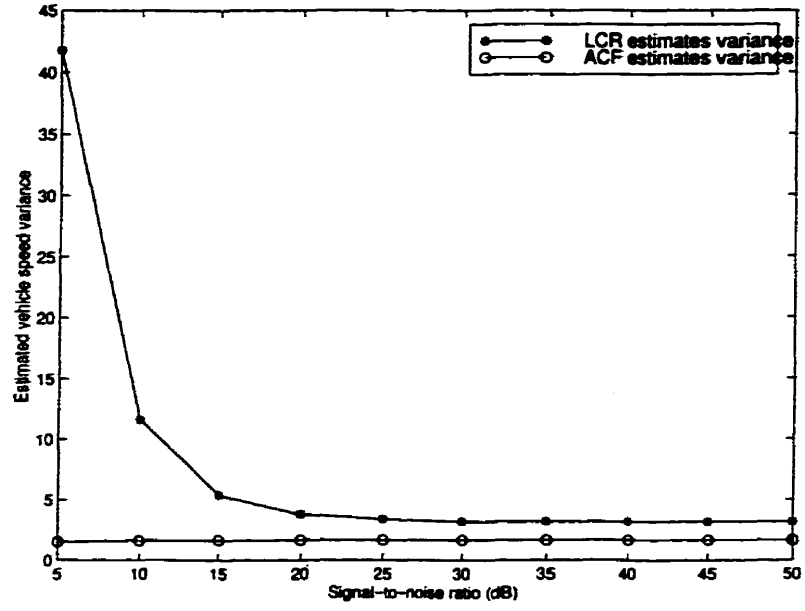

Figure 4.12: Simulation results of actual vehicle speed of 70 km/h in presence of additive Gaussian noise, estimated vehicle speed variance

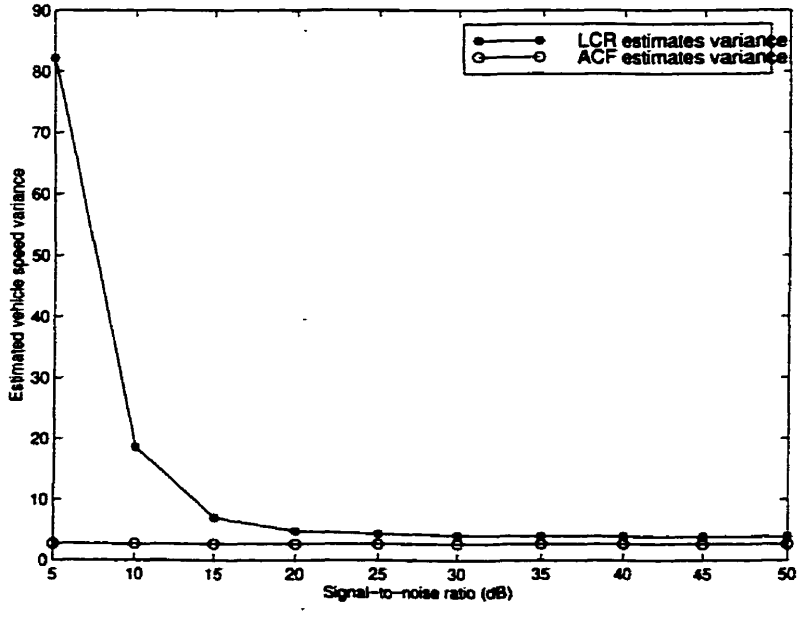

Figure 4.13: Simulation results of actual vehicle speed of 100 km/h in presence of additive Gaussian noise, estimated vehicle speed variance

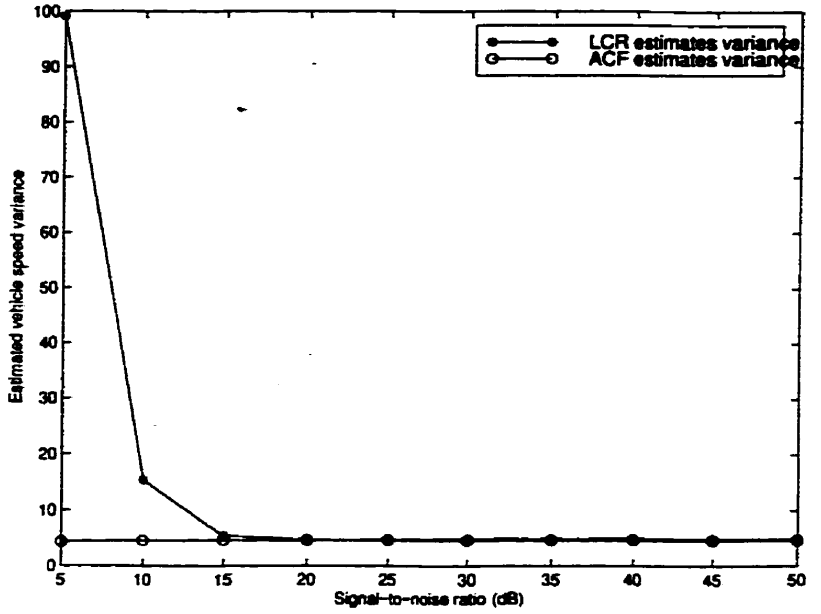

Figure 4.14: Simulation results of actual vehicle speed of 120 km/h in presence of additive Gaussian noise, estimated vehicle speed variance

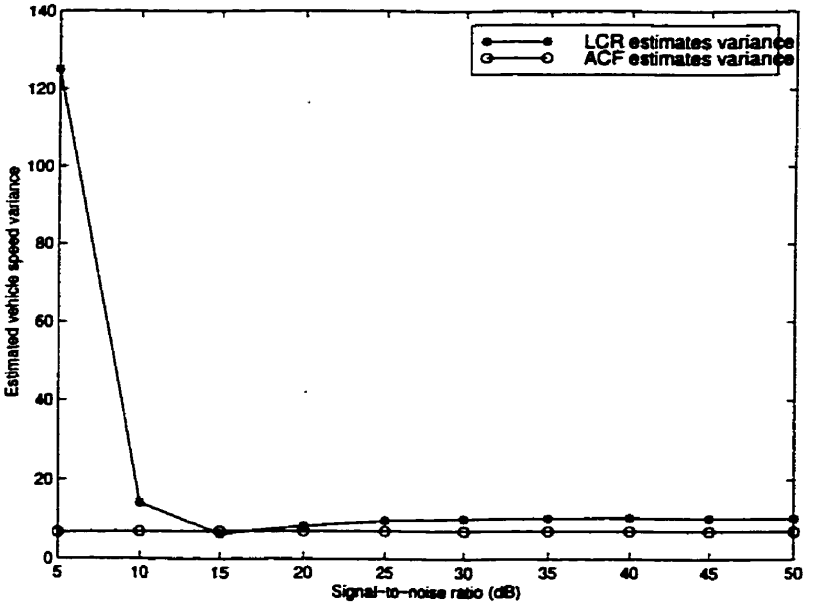

Figure 4.15: Simulation results of actual vehicle speed of 150 km/h in presence of additive Gaussian noise, estimated vehicle speed variance

Figures 4.22 to 4.27, where circle-lines represent ACF estimates and star-lines represent LCR estimates. The sampling rates for both methods are 1600 Hz for the case of the mobile speeds are less than 100 km/h, and 3200 Hz for the case of the mobile speeds are larger than 100 km/h.

These figures show that ACF estimates of mobile speeds obtained from the signal corrupted by two-term mixture Gaussian noise are close to the actual speeds for various SNR's. Correctness of ACF estimator in the presence of two-term mixture Gaussian noise is then justified. Compared to the LCR estimates, the ACF estimator has much better performance in low SNR. However, when the mobile speeds and SNR are large, LCR estimates are close to ACF estimates.

4.3 Summary

In Section 4.1, we described the algorithm of ACF method of mobile velocity. We also showed implementation procedure and simulation results of the ACF estimator in Section 4.2. From the simulation results, we learned that ACF estimates are accurate. Compared to the LCR mobile velocity estimator, the ACF estimator uses a single sampling rate of the continuous-time received signal for different mobile speeds, which simplifies the implementation of the mobile velocity estimation. Furthermore, ACF estimates of mobile speeds are more accurate than LCR estimates in low SNR conditions.

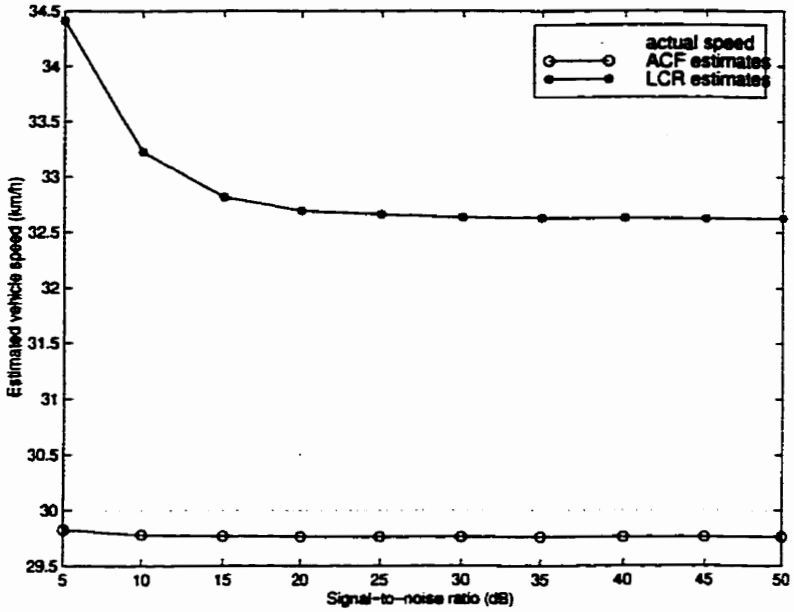

Figure 4.16: Simulation results of actual vehicle speed of 30 km/h in presence of two-term mixture Gaussian noise

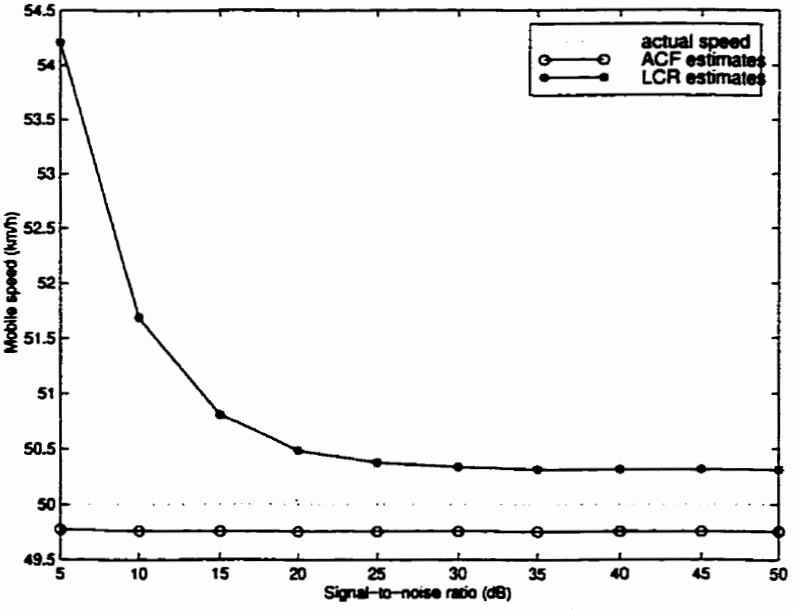

Figure 4.17: Simulation results of actual vehicle speed of 50 km/h in presence of two-term mixture Gaussian noise

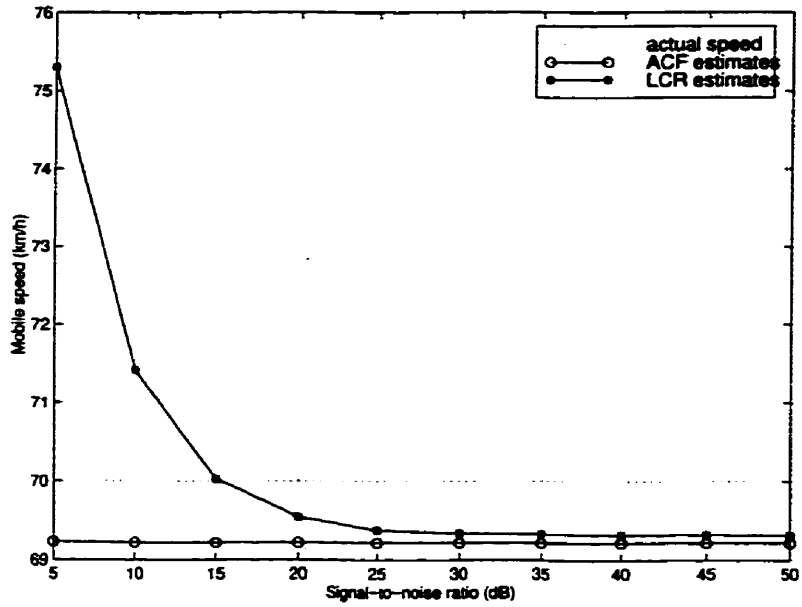

Figure 4.18: Simulation results of actual vehicle speed of 70 km/h in presence of two-term mixture Gaussian noise

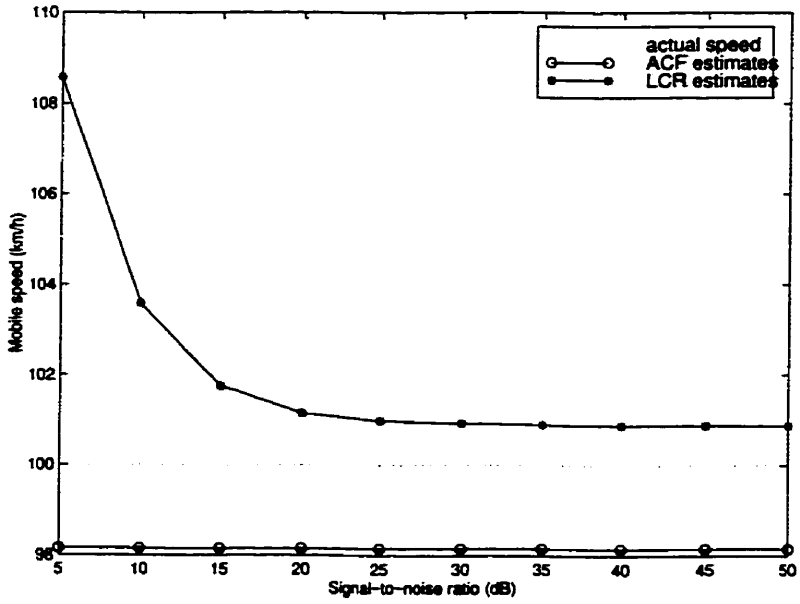

Figure 4.19: Simulation results of actual vehicle speed of 100 km/h in presence of two-term mixture Gaussian noise

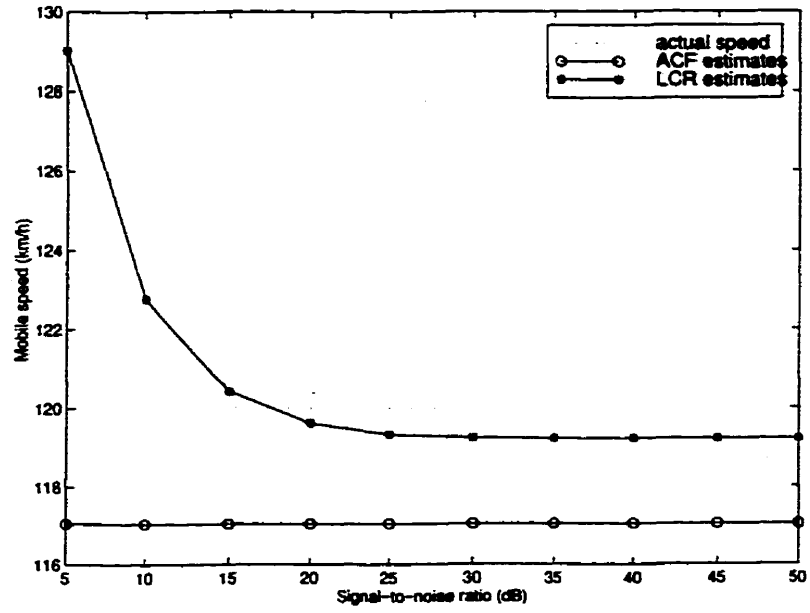

Figure 4.20: Simulation results of actual vehicle speed of 120 km/h in presence of two-term mixture Gaussian noise

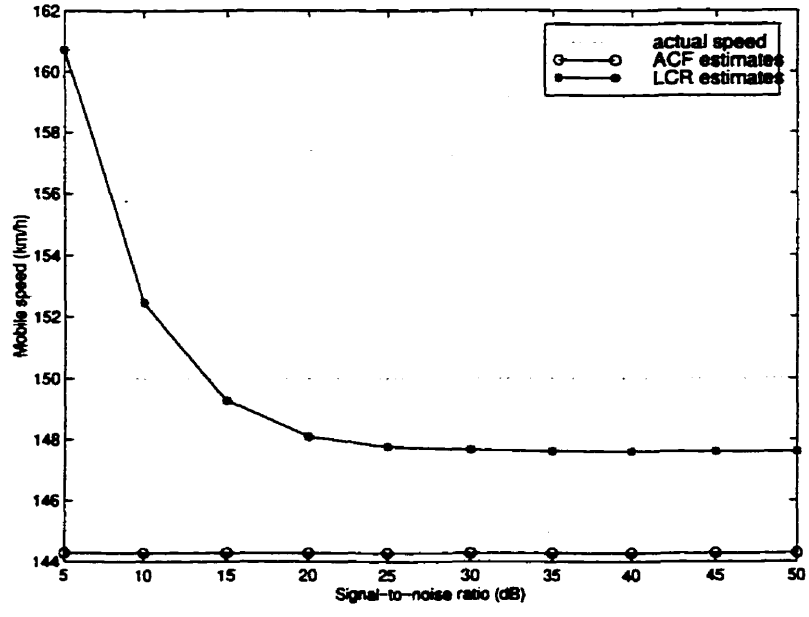

Figure 4.21: Simulation results of actual vehicle speed of 150 km/h in presence of two-term mixture Gaussian noise

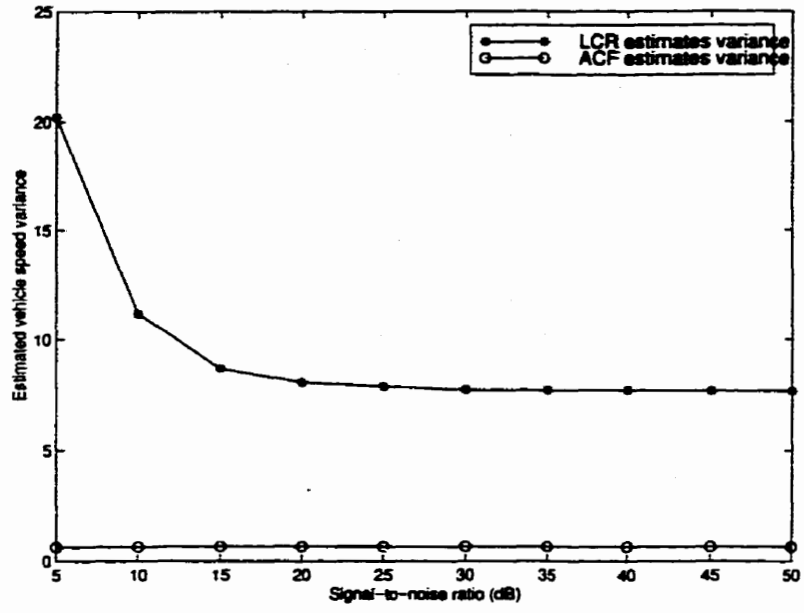

Figure 4.22: Simulation results of actual vehicle speed of 30 km/h in presence of two-term mixture Gaussian noise, estimated vehicle speed variance

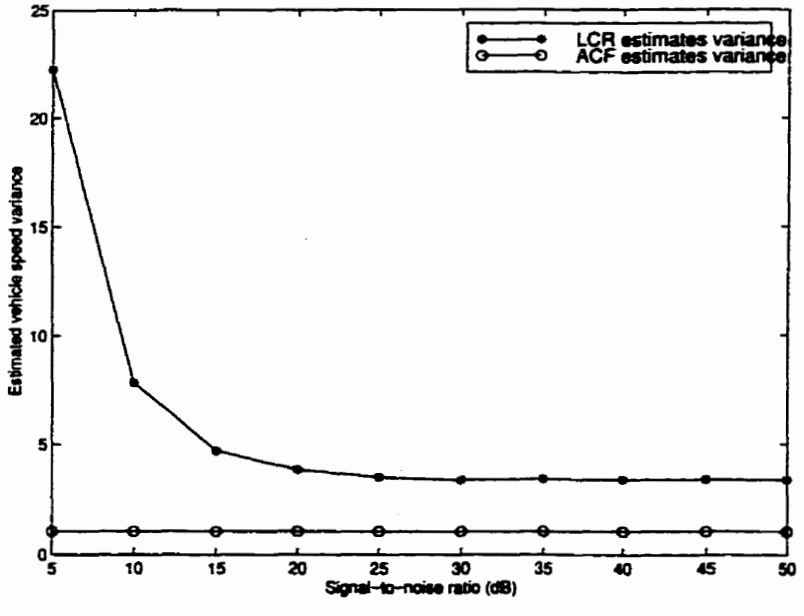

Figure 4.23: Simulation results of actual vehicle speed of 50 km/h in presence of two-term mixture Gaussian noise, estimated vehicle speed variance

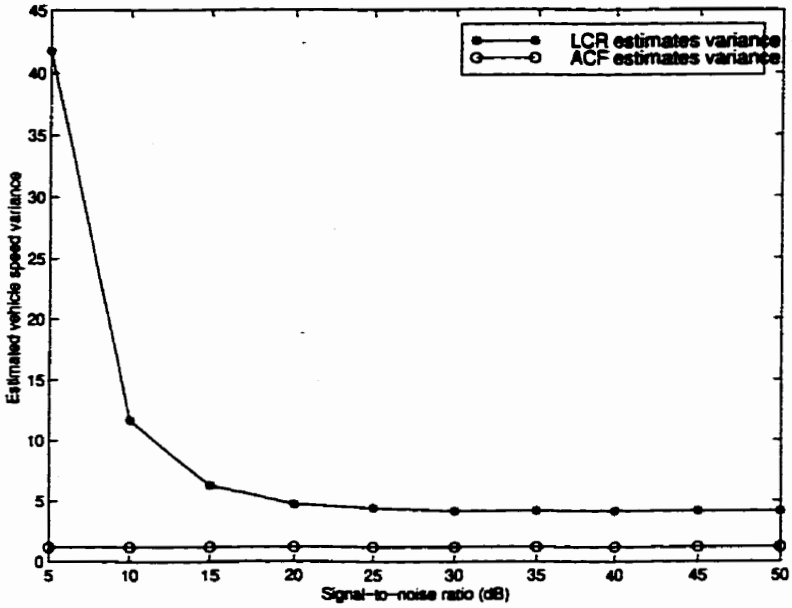

Figure 4.24: Simulation results of actual vehicle speed of 70 km/h in presence of two-term mixture Gaussian noise, estimated vehicle speed variance

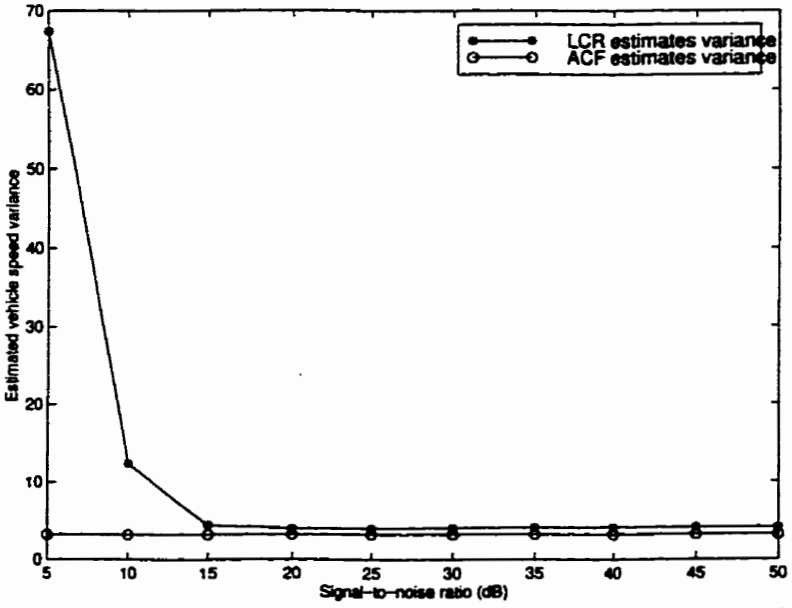

Figure 4.25: Simulation results of actual vehicle speed of 100 km/h in presence of two-term mixture Gaussian noise, estimated vehicle speed variance

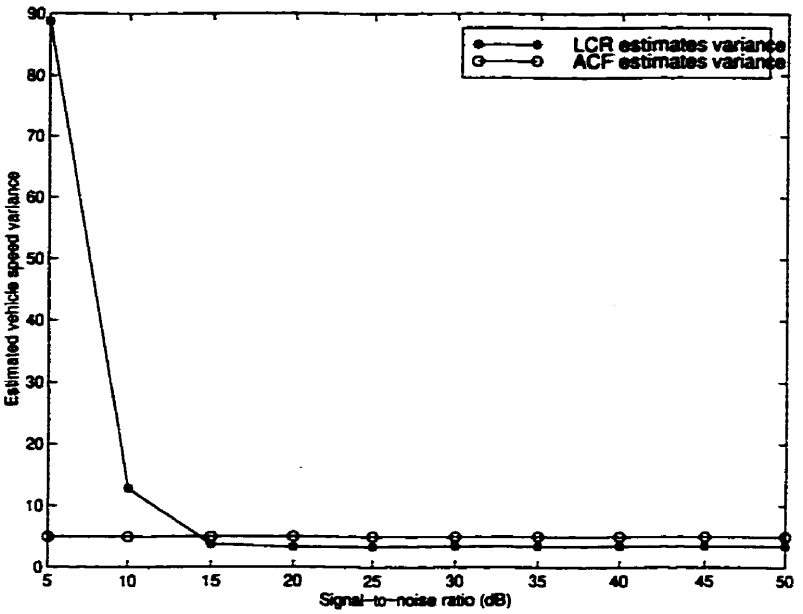

Figure 4.26: Simulation results of actual vehicle speed of 120 km/h in presence of two-term mixture Gaussian noise, estimated vehicle speed variance

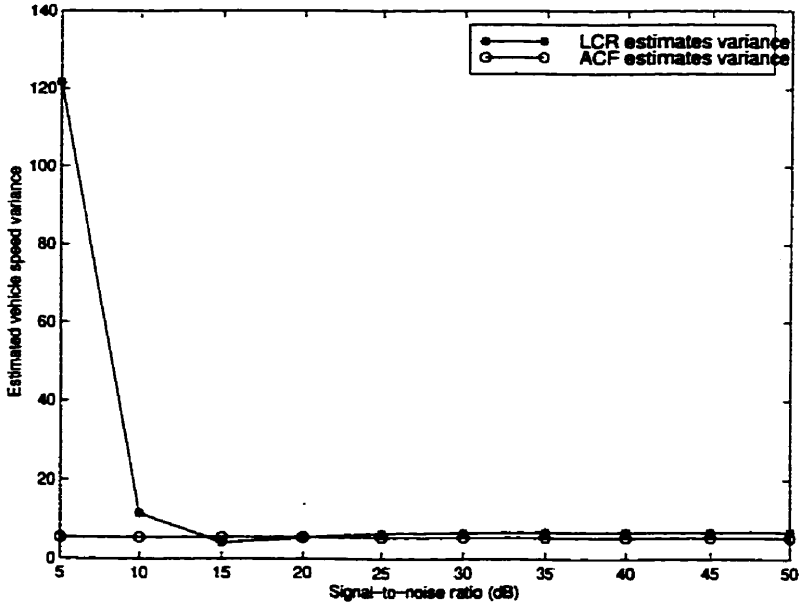

Figure 4.27: Simulation results of actual vehicle speed of 150 km/h in presence of two-term mixture Gaussian noise, estimated vehicle speed variance

Chapter 5

Application to Mobile Location Tracking

5.1 Introduction to Mobile Geolocation

Emergency services for cellular phone users have drawn significant attention over the past few years. In 1996, in order to achieve adequate provision of emergency services, the Federal Communications Commission (FCC) in the U.S. announced its mandate for enhanced emergency services (E-911) for cellular phone users. The wireless services providers, including cellular, personal communications services (PCS) and special mobile radio (SMR), are required to provide latitude and longitude estimates of the 911 caller's position within an accuracy of 125 m RMS in 67 percent of all measurement by October, 2001[13]. Recently, to conform the FCC requirement being concerned primarily with the ability to locate mobile telephones originating emergency phone calls is the main goal for implementing position location.

Geolocation systems may be loosely separated into unilateral systems and multiteral systems [30]. In a unilateral system, a mobile unit estimates its own position based on received signal from transmitters at known locations. The Global Positioning System (GPS) is the classic example of unilateral system. In a multilateral system, an estimate of the mobile location is based on a signal transmitted by the mobile and received at multiple fixed base stations. Most cellular geolocation systems are multilateral, where the estimate of the mobile's position is made by the network, rather than by the mobile itself. In this section, we review some basic mobile positioning technologies that are available for accurate position location in recent years.

5.1.1 Global Positioning Systems

A GPS receiver makes the appropriate signal measurements from signals transmitted from a network of 24 satellites and uses these measurements to determine its position [11, 15, 18, 21]. These satellites with precise timing transmit L-band signals (centered at 1575.42 MHz) to earth. The receiver measures the time delay between the signals leaving the satellites and arriving at the receiver with a built-in clock. The exact distance from the receiver to each satellite is then calculated. A sphere about each satellite can be described by the calculated distance from each satellite to the receiver. If three satellites are visible to the receiver, the receiver's position lies at the intersection of these three spheres, providing coordinates in latitude, longitude, and altitude. In practice, signals from the fourth satellite are used to correct receiver clock errors, due to the lower-accuracy built-in clock of the receiver.

Commercial GPS receivers that are available now accurately determine position to within approximately 50 m [18]. However, wireless services providers are not intending to use GPS as their principal geolocation technology. This may be due to cost, size, complexity, and power consumption associated with integrating a GPS receiver into a handset and to the susceptibility to radio frequency interference. Furthermore, the reliability of GPS measurements is greatly reduced in urban environments, when one or more satellites are obscured by buildings, or when the mobile antenna is located inside a vehicle.

5.1.2 Cellular Geolocation Systems

Cellular geolocation relies on the existing infrastructure of cellular base stations. It has some advantages over GPS since it does not need the extra GPS equipment at the mobile. Geolocation systems estimate the target mobile's position by monitoring the reverse signal channel transmissions from the mobile. Multiple base stations receive the mobile signal, and the mobile position can be determined that are based on either angle of arrival (AOA) estimates from each base station, time of arrial (TOA), or time difference of arrival (TDOA) measurements between multiple base stations, or their combinations.

Angle of Arrival

Angle of arrival, also called direction of arrival (DOA), has been used widely in surveying, radar tracking, and vehicle navigation systems [23, 34]. The position of the desired target mobile can be found by the intersection of two lines of bearing (LOBs), each formed by a radial from a base station to the target mobile. Instead of using the intersection of just two lines, many pairs of LOBs are used in practice, and highly directional antennas are required, which makes AOA estimation difficult at the mobile end. Figure 5.1 shows an AOA method using three base stations located at points (A, B, C). This method may be solved using trigonometry or analytic geometry, or through table lookup [23].

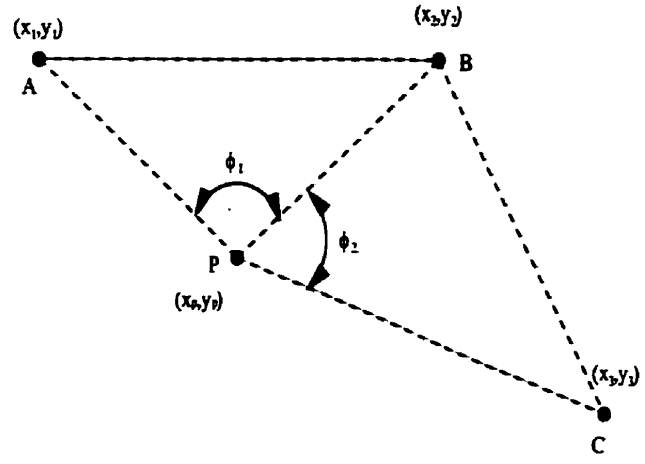

Figure 5.1: AOA method using three base stations.

AOA is usually determined at a base station by electronically steering the main lobe of an adaptive phased array antenna in the direction of the arriving mobile signal. In practice, two closely spaced antenna arrays are used to determine the exact direction of peak incoming energy (Figure 5.2). In general, the antenna element spacing used in AOA measurement is on the order of half the wavelength of the signal carrier frequency. The relatively close spacing of the antenna elements allows the time delay seen by a signal as it propagates across the array to be modeled as a phase shift. This is referred to as the "narrowband model".

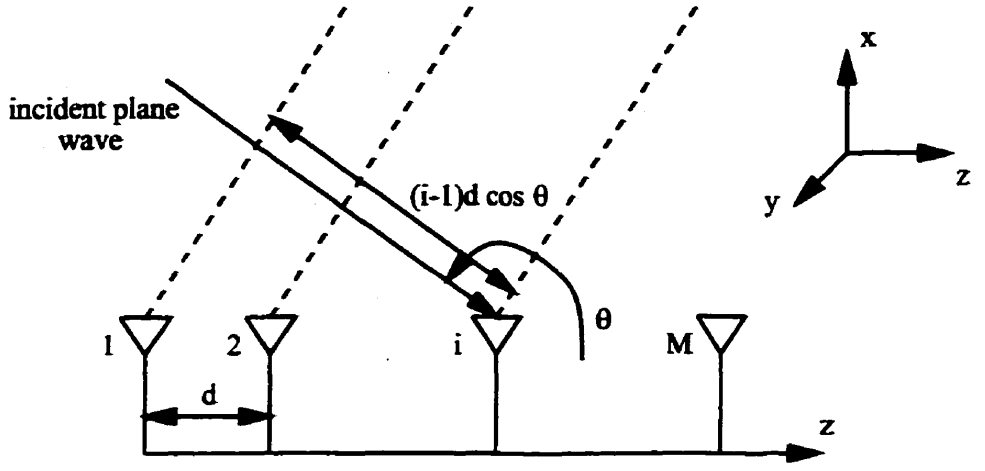

Figure 5.2: Illustration of a plane wave incident on a linear equispaced array.

For high SNR, the most straightforward AOA estimation approaches are phase interferometry and beamforming. However, they will fail for strong co-channel interference and/or multipath [30]. Maximum likelihood (ML) methods work well in multipath but implementation of these methods is very complicated [23, 37, 44]. To simplify the implementation of the ML methods, Xu and Liu proposed subspace-based algorithms combining spatially smoothed covariance matrices [42].

For code-division multiple access (CDMA) signals where there exists a very large number of co-channel signals, all of the AOA estimation algorithms proposed so far will fail, since they assume that the number of antennas in the array exceeds the number of co-channel signals [3]. However, by assuming that the CDMA signal may be demodulated with low bit error rate (BER), an estimated waveform may be substituted for the known waveform. One implementation of this approach uses the despread soft decisions from each antenna together with the hard decisions made by the existing CDMA demodulation process. Results presented in [3] show that accurate AOA estimates of CDMA waveforms can be obtained even in highly overloaded environments.

Time of Arrival

Time of arrival (TOA) is the second primary method for determining position location. Since electromagnetic waves propagate at the constant speed of light in a free-space medium, the distance from the mobile target to the receiving base station is directly proportional to the propagation time. If the signal propagates in time t_i from the target transmitter to the ith fixed receiver, then the receiver lies on a sphere of radius R_i, where

$$R_i = ct_i \tag{5.1}$$

If TOA measurements are made at a second base station at a second location, the target position can be determined to lie on a circle. The position of a transmitter is then uniquely determined by the intersection of three spheres using TOA measurements from three base stations [12, 36].

Time Difference of Arrival

In general, direct TOA requires all transmitters and receivers in the system have precisely synchronized clocks, for example, just 1 μs of timing error could result in a 300 meter position location error. Furthermore, the transmitting signal must be labeled with a timestamp in order for the receiver to discern the distance the signal has traveled. Therefore, time difference of arrival (TDOA) measurements are a more parctical means of position location for commercial systems [5].

The idea behind TDOA is to determine the relative position of the mobile transmitter by examining the difference in time at which the signal arrives at multiple base station receivers, rather than the absolute arrival time. Therefore, each TDOA measurement determines that the transmitter must lie on a hyperboloid with a constant range difference between the two receivers. The equation of this hyperboloid is given by

$$\begin{aligned} R_{i,j} &= \sqrt{(X_i - x)^2 + (Y_i - y)^2 + (Z_i - z)^2} \\ &\quad -\sqrt{(X_j - x)^2 + (Y_j - y)^2 + (Z_j - z)^2} \end{aligned} \tag{5.2}$$

where $R_{i,j}$ is the length difference between two base stations to the mobile transmitter, the coordinates (X_i, Y_i, Z_i) and (X_j, Y_j, Z_j) represent the fixed receivers i and j, and

determine the unknown coordinates (x, y, z) of the target transmitter [14]. A mobile location can be estimated from the intersection of two or more hyperboloids generated from three or more TDOA measurements. Figure 5.3 illustrates mobile position estimation using TDOA measurements from three base stations.

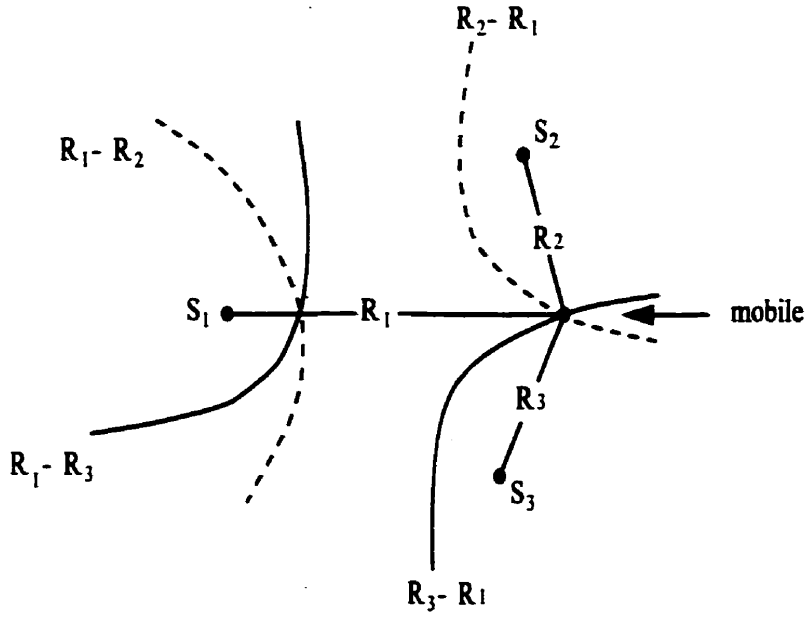

Figure 5.3: Mobile position location solution using TDOA measurements from three base stations, where S_1, S_2, and S_3 represent the fixed base station locations.

Using the TDOA measurements, the transmitted signal does not have to contain a timestamp, and only base stations are required to have precisely synchronized clocks. This makes TDOA more realistic than TOA, which requires each mobile unit to have an accurate clock.

A two-stage process is required to obtain position estimates from TDOA measurements. First, we must accurately compute the TDOA estimates from noisy signals, and then we determine the mobile position from the TDOA estimates and Equation (5.2). Generalized cross-correlation methods and filtering techniques are usually used in the first stage [30]. Once TDOA estimates are available, the position of the mobile may be located by substituting the corresponding range difference estimates

$R_{i,j}$ into the hyperbolic equations, Equation (5.2), and solving for the Cartesian coordinates of the mobile. There exist several methods to solve for the hyperbolic equations, which are summarized in [30].

5.2 Mobile Motion Tracking Using Kalman Filtering

We have introduced static mobile geolocation techniques in the previous section. In order to track to motion of mobiles, a Kalman filter can be applied. In this section, we introduce the mobile motion tracking application in terms of Kalman filter. We then try to improve tracking performance through the use of mobile velocity estimates which were developed in previous chapters.

Assuming that we are estimating the motion trajectory of a mobile with a constant velocity v. Along the x- and y-axis, we know that

$$\frac{d^2x(t)}{dt^2} = 0 \tag{5.3}$$

and

$$\frac{d^2y(t)}{dt^2} = 0 \tag{5.4}$$

where $x(t)$ and $y(t)$ are the position of the mobile at x- and y-axis, respectively.

In practice, the velocities undergo at least slight changes. These can be modeled by the continuous-time white Gaussian noises $\tilde{v}_x(t)$ and $\tilde{v}_y(t)$, respectively. Therefore,

$$\frac{d^2x(t)}{dt^2} = \tilde{v}_x(t) \tag{5.5}$$

and

$$\frac{d^2y(t)}{dt^2} = \tilde{v}_y(t) \tag{5.6}$$

where

$$\begin{cases} E\{\tilde{v}_x(t)\} = 0 \\ E\{\tilde{v}_x(t)\tilde{v}_x(\tau)\} = q_x\delta(t-\tau) \end{cases} \tag{5.7}$$

and

$$\begin{cases} E\{\tilde{v}_y(t)\} = 0 \\ E\{\tilde{v}_y(t)\tilde{v}_y(\tau)\} = q_y\delta(t-\tau) \end{cases} \tag{5.8}$$

where $\tilde{v}_x(t)$ and $\tilde{v}_y(t)$ are assumed mutually independent, q_x and q_y are variances of $\tilde{v}_x(t)$ and $\tilde{v}_y(t)$, respectively.

The state vector corresponding to Equations (5.5) and (5.6) is

$$\mathbf{x}(t) = \begin{bmatrix} x(t) \\ y(t) \\ \frac{dx(t)}{dt} \\ \frac{dy(t)}{dt} \end{bmatrix} \tag{5.9}$$

The continuous-time state equation is

$$\frac{d\mathbf{x}(t)}{dt} = \mathbf{A}\mathbf{x}(t) + \mathbf{B}\begin{bmatrix} \tilde{v}_x(t) \\ \tilde{v}_y(t) \end{bmatrix} \tag{5.10}$$

where

$$\mathbf{A} = \begin{bmatrix} 0 & 0 & 1 & 0 \\ 0 & 0 & 0 & 1 \\ 0 & 0 & 0 & 0 \\ 0 & 0 & 0 & 0 \end{bmatrix} \tag{5.11}$$

and

$$\mathbf{B} = \begin{bmatrix} 0 & 0 \\ 0 & 0 \\ 1 & 0 \\ 0 & 1 \end{bmatrix} \tag{5.12}$$

Using Equations (2-192)–(2-199) in [4], the discrete-time state equation with sampling period T_s is

$$\mathbf{x}_{k+1} = \mathbf{F}\mathbf{x}_k + \mathbf{v}_k \tag{5.13}$$

where

$$\mathbf{F} = e^{\mathbf{A}T_s} = \begin{bmatrix} 1 & 0 & T_s & 0 \\ 0 & 1 & 0 & T_s \\ 0 & 0 & 1 & 0 \\ 0 & 0 & 0 & 1 \end{bmatrix} \tag{5.14}$$

and $\mathbf{v}_k$ is a 4×1 process noise vector. For simplicity, we assume that $\mathbf{v}_k$ is a white Gaussian noise vector with

$$E\{\mathbf{v}_k\} = \mathbf{0} \tag{5.15}$$

and the covariance matrix $\mathbf{Q}$ is

$$\mathbf{Q} = \begin{bmatrix} \frac{1}{2}T_s^2 q_x & 0 & 0 & 0 \\ 0 & \frac{1}{2}T_s^2 q_y & 0 & 0 \\ 0 & 0 & T_s q_x & 0 \\ 0 & 0 & 0 & T_s q_y \end{bmatrix} \tag{5.16}$$

5.2.1 Mobile Motion Tracking without Velocity Measurement

If we only know x_k and y_k, the mobile position measurements at x- and y-axis, the measurement equation for mobile motion tracking can be written as

$$\mathbf{y}_k = \mathbf{H}\mathbf{x}_k + \mathbf{w}_k \tag{5.17}$$

where $\mathbf{x}_k$ is the state vector, $\mathbf{y}_k$ is the measurement vector

$$\mathbf{y}_k = \begin{bmatrix} x_k \\ y_k \end{bmatrix} \tag{5.18}$$

and $\mathbf{w}_k$ is the measurement noise vector,

$$\mathbf{w}_k = \begin{bmatrix} w_{x,k} \\ w_{y,k} \end{bmatrix} \tag{5.19}$$

with

$$\begin{cases} E\{\mathbf{w}_k\} = \mathbf{0} \\ E\{\mathbf{w}_k \mathbf{w}_i'\} = \mathbf{R}\delta_{ki} \end{cases} \tag{5.20}$$

where

$$\mathbf{R} = \begin{bmatrix} r_x & 0 \\ 0 & r_y \end{bmatrix} \tag{5.21}$$

r_x, r_y are variances of $w_{x,k}$ and $w_{y,k}$, respectively, and $\mathbf{w}'$ is the transpose of vector $\mathbf{w}$.

To implement the Kalman filter algorithm, we should first initialize the state vector $\mathbf{x}$ and its covariance matrix $\mathbf{P}$. Then we obtain the one-step prediction by taking expection of Equation (5.13) conditioned on $Y^k \triangleq \{\mathbf{y}(j), j = 1, \ldots, k\}$, which results in

$$\hat{\mathbf{x}}_{k+1|k} = \mathbf{F}\hat{\mathbf{x}}_{k|k} \tag{5.22}$$

and the one-step prediction covariance matrix is

$$\mathbf{P}_{k+1|k} = \mathbf{F}\mathbf{P}_{k|k}\mathbf{F}' + \mathbf{Q} \tag{5.23}$$

where $\mathbf{F}'$ is the transpose of matrix $\mathbf{F}$.

The predicted measurement follows similarly by taking the expected value of Equation (5.17) at time $k+1$, conditioned on Y^k:

$$\hat{\mathbf{y}}_{k+1|k} = \mathbf{H}\hat{\mathbf{x}}_{k+1|k} \tag{5.24}$$

and the Kalman gain is

$$\mathbf{K}_{k+1} = \mathbf{P}_{k+1|k}\mathbf{H}'[\mathbf{H}\mathbf{P}_{k+1|k}\mathbf{H}' + \mathbf{R}] \tag{5.25}$$

and thus

$$\hat{\mathbf{x}}_{k+1|k+1} = \hat{\mathbf{x}}_{k+1|k} + \mathbf{K}_{k+1}[\mathbf{y}_{k+1} - \mathbf{H}\hat{\mathbf{x}}_{k+1|k}] \tag{5.26}$$

Finally, the state covariance matrix at time $k+1$ is

$$\mathbf{P}_{k+1|k+1} = [\mathbf{I} - \mathbf{K}_{k+1}\mathbf{H}]\mathbf{P}_{k+1|k}[\mathbf{I} - \mathbf{K}_{k+1}\mathbf{H}]' + \mathbf{K}_{k+1}\mathbf{R}\mathbf{K}'_{k+1} \tag{5.27}$$

The algorithm implementation procedure is summarized as:

1. Initialize the state vector $\hat{\mathbf{x}}_0$ and its covariance matrix $\mathbf{P}_0$;
2. Obtain the time update using Equations (5.22) and (5.23);
3. Obtain the measurement update using Equations (5.24) – (5.27);
4. Go back to step 2 and repeat until all samples have been processed.

5.2.2 Mobile Motion Tracking with Velocity Measurement

If we have the position and velocity measurements, x_k, y_k and v_k, of the mobile, the measurement equation can then be written as

$$\mathbf{y}_k = \mathbf{h}[k, \mathbf{x}_k] + \mathbf{w}_k \tag{5.28}$$

where

$$\mathbf{y}_k = \begin{bmatrix} x_k \\ y_k \\ v_k \end{bmatrix} \tag{5.29}$$

and

$$\mathbf{h}[\cdot] \triangleq \begin{bmatrix} x_k \\ y_k \\ \sqrt{v_{x,k}^2 + v_{y,k}^2} \end{bmatrix} \tag{5.30}$$

and the measurement noise vector

$$\mathbf{w}_k = \begin{bmatrix} w_{x,k} \\ w_{y,k} \\ w_{v,k} \end{bmatrix} \tag{5.31}$$

is assumed as a white Guassian noise vector with

$$\begin{cases} E\{\mathbf{w}_k\} = \mathbf{0} \\ E\{\mathbf{w}_k \mathbf{w}_i'\} = \mathbf{R}\delta_{ki} \end{cases} \tag{5.32}$$

where

$$\mathbf{R} = \begin{bmatrix} r_x & 0 & 0 \\ 0 & r_y & 0 \\ 0 & 0 & r_v \end{bmatrix} \tag{5.33}$$

and r_v is the variance of $w_{v,k}$.

Since the measurement equation (5.28) is nonlinear, we have to linearize it before we implement the Kalman filter algorithm. It is done by replacing $\mathbf{H}$ in Equations (5.24)–(5.27) by the Jacobian of $\mathbf{h}[\cdot]$ with respect to the state vector:

$$\mathbf{h}_{\mathbf{x},k} = \left. \frac{d\mathbf{h}[k, \mathbf{x}_k]}{d_{\mathbf{x}_k}} \right|_{\mathbf{x}_k = \hat{\mathbf{x}}_k} \tag{5.34}$$

Substituting Equation (5.30) into (5.34), we obtain

$$\mathbf{h}_{\hat{\mathbf{x}},k} = \begin{bmatrix} 1 & 0 & 0 & 0 \\ 0 & 1 & 0 & 0 \\ 0 & 0 & \frac{v_{x,k}}{\sqrt{v_{x,k}^2 + v_{y,k}^2}} & \frac{v_{y,k}}{\sqrt{v_{x,k}^2 + v_{y,k}^2}} \end{bmatrix} \tag{5.35}$$

Therefore, the implementation procedure is the same as the one in the previous section, but using $\mathbf{h}_{\hat{\mathbf{x}},k}$ rather than $\mathbf{H}$ in Equations (5.24)–(5.27).

5.3 Simulation and Comparison

We have introduced two mobile motion tracking models in the previous section, one is without mobile velocity measurement and another uses mobile velocity measurement. We will simulate these two motion trackers and compare their performance in this section. At the very first, the measurement covariance matrices for each tracker and the process noise covariance matrix should be determined. Then the initial state estimate is specified.

5.3.1 Measurement Noise Covariance Matrices

It is assumed that position errors on x- and y-axis are Gaussian and identically distributed with zero mean and variances, r_x and r_y, which are listed in Table (5.1).

r_x, r_y (m^2)	33.33	133.33	833.33

Table 5.1: Various position error variances

From the previous two chapters, we know that both of the LCR and ACF estimates of mobile velocity have estimate errors within 10% of the actual mobile velocity. We then list mobile velocity measurement error variances r_v in Table (5.2).

	pedestrian	slow moving vehicle	fast moving vehicle	faster moving vehicle
v (km/h)	5	20	50	100
r_v (m^2/s^2)	0.0064	0.1029	0.6430	2.5720

Table 5.2: Various velocity error variances

5.3.2 Process Noise Covariance Matrix

The process noise covariance matrix $\mathbf{Q}$ in Equation (5.16) is related to sampling period T_s and q_x, q_y, the variances of acceleration error on x- and y-axis, respectively. Here we assume that

$$T_s = 1 \tag{5.36}$$

Then $\mathbf{Q}$ is determined mainly by q_x and q_y.

One must notice that the Kalman gain is directly proportional to the process noise covariance matrix. However, if the Kalman gain is too small, the contribution of the current measurement will be ignored. On the other hand, if the Kalman gain is too large, small residual errors will be magnified, thus affecting the accuracy of the updated state estimates.

Unfortunately, there does not exist any sysematic procedure to determine the "proper amount" of the process noise covariance matrix. The following process noise covariance matrix will be used in all the simulations.

$$\mathbf{Q} = \begin{bmatrix} 0.005 & 0 & 0 & 0 \\ 0 & 0.005 & 0 & 0 \\ 0 & 0 & 0.01 & 0 \\ 0 & 0 & 0 & 0.01 \end{bmatrix} \tag{5.37}$$

5.3.3 Initial State Estimates

A Kalman filter needs to be initialized. Specifically, inital values for the estimated state vector and error covariance matrix must be given. The following formula is used in specifying initial state estimates:

$$\hat{\mathbf{x}_0} = [1 \pm (1 + r)e]\mathbf{x}_0 \tag{5.38}$$

where r is a random number uniformly distributed in the interval $(0, 1)$ and e is used to control the magnitude of the errors. By setting $e = 0.2$, for example, errors can be introduced in the range 20%–40%. $e = 0.2$ will be used for all the simulations.

The initial error covariance matrix is computed as

$$\mathbf{P}_0 = \begin{bmatrix} (x_{0,1} - \hat{x}_{0,1})^2 & 0 & 0 & 0 \\ 0 & (x_{0,2} - \hat{x}_{0,2})^2 & 0 & 0 \\ 0 & 0 & (x_{0,3} - \hat{x}_{0,3})^2 & 0 \\ 0 & 0 & 0 & (x_{0,4} - \hat{x}_{0,4})^2 \end{bmatrix} \tag{5.39}$$

5.3.4 Simulation Results

We assume that the mobile is traveling along a line $y = x$ on a x-y plane, and the initial position of the mobile is (1000, 1000). Then we can obtain the estimated initial state vector and its error covariance matrix using Equation (5.38) and (5.39). Due to the correlation between computer-generated "pseudo" white noise samples, we have to use Monte-Carlo method to get rid of the correlation. For all the simulations, we set the number of Monte-Carlo trials be 50.

According to Table 5.1 and 5.2, we simulate the mobile trackers with various velocities and position errors. Figure 5.4–5.51 depict the simulation results. In each figure, the solid line and dashed line represent simulation results of mobile motion tracker with and without mobile velocity measurement, respectively. From these figures, we see that when the mobile is moving slowly (i.e., velocity at 5 or 20 km/h), the mobile velocity measurements do not improve the performance of the mobile motion tracker. On the other hand, when the mobile velocity is large (i.e., velocity at 50 or 100 km/h), the performance of the mobile motion tracker is improved significantly with velocity measurement being taken into account.

This phenomenon occurs becuase of the relatively large position measurement errors. With relatively large position measurement errors, the mobile velocity measurements at 5 or 20 km/h will not change the Kalman gain in Equation (5.25) significantly. Therefore, the state estimates remain the same as those without velocity measurements. Once the mobile velocity measurements are large (for example, 50 or 100 km/h), the Kalman gain will be affected accordingly, then we obtain more accurate state estimates than those without velocity measurements being considered.

5.4 Summary

In this chapter, we have applied the mobile velocity estimates in mobile motion tracking problem. Then we simulated the mobile motion trackers and compared the performance of trackers with and without velocity measurements. From the simulation results, we found that when the mobile is moving slowly, the velocity measurements do not increase the accuracy of the mobile position estimates. However, when the mobile velocity is large, the performance of mobile motion tracker with velocity measurements being taken into account is improved significantly.

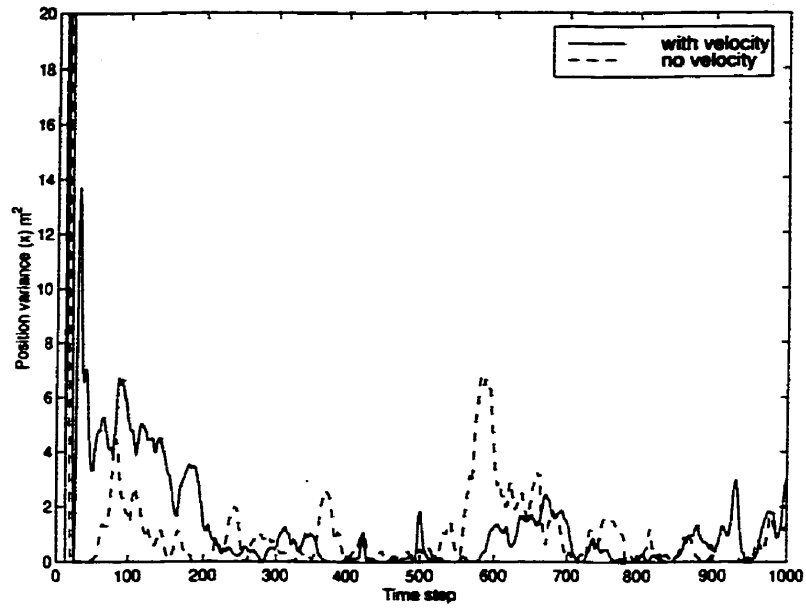

Figure 5.4: x position variance, mobile velocity: 5 km/h, position measurement error: 20 m

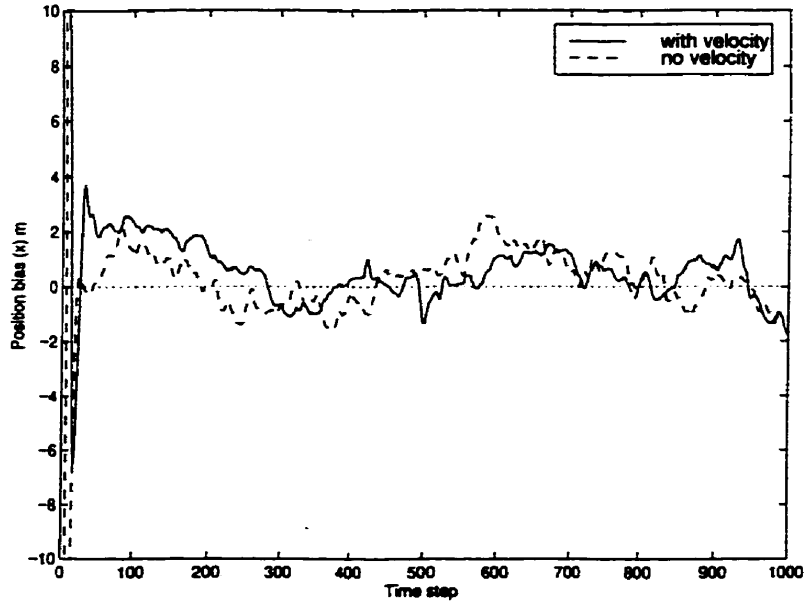

Figure 5.5: x position bias, mobile velocity: 5 km/h, position measurement error: 20 m

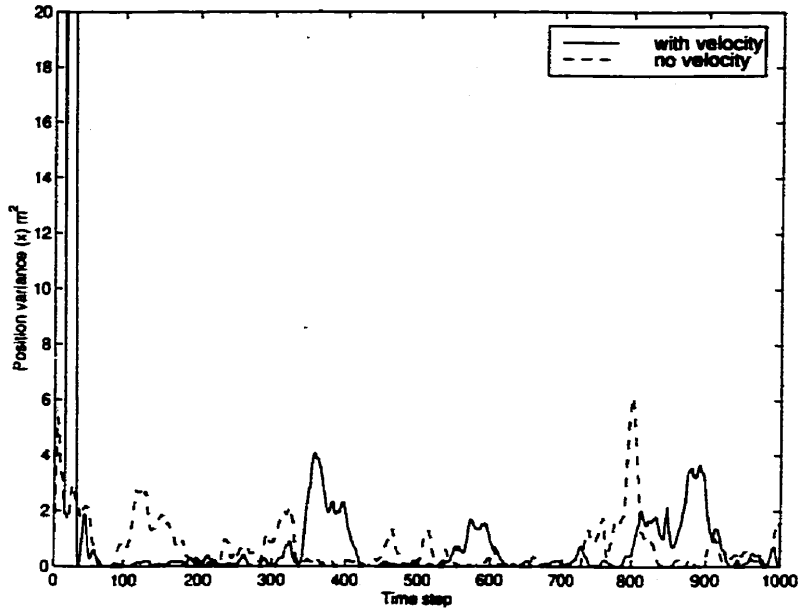

Figure 5.6: y position variance, mobile velocity: 5 km/h, position measurement error: 20 m

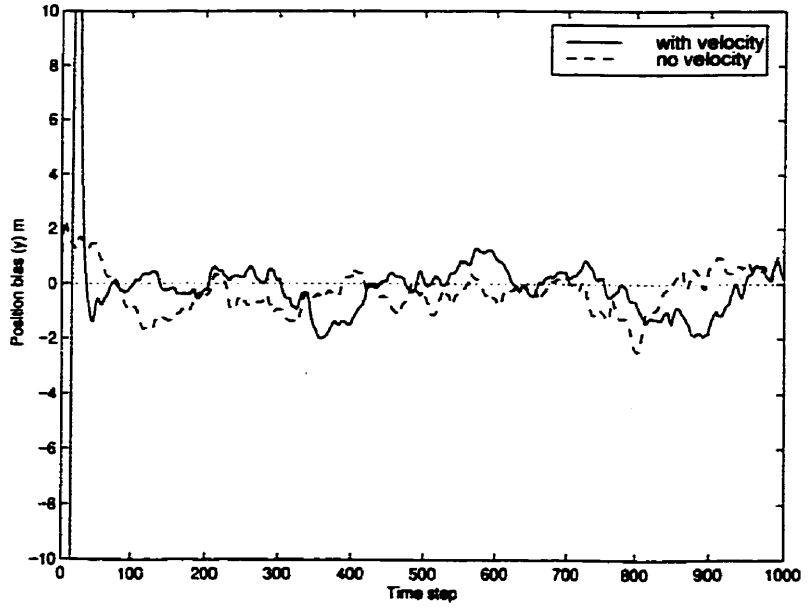

Figure 5.7: y position bias, mobile velocity: 5 km/h, position measurement error: 20 m

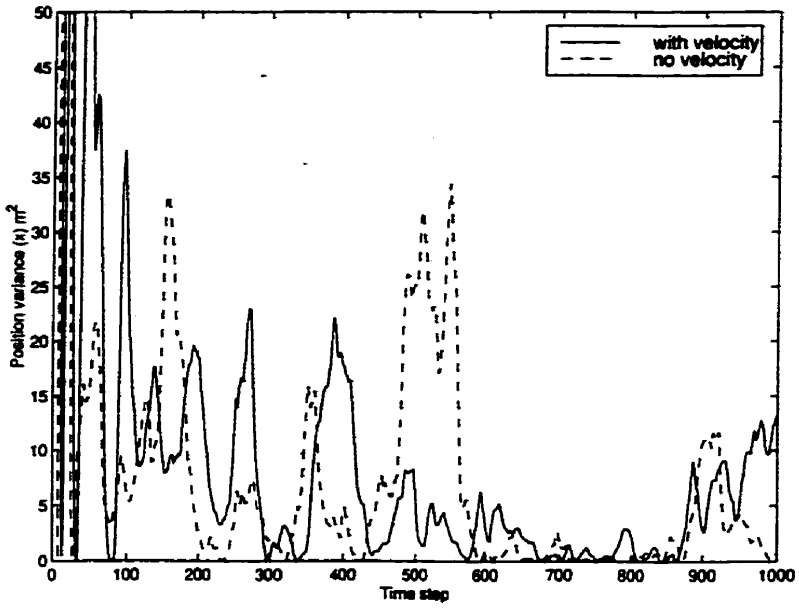

Figure 5.8: x position variance, mobile velocity: 5 km/h, position measurement error: 40 m

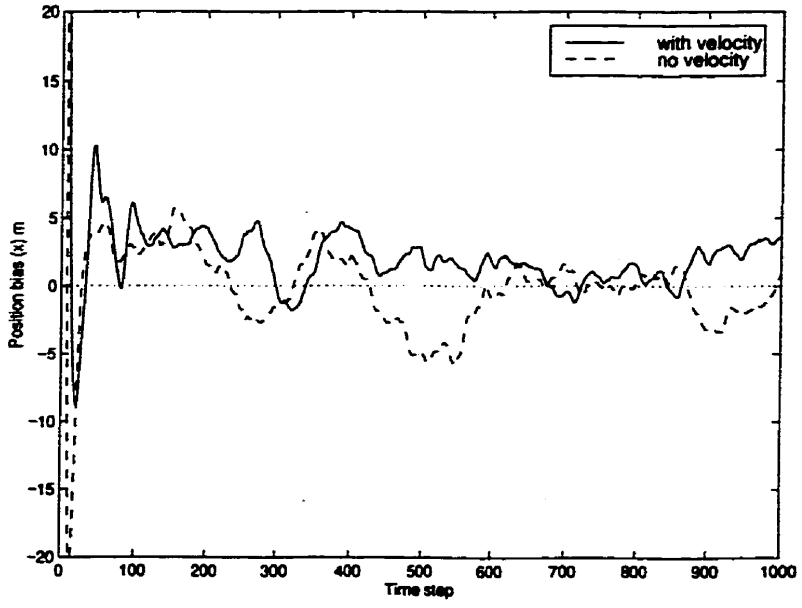

Figure 5.9: x position bias, mobile velocity: 5 km/h, position measurement error: 40 m

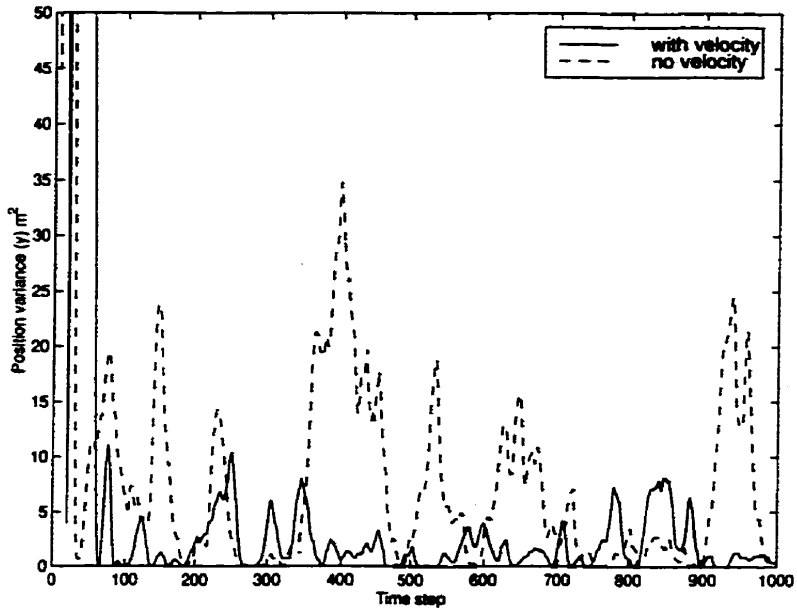

Figure 5.10: y position variance, mobile velocity: 5 km/h, position measurement error: 40 m

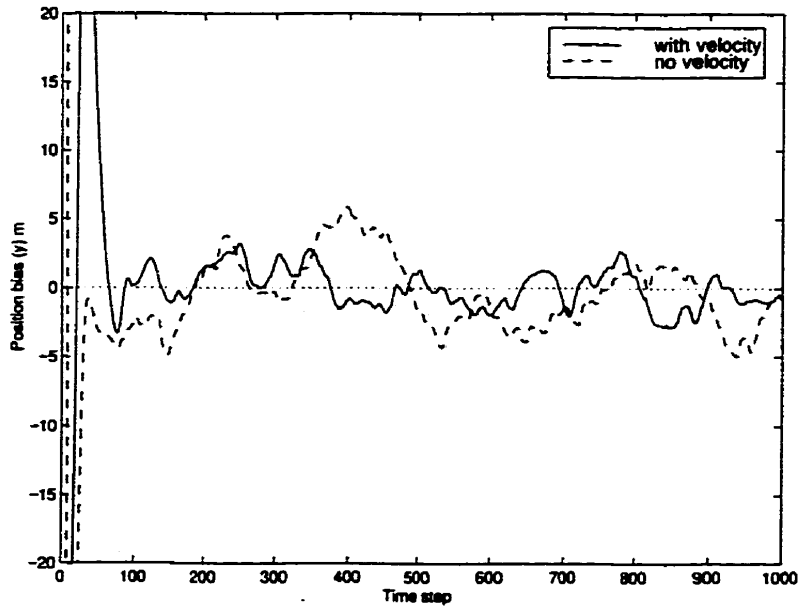

Figure 5.11: y position bias, mobile velocity: 5 km/h, position measurement error: 40 m

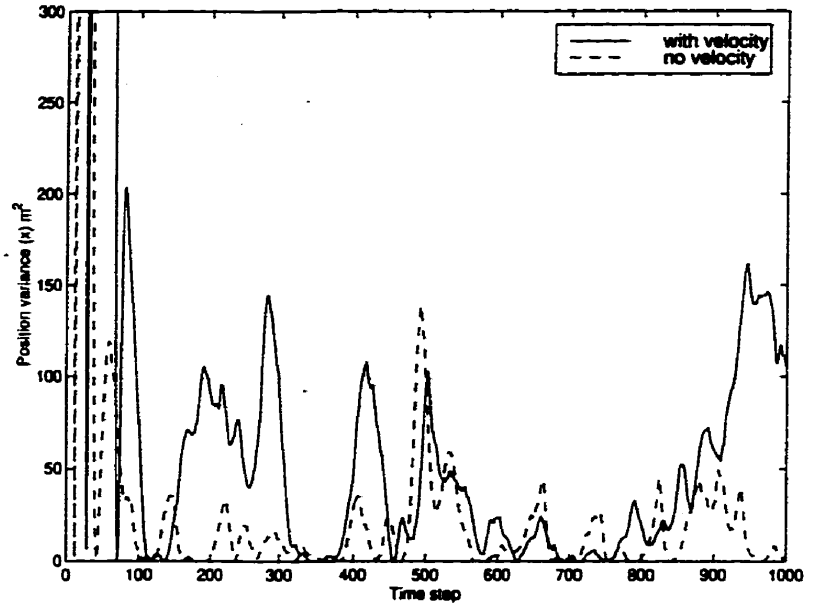

Figure 5.12: x position variance, mobile velocity: 5 km/h, position measurement error: 100 m

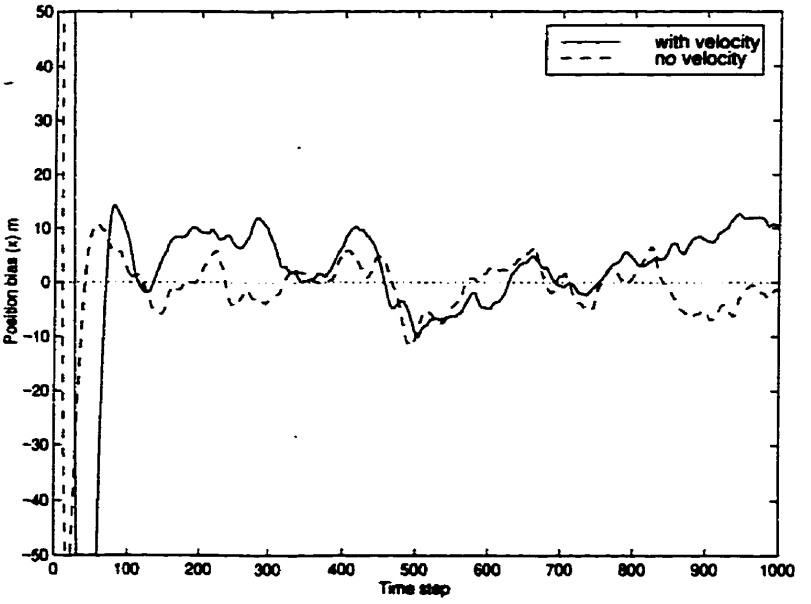

Figure 5.13: x position bias, mobile velocity: 5 km/h, position measurement error: 100 m

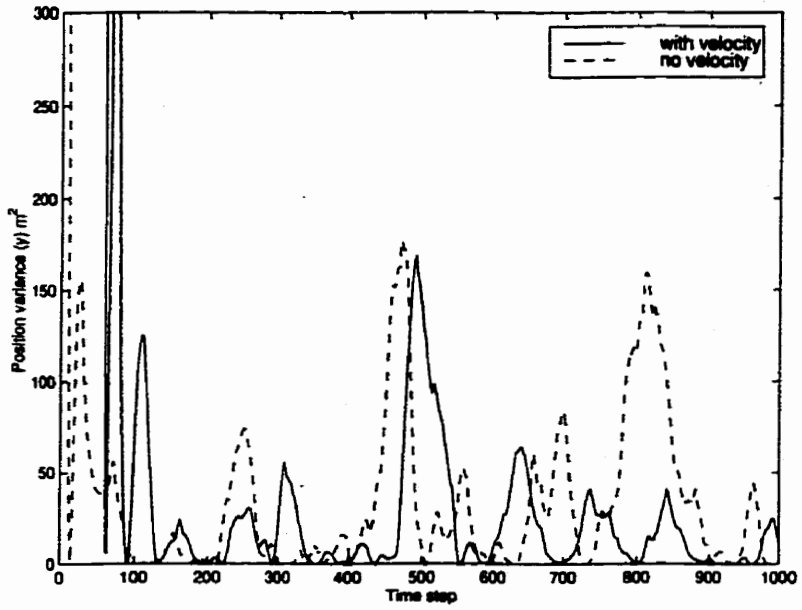

Figure 5.14: y position variance, mobile velocity: 5 km/h, position measurement error: 100 m

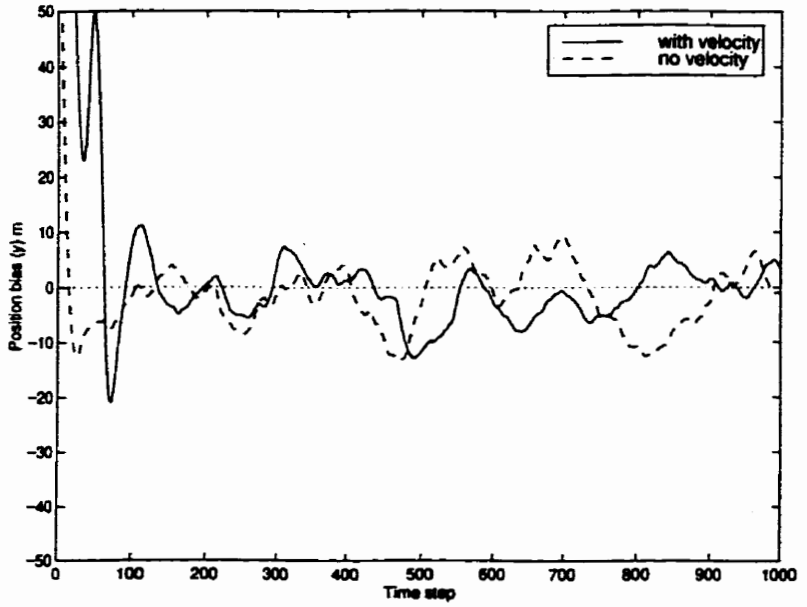

Figure 5.15: y position bias, mobile velocity: 5 km/h, position measurement error: 100 m

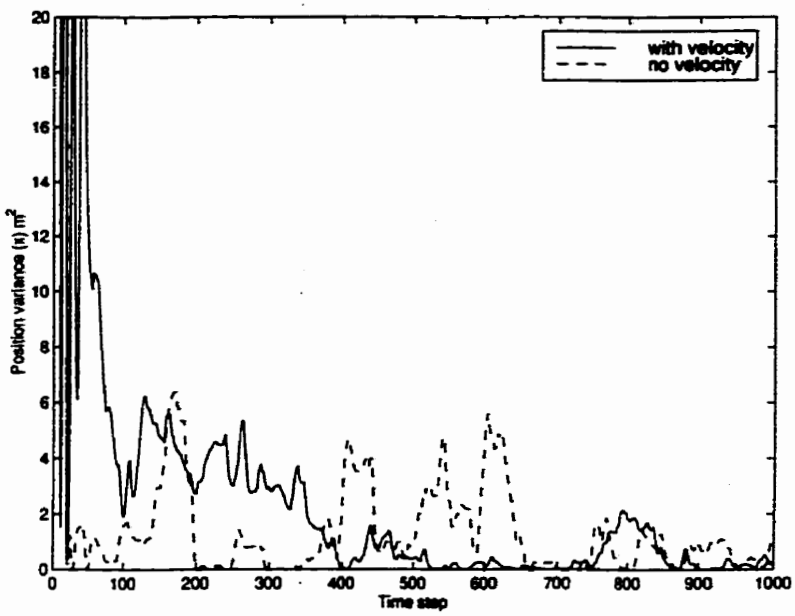

Figure 5.16: x position variance, mobile velocity: 20 km/h, position measurement error: 20 m

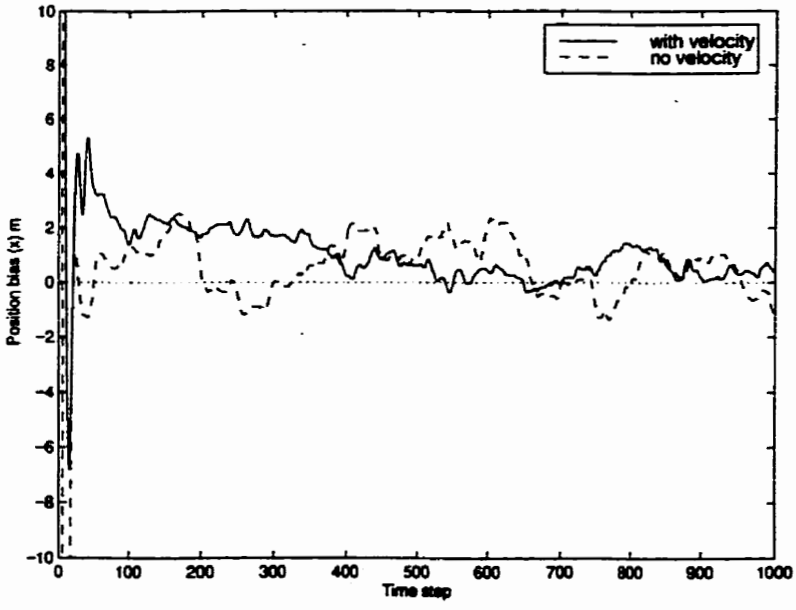

Figure 5.17: x position bias, mobile velocity: 20 km/h, position measurement error: 20 m

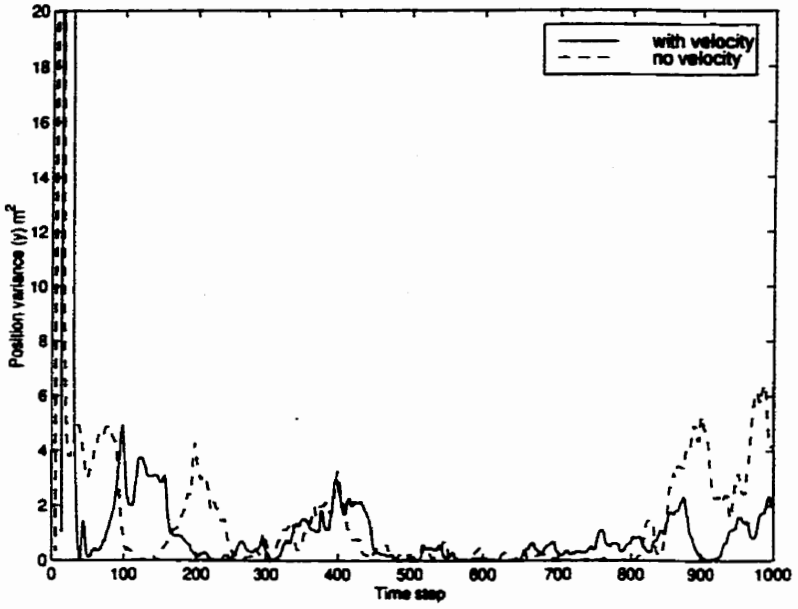

Figure 5.18: y position variance, mobile velocity: 20 km/h, position measurement error: 20 m

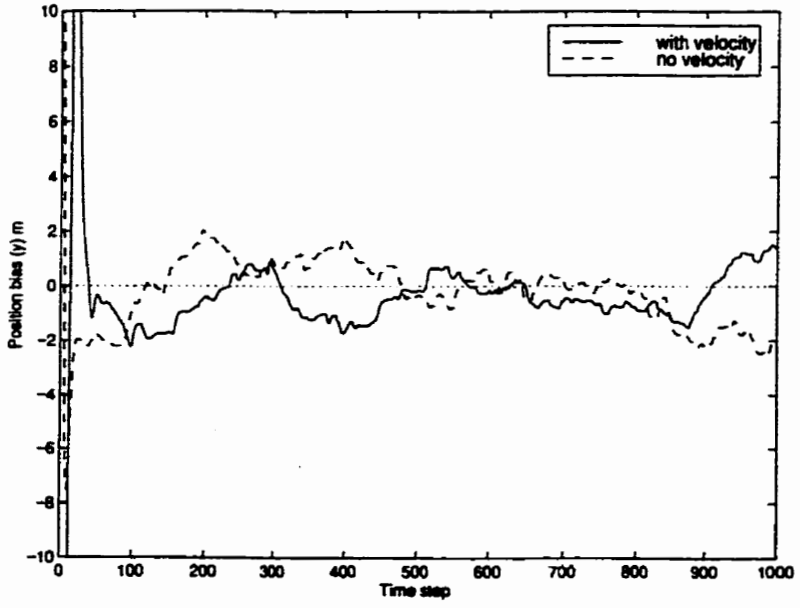

Figure 5.19: y position bias, mobile velocity: 20 km/h, position measurement error: 20 m

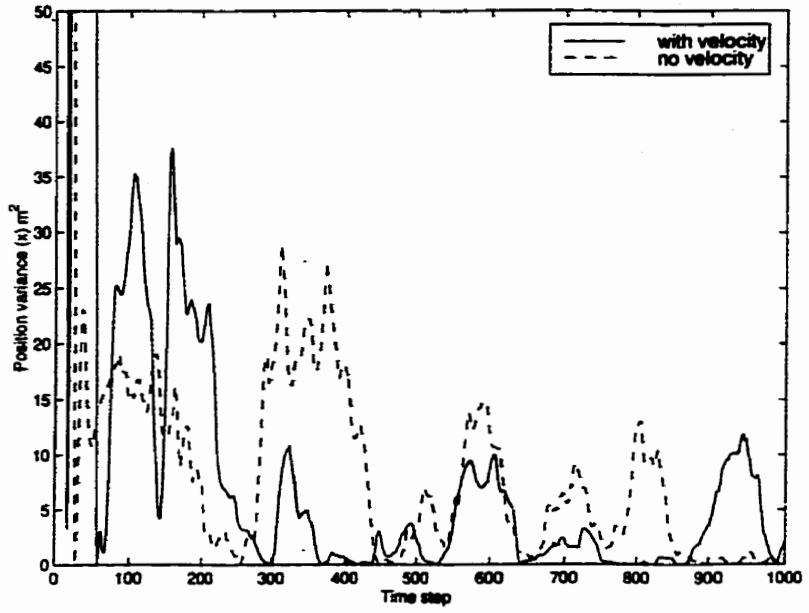

Figure 5.20: x position variance, mobile velocity: 20 km/h, position measurement error: 40 m

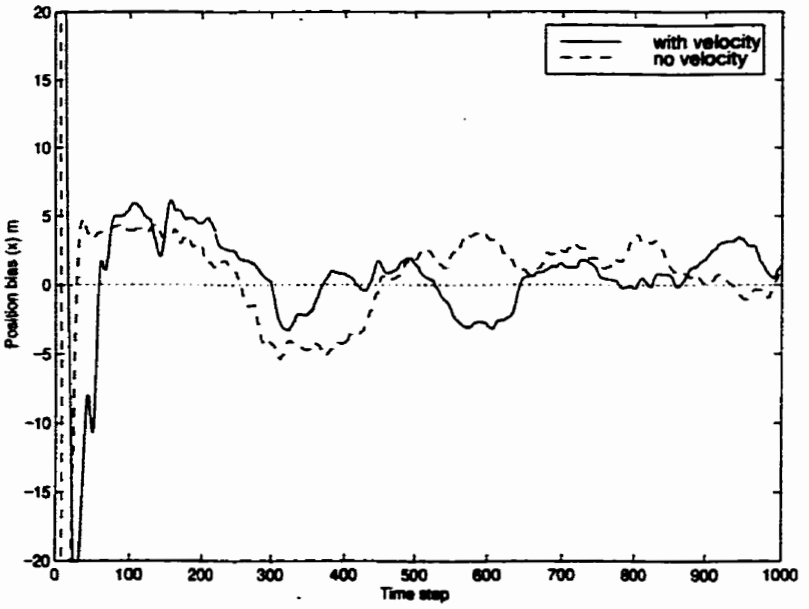

Figure 5.21: x position bias, mobile velocity: 20 km/h, position measurement error: 40 m

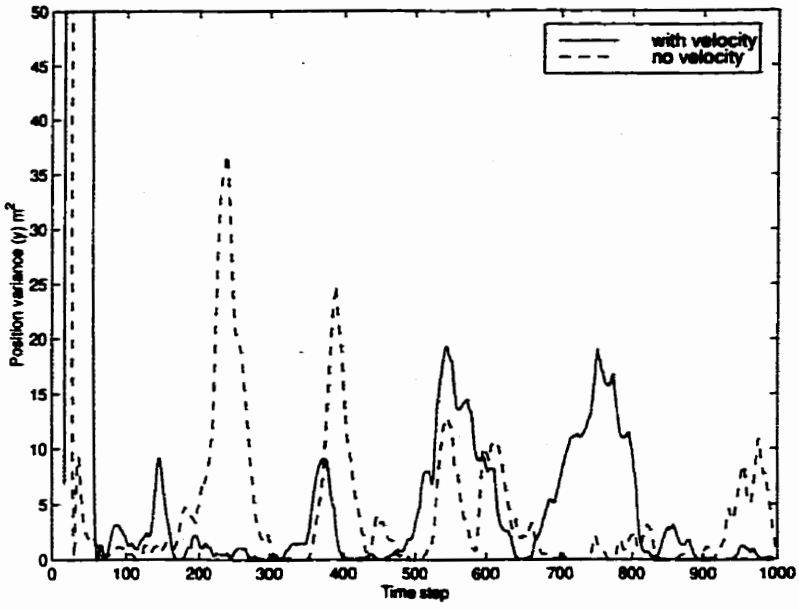

Figure 5.22: y position variance, mobile velocity: 20 km/h, position measurement error: 40 m

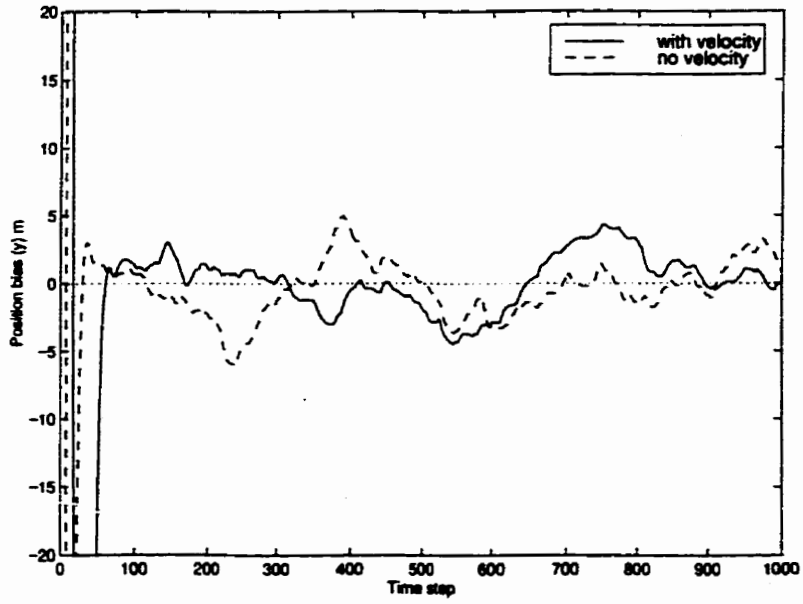

Figure 5.23: y position bias, mobile velocity: 20 km/h, position measurement error: 40 m

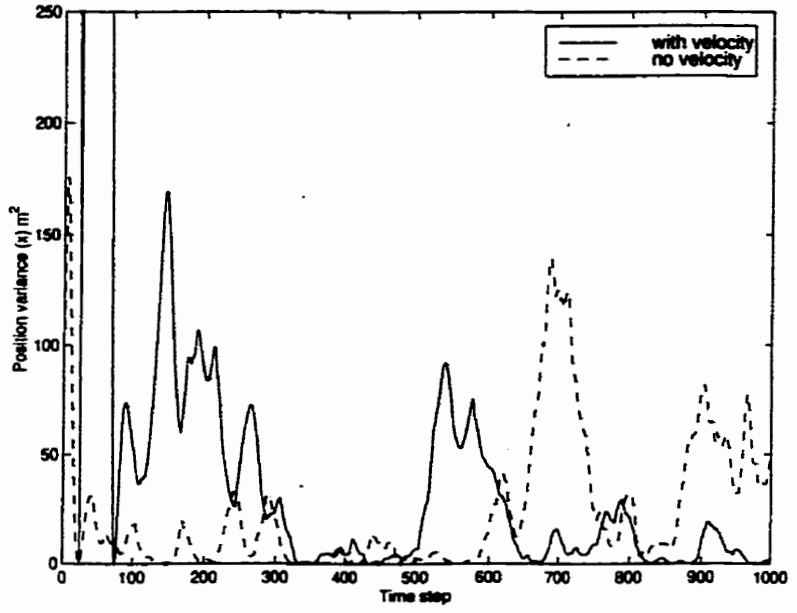

Figure 5.24: x position variance, mobile velocity: 20 km/h, position measurement error: 100 m

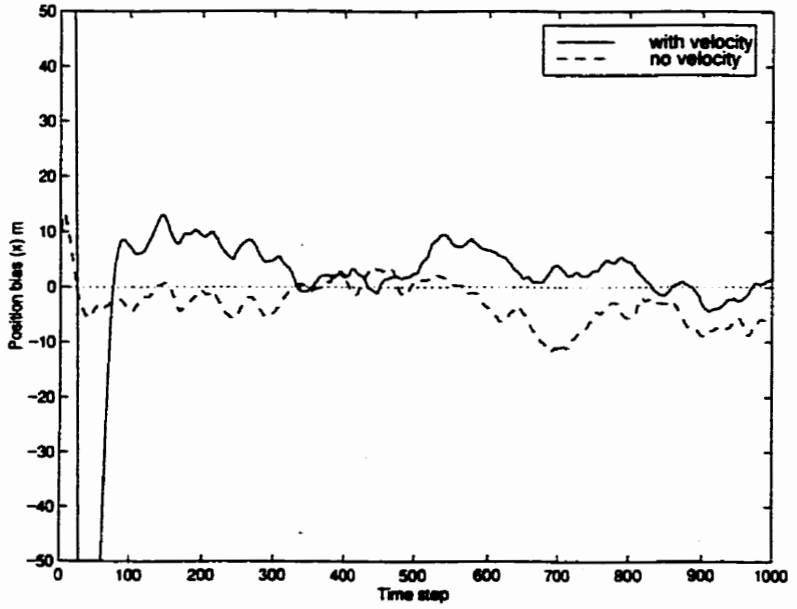

Figure 5.25: x position bias, mobile velocity: 20 km/h, position measurement error: 100 m

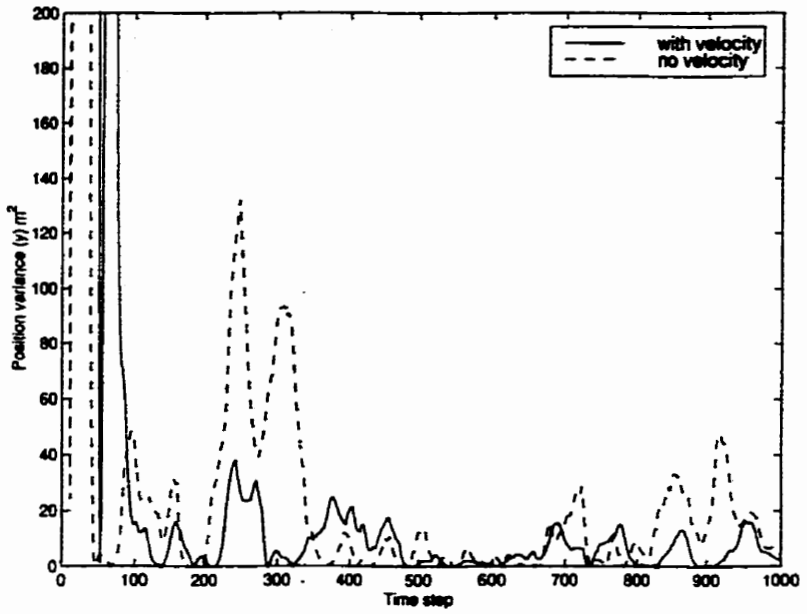

Figure 5.26: y position variance, mobile velocity: 20 km/h, position measurement error: 100 m

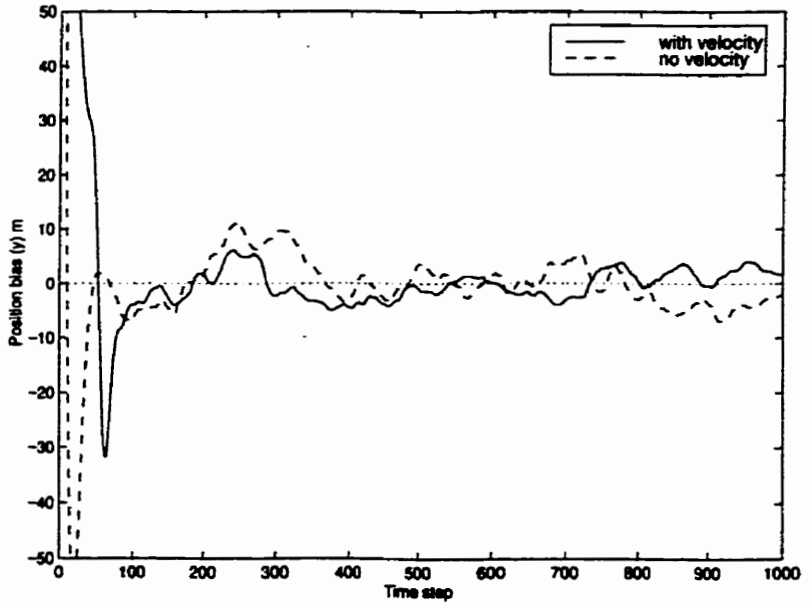

Figure 5.27: y position bias, mobile velocity: 20 km/h, position measurement error: 100 m

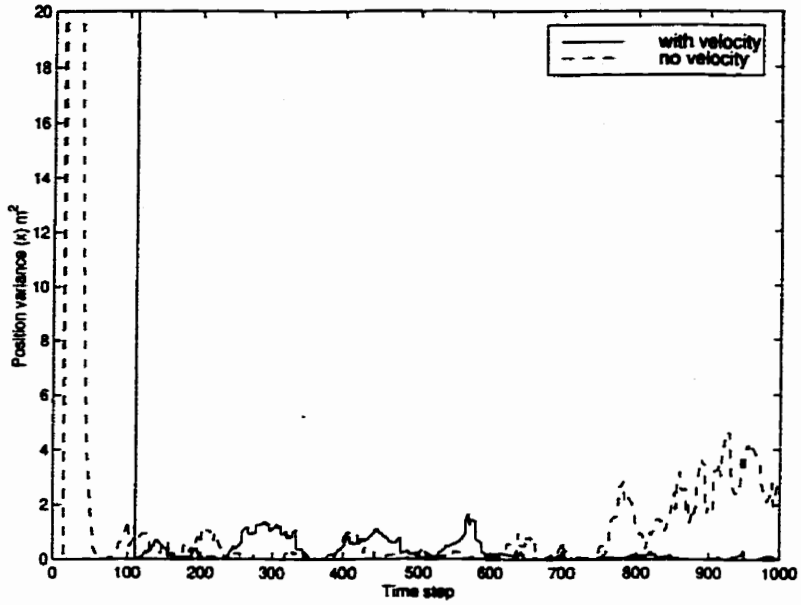

Figure 5.28: x position variance, mobile velocity: 50 km/h, position measurement error: 20 m

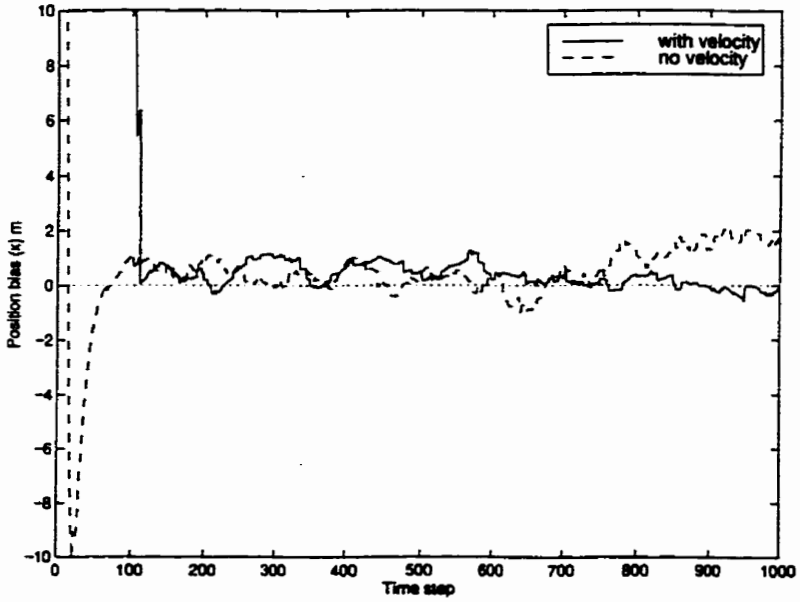

Figure 5.29: x position bias, mobile velocity: 50 km/h, position measurement error: 20 m

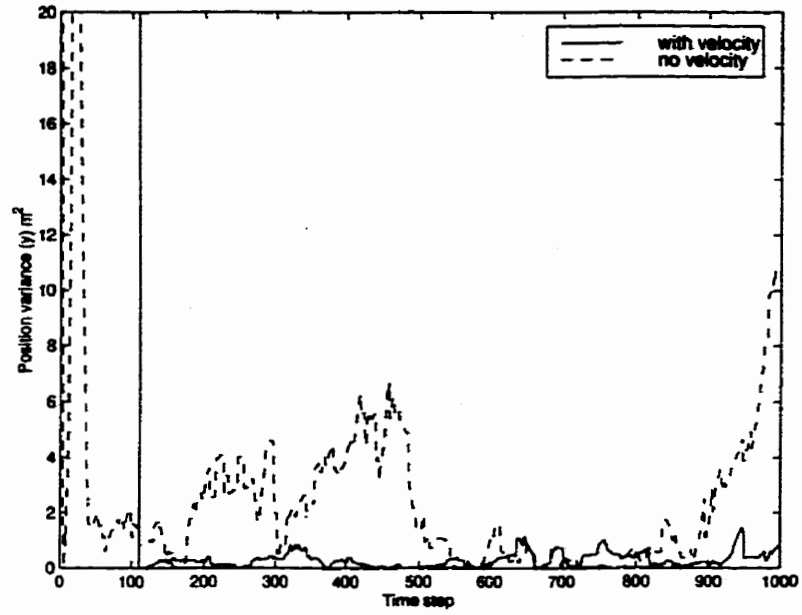

Figure 5.30: y position variance, mobile velocity: 50 km/h, position measurement error: 20 m

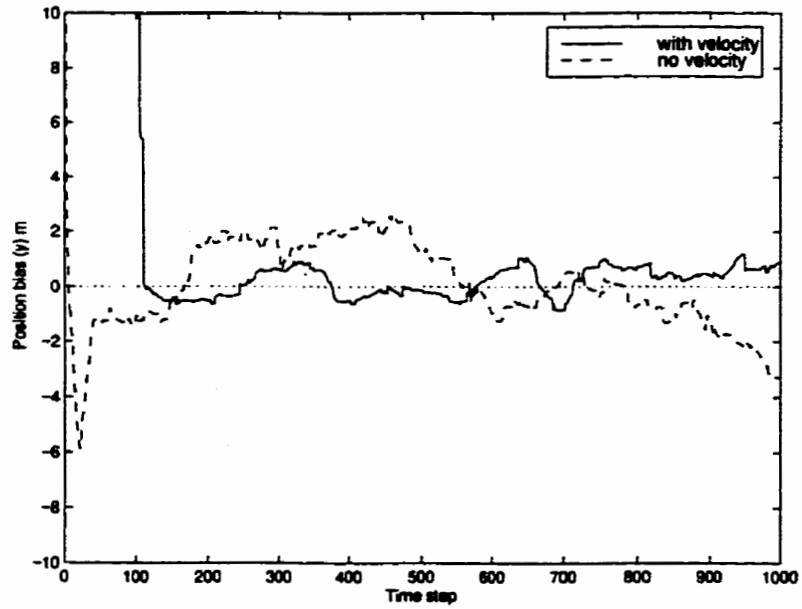

Figure 5.31: y position bias, mobile velocity: 50 km/h, position measurement error: 20 m

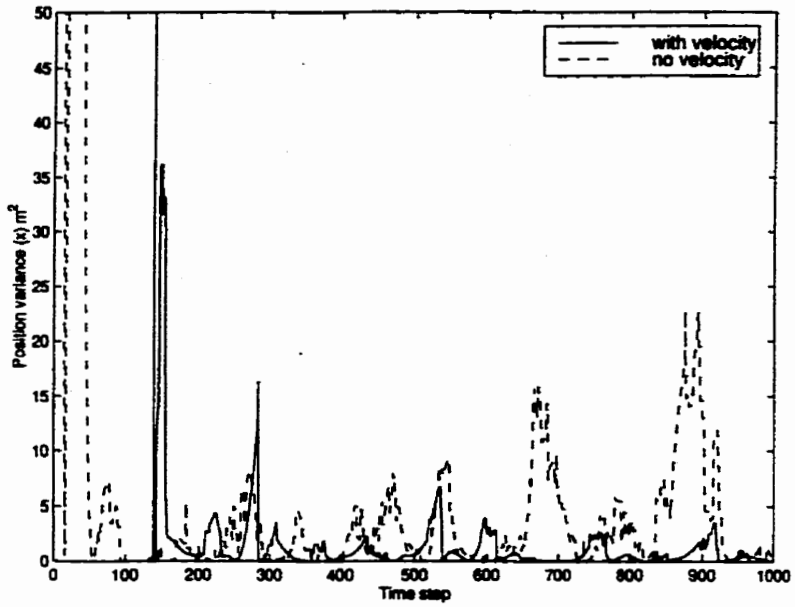

Figure 5.32: x position variance, mobile velocity: 50 km/h, position measurement error: 40 m

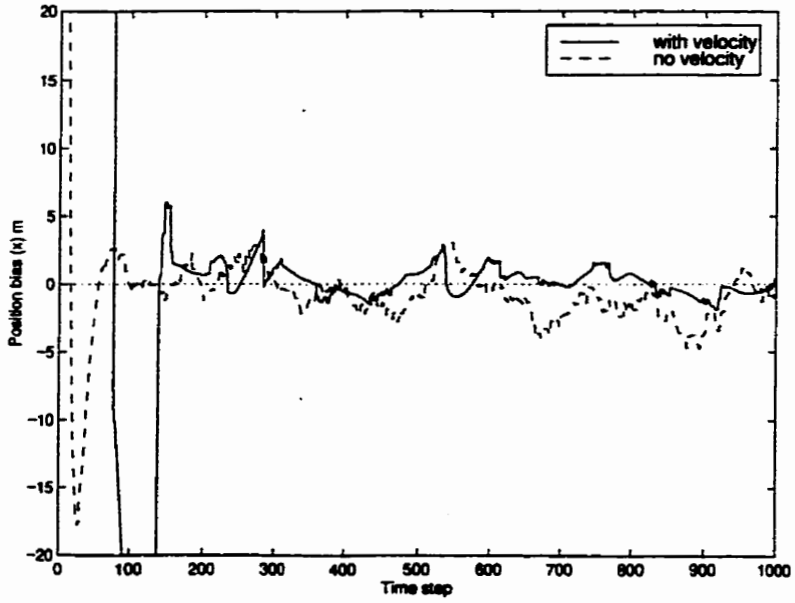

Figure 5.33: x position bias, mobile velocity: 50 km/h, position measurement error: 40 m

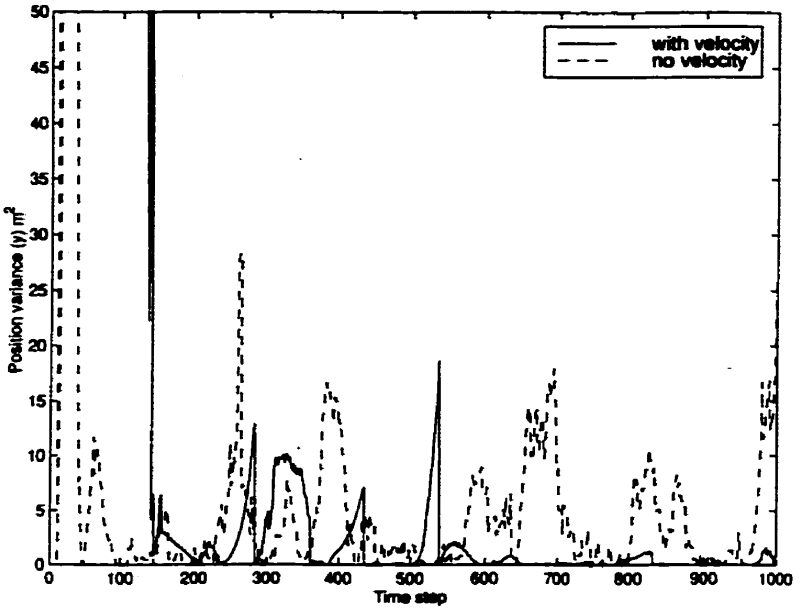

Figure 5.34: y position variance, mobile velocity: 50 km/h, position measurement error: 40 m

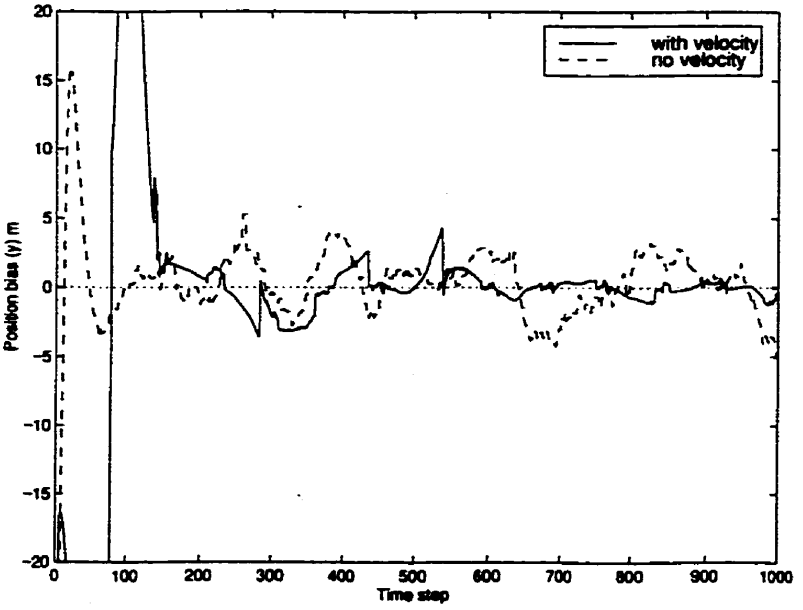

Figure 5.35: y position bias, mobile velocity: 50 km/h, position measurement error: 40 m

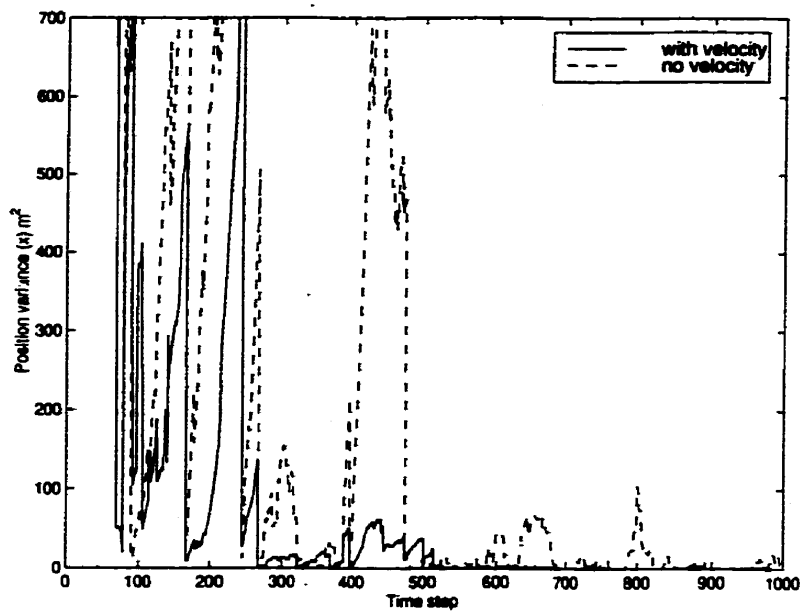

Figure 5.36: x position variance, mobile velocity: 50 km/h, position measurement error: 100 m

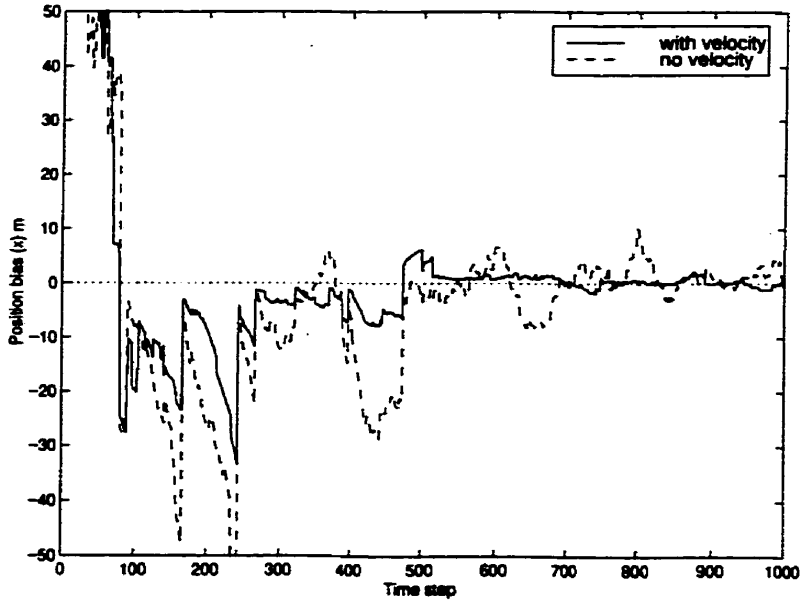

Figure 5.37: x position bias, mobile velocity: 50 km/h, position measurement error: 100 m

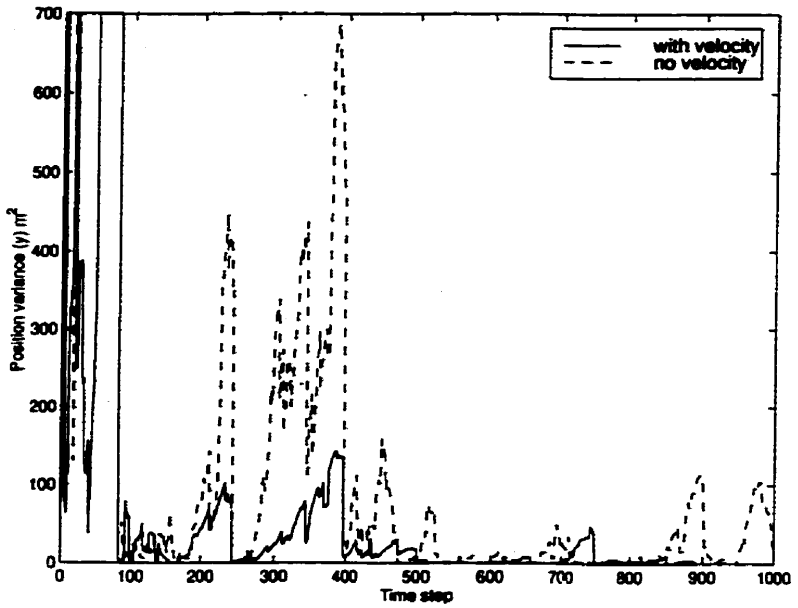

Figure 5.38: y position variance, mobile velocity: 50 km/h, position measurement error: 100 m

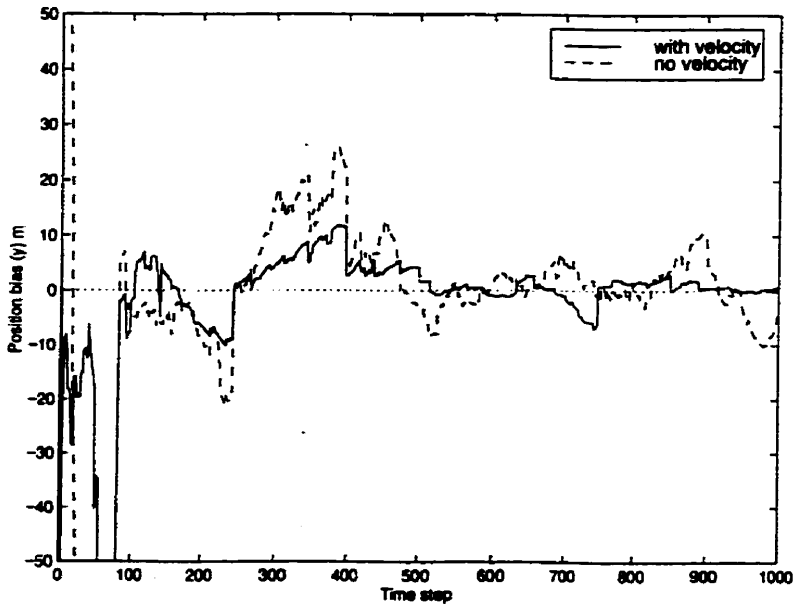

Figure 5.39: y position bias, mobile velocity: 50 km/h, position measurement error: 100 m

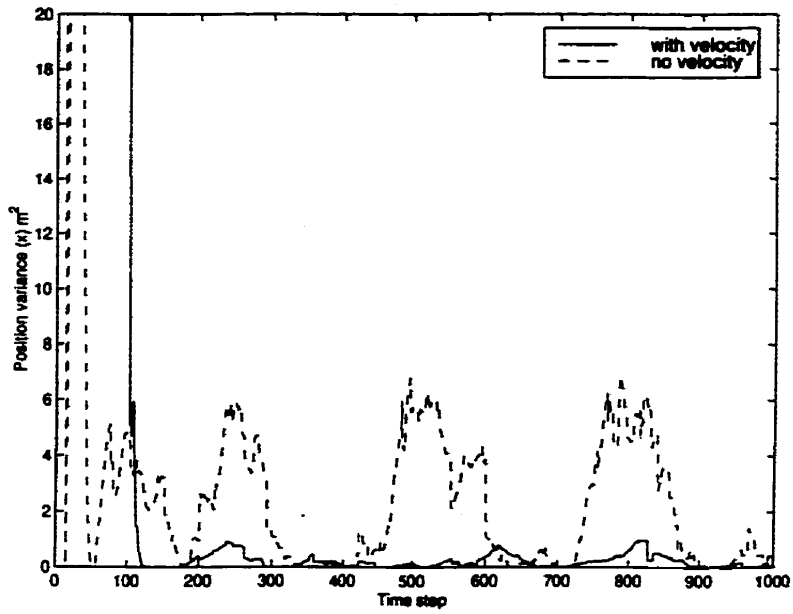

Figure 5.40: x position variance, mobile velocity: 100 km/h, position measurement error: 20 m

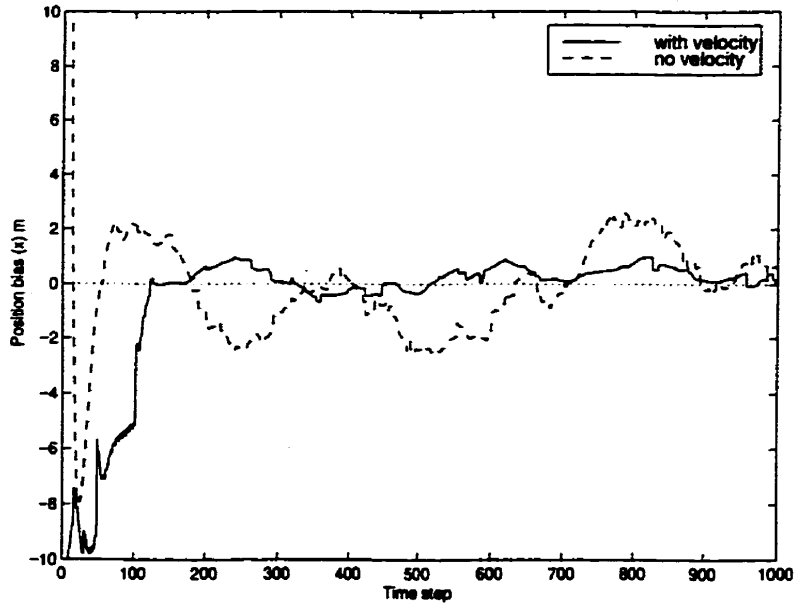

Figure 5.41: x position bias, mobile velocity: 100 km/h, position measurement error: 20 m

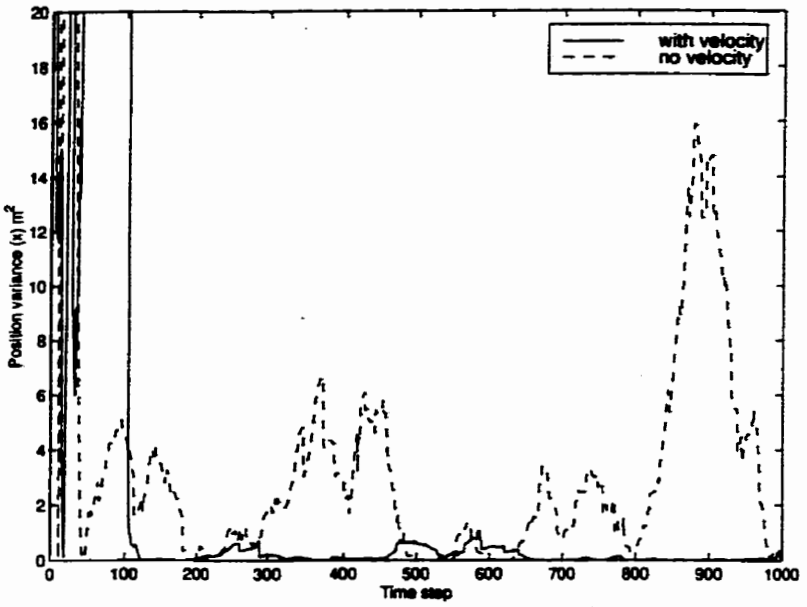

Figure 5.42: y position variance, mobile velocity: 100 km/h, position measurement error: 20 m

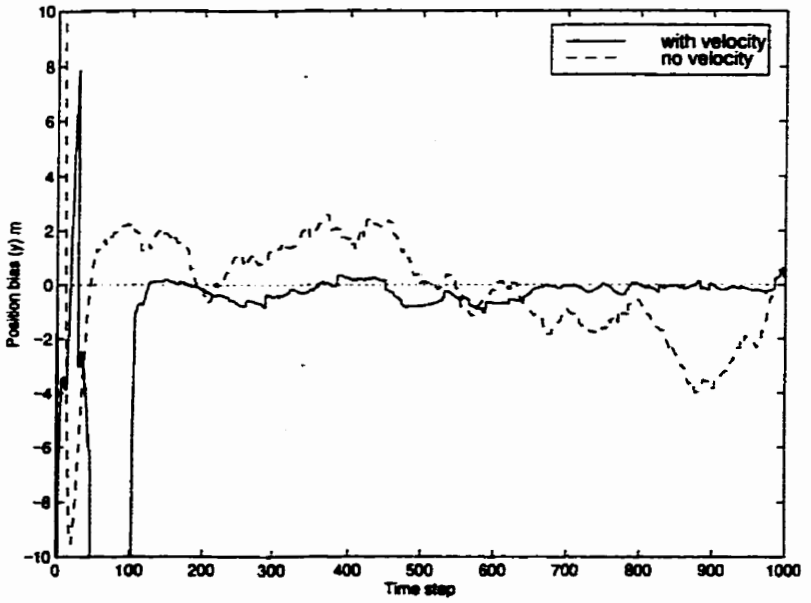

Figure 5.43: y position bias, mobile velocity: 100 km/h, position measurement error: 20 m

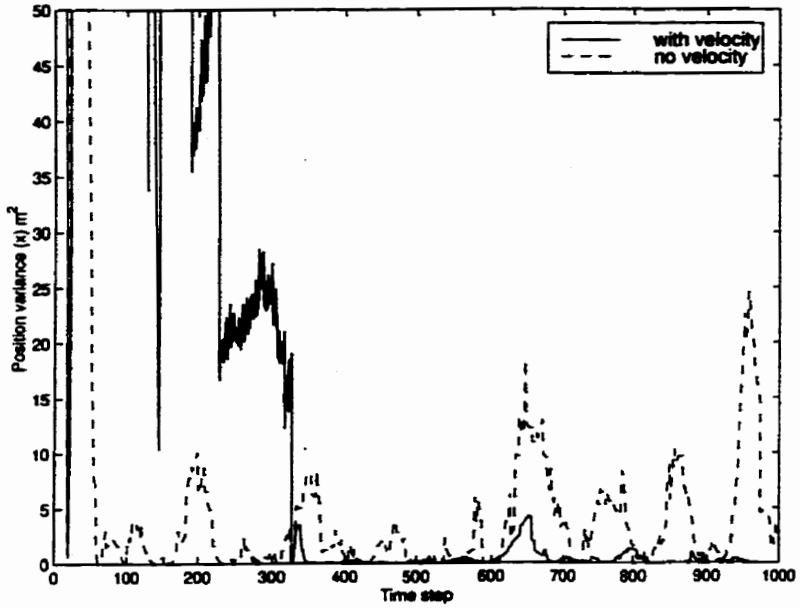

Figure 5.44: x position variance, mobile velocity: 100 km/h, position measurement error: 40 m

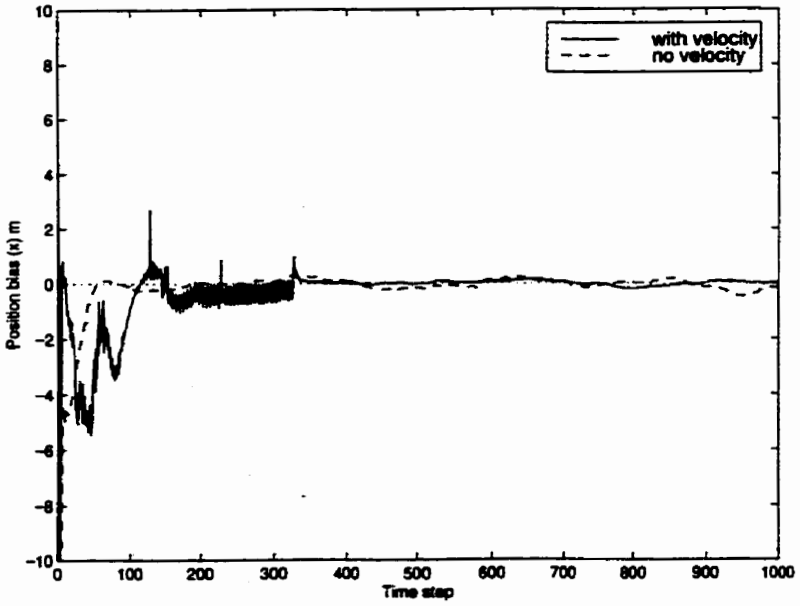

Figure 5.45: x position bias, mobile velocity: 100 km/h, position measurement error: 40 m

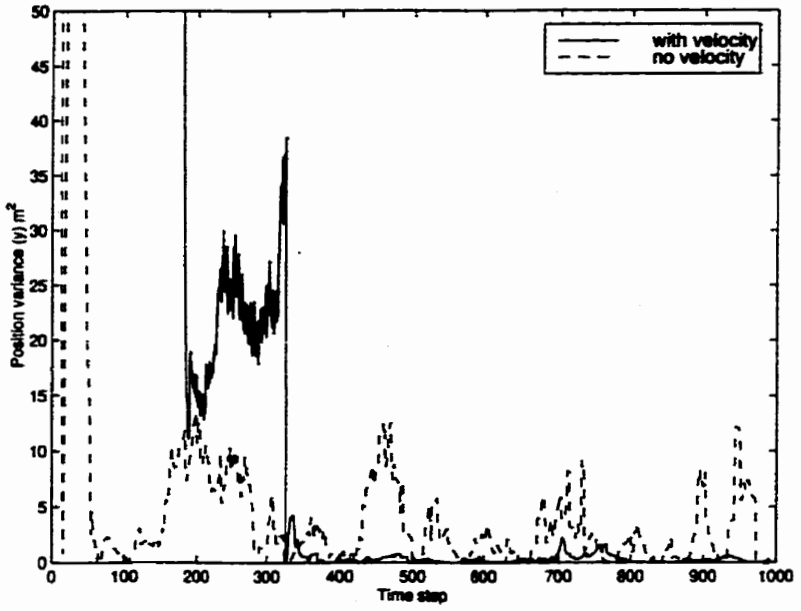

Figure 5.46: y position variance, mobile velocity: 100 km/h, position measurement error: 40 m

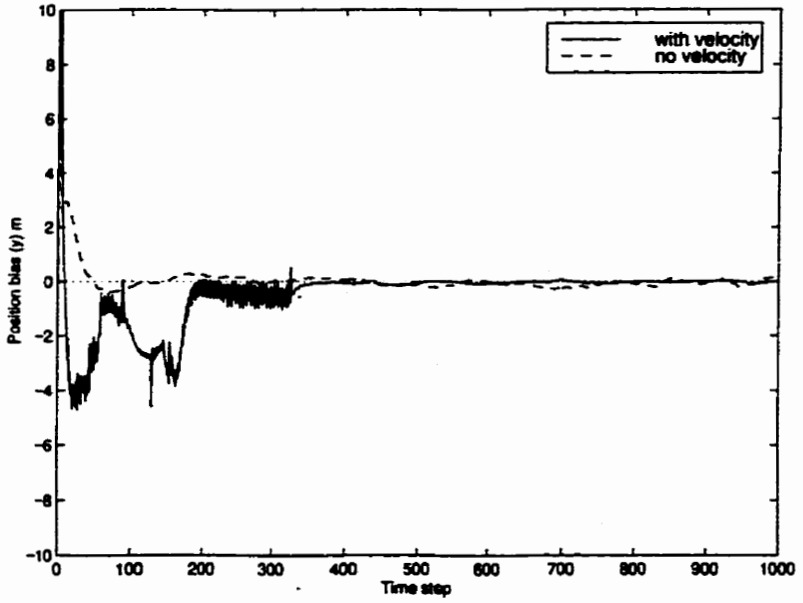

Figure 5.47: y position bias, mobile velocity: 100 km/h, position measurement error: 40 m

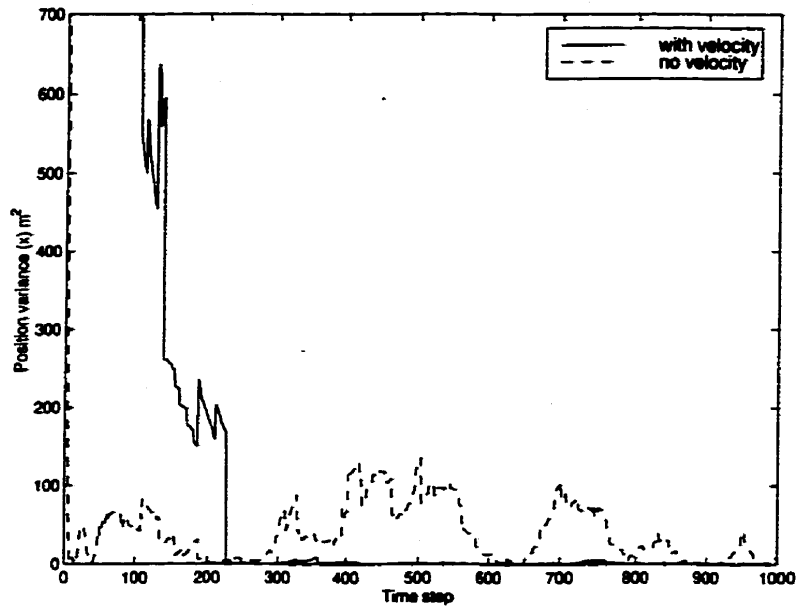

Figure 5.48: x position variance, mobile velocity: 100 km/h, position measurement error: 100 m

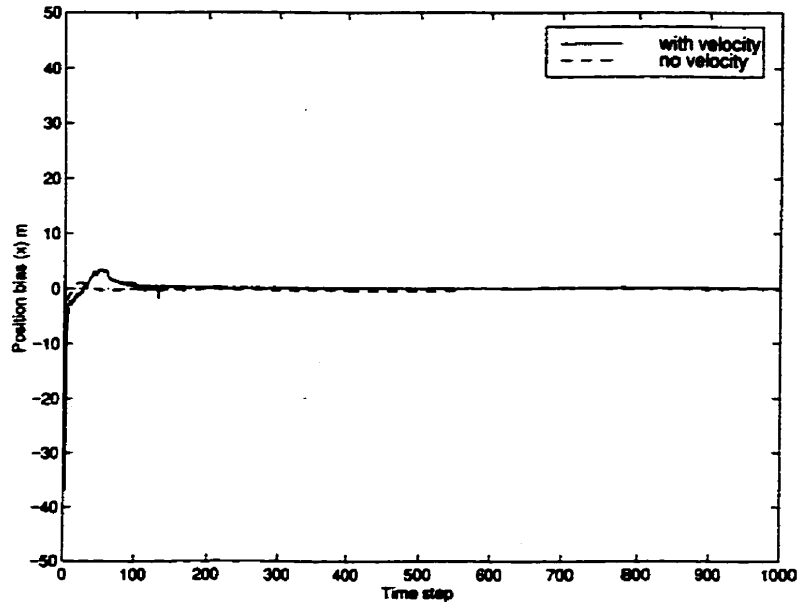

Figure 5.49: x position bias, mobile velocity: 100 km/h, position measurement error: 100 m

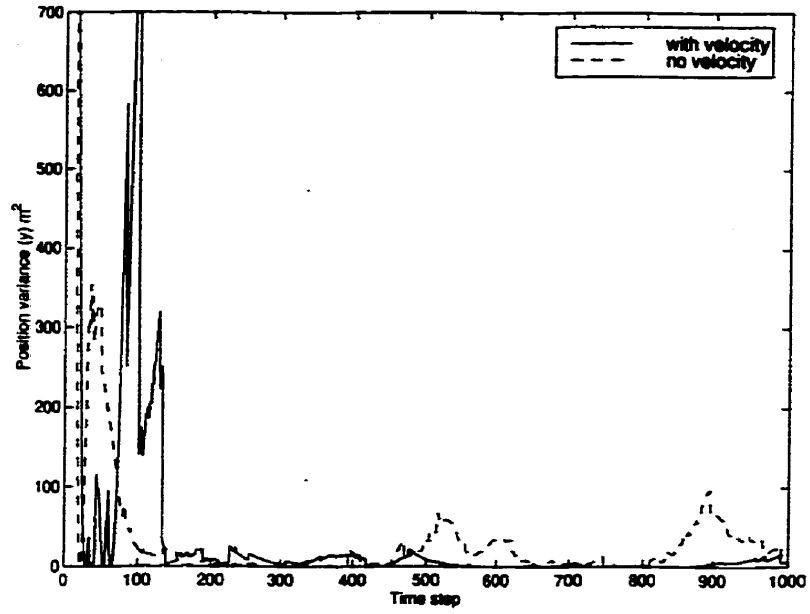

Figure 5.50: y position variance, mobile velocity: 100 km/h, position measurement error: 100 m

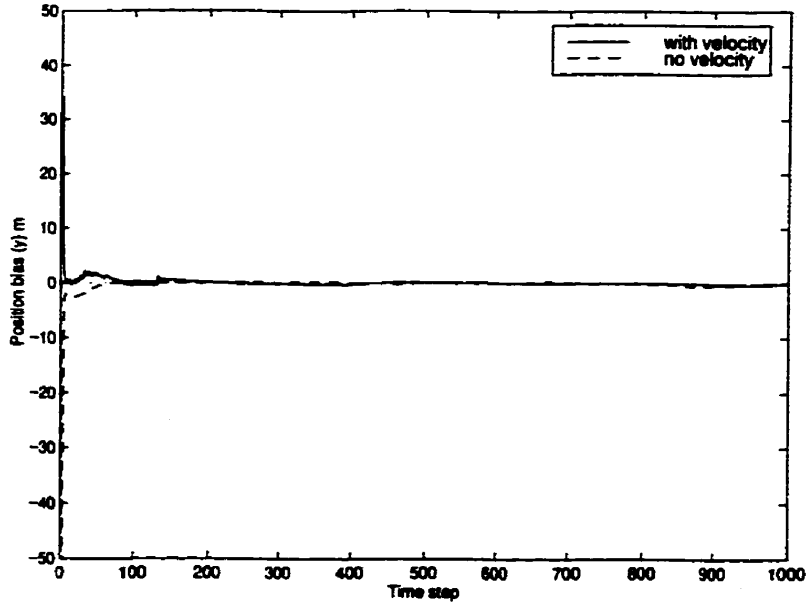

Figure 5.51: y position bias, mobile velocity: 100 km/h, position measurement error: 100 m

Chapter 6

Conclusion and Future Work

In a mobile radio system, the received signal at the mobile always consists of multiple components from different directions and with different delays. Small changes in the differential delays introduced by the moving mobile will cause large variations in the envelope amplitude and phase of the composite received signal. This phenomenon is called multipath fading. The fading depends on the mobile velocity. The faster the mobile, the larger the fading rate of received signal. Therefore, the statistical characteristics of the fading signal can be used for mobile velocity estimation. At the beginning of this thesis, we introduced the mathematical model for continuous-time fading signal derived by Rice *et al.* and some mobile velocity estimation techniques based on it in the background chapter.

The main contribution of this thesis is the development of discrete-time fading signal model and level crossing rate (LCR) and autocorrelation function (ACF) estimation techniques for mobile velocity using a discrete-time fading signal. In Chapter 3, we introduced the definition of level crossings for discrete-time model, and then defined the level crossing rate over N given samples as the ratio of the expected number of level crossings to the number of samples. From the statistical characteristics of the discrete-time fading signal model, we obtained an expression for LCR as a function of the signal envelope and the mobile velocity. In Chapter 4, we derived the ACF method by exploiting the feature that the autocorrelation function of the in-phase and/or quadrature components of fading signal are functions of mobile velocity.

Based on our simulation results, we are able to conclude that both methods can

obtain accurate estimates of mobile velocity. We also carried out a comparison between these two methods. We found that by using the ACF method, we obtained more accurate results, especially when the SNR is small. Furthermore, if the sampling rate of the continuous-time fading signal is relatively small and the actual mobile velocity is large, the LCR method would underestimate the actual values. However, when we increase the sampling rate, we still can obtain accurate results. While the ACF method overcomes this drawback of LCR method, it requires coherently received in-phase or quadrature signal components rather than the signal envelopes.

In Chapter 5, we applied the estimates of mobile velocity into the mobile motion tracking application. We proposed a simple Kalman filter tracking model taking into account the mobile position and velocity measurements. We then compared it with the tracking model using only position measurements. From the simulation results, we found that when the mobile velocity is large, the performance of the velocity-based mobile motion tracker is significantly better than the tracker only using position measurements. On the other hand, when the mobile is moving slowly, there is no obvious difference in the performance of these two mobile motion trackers.

Suggestions for Future Research

In the future, the accuracy of the discrete-time mobile velocity estimation model needs to be investigated further. In particular, the assumption in Section 3.2 that only one level crossing occurs per sample may be improved upon. The choice of the signal level, A, should be optimized in view of this assumption.

The purpose of the introduction of the mobile tracking model in Chapter 5 is to illustrate the advantages of employing the mobile velocity measurements in addition to the mobile position measurements. The simulation results show that we have accomplished this purpose. However, this model should be further refined in order to be used in practical mobile motion tracking applications. For example, we assumed that the measurements are independent of each other and the measurement noise matrix is time-invariant for the sake of simplicity. One should develop a real-world model which takes account of correlated measurements and time-varying measurement noise.

We have observed that there is no improvement in adding mobile velocity estimates

to the tracker for the case of small mobile velocity. This observation should be investigated in more detail.

Bibliography

[1] T. Aulin, *A Modified Model for the Fading Signal at a Mobile Radio Channel*, IEEE Trans. Veh. Technol., Vol. 28, pp. 182–203, Aug. 1979.

[2] M. D. Austin, G. L. Stuber, *Velocity Adaptive Handoff Algorithms for Microcellular Systems*, IEEE Trans. Veh. Technol., Vol. 43, pp. 549–561, Aug. 1994.

[3] T. E. Biedka and J. H. Reed, *Direction Finding Methods for CDMA wireless Systems*, Virginia Tech., MPRG-TR-96-20, May, 1996.

[4] Y. Bar-Shalom and T. E. Fortmann, *Tracking and Data Association*, Academic Press, 1988.

[5] Y. T. Chan and K. C. Ho, *A Simple and Efficient Estimator for Hyperbokic Location*, IEEE Trans. Signal Processing, vol. 42, no. 8, Aug. 1994, pp. 1905–1915.

[6] G. C. Clark, J. B. Cain, *Error-Correction Coding for Digital Communications*, New York, NY: Plenum, 1981.

[7] R. H. Clarke, *A Statistical Theory of Mobile Radio Reception*, Bell Syst. Tech. J., Vol 47, pp. 957–1000, July 1968.

[8] G. Colman, S. D. Blostein, and N. C. Beaulieu, *An ARMA Multipath Fading Simulator*, in Advances in Wireless Communications, Chapter 4 in Wireless Personal Communications: Improving Capacity, Services and Reliability, ed. T. S. Rappaport, B. D. Woerner, J. H. Reed and W. H. Tranter, Kluwer Pub., pp. 37–48, NY, 1997.

[9] W. B. Davenport Jr., W. L. Root, *An Introduction to the Theory of Random Signals and Noise*, McGraw-Hill, 1958, pp. 152.

[10] E. J. Dudewicz and S. N. Mishra *Modern Mathematical Statistics*, John Wiley & Sons, 1988.

[11] P. K. Enge, *Global Positioning System: Signals, Measurements and Performance*, Int'l. J. Wireless Info. Networks, Vol. 1, NO. 2, Apr. 1994.

[12] B. T. Fang, *Simple Solutions for Hyperbolic and Related Position Fixes*, IEEE Trans. Aerospace and Elect. Sys., vol. 29, no. 5, Sept. 1990, pp. 748–753.

[13] FCC Docket No. 94-102, *Revision of the Commission's Rules to Ensure Compatibility with Enhanced 911 Emergency Calling Systems*, RM-8143, July 26, 1996.

[14] W. H. Foy, *Position-Location Solutions by Taylor-Series Estimation*, IEEE Trans. Aerospace and Elect. Sys., vol. AES-12, no. 2, Mar. 1976, pp. 187–193.

[15] *The Global Positioning System*, IEEE Specturm, Dec. 1993, pp. 36–47.

[16] M. Hata, T. Nagatsu, *Mobile Location Using Signal Strength Measurements in a Cellular System*, IEEE Trans. Veh. Technol., Vol. 29, no. 2, pp. 245–252, May 1980.

[17] C. W. Helstrom, *Statistical Theory of Signal Detection*, 2nd Ed., Pergamon, 1968.

[18] T. A. Herring, *The Global Positioning System*, Sci. Amer., Feb. 1996, pp. 44–50.

[19] J. Holtzman, *Adaptive Measurement Intervals for Handoffs*, IEEE Int. Conf. on Commun., Chicago, IL, pp. 1032–1036, June 1992.

[20] J. Holtzman, A. Sampath, *Adaptive Handoffs through the Estimation of Fading Parameter*, IEEE Int. Conf. on Commun., pp. 1131–1135, 1994.

[21] E. D. Kaplan, ed., *Understanding GPS: Principles and Applications*, Boston: Artech House, 1996.

[22] W. C. Jakes, *Microwave Mobile Communications*, IEEE Press, 1974.

[23] C. D. McGillem and T. S. Rappaport, *A Beacon Navigation Method for Autonomous Vehicles*, IEEE Trans. Vehic. Tech., vol. 38, no. 3, Aug. 1989, pp. 132–139.

[24] R. Muhamed and T. S. Rappaport, *Comparison of Coventional Subspaced-Based DOA Estimation Algorithms with Those Employing Property-Restoral Techniques: Simulation and Measurements*, IEEE ICUPC, Cambridge, MA, Oct. 2, 1996.

[25] C. T. Mullis and L. L. Scharf, *Quadratic Estimators of the Power Spectrum* in *Advances in Spectral Analysis and Array Processing*, Vol. I, S. Haykin (Editor), Prentice Hall, 1989.

[26] J. F. Ossanna, Jr., *A Model for Mobile Radio Fading Due to Building Reflections: Theoretical and Experimental Waveform Power Spectra*, Bell. Syst. Tech. J., Vol 43, pp. 2935–2971, Nov. 1964.

[27] A. Popoulis, *Probabilitiy, Random Variables, and Stochastic Processes*, 2nd Ed., McGraw-Hill, 1984

[28] J. G. Proakis, *Digital Communications*, 3rd Ed., McGraw-Hill, 1995.

[29] J. G. Proakis, D. G. Manolakis, *Digital Signal Processing: Principles, Algorithms and Applications*, 2nd Ed., Macmillan, 1992, pp. 405-410.

[30] T. S. Rappaport, J. H. Reed, and B. D. Woerner, *Position Location Using Wireless Communications on Highways of the Future*, IEEE Commun. Mag., Oct. 1996, pp. 33–41.

[31] S. O. Rice, *Mathematical Analysis of Random Noise*, Bell System Technical Journal, Vol. 23, July 1944, pp. 282–332, Vol. 24, Jan. 1945, pp. 46–156.

[32] S. O. Rice, *Statistical Properties of a Sine Wave plus Noise*, Bell System Technical Journal, Vol. 27, Jan. 1948, pp. 109–157.

[33] A. Sampath, J. Holtzman, *Estimation of Maximum Doppler Frequency for Handoff Decisions*, IEEE Veh. Technol. Conf., Secaucus, NJ, pp. 859–862, May 1993.

[34] S. V. Schell and Gardner, *High Resolution Direction Finding*, Handbook of Statistics: Volume 10, Elsevier, 1993.

[35] J. I. Smith, *A Computer Generated Multipath Fading Simulation for Mobile Radio*, IEEE Trans. Veh. Technol., Vol 24, Aug. 1975, pp. 39–40.

[36] O. J. Smith and J. S. Abel, *The Spherical Interpolation Method of Source Localization*, IEEE J. Oceanic Eng., vol. OE-12, no. 1, Jan. 1987, pp. 246–252.

[37] P. Stoica and A. Nehorai, *MUSIC, Maximum Likelihood, & Cramer-Rao Bound*, Proc. IEEE, vol. 57, no. 8, Aug. 1969, pp. 1408–1418.

[38] G. L. Stuber, *Principles of Mobile Communication*, Kluwer Academic Publishers, 1996.

[39] R. G. Vaughan, *Signals in Mobile Communications: A Review*. IEEE Trans. Veh. Technol., Vol 35, Nov. 1986.

[40] R. Vijayan, J. Holtzman, *Foundations of Level Crossing Analysis of Handoff Algorithms*, Int. Conf. on Commun., pp. 935–938, 1993.

[41] X. Wang and H. V. Poor, *Blind Adaptive Interference Suppression in DS-CDMA Communications with Impulsive Noise*, Int. Conf. on Acoustics, Speech, and Signal Processing, 1998

[42] G. Xu and H. Liu, *An Effective Transmission Beamforming Scheme for Frequency-Division-Duplex Digital Wireless Communication Systems*, Proc. IEEE ICASSP, 1995, pp. 1729–1732.

[43] D. J. Young, N. C. Beaulieu, *On the Generation of Correlated Rayleigh Random Variates by Inverse Discrete Fourier Transform*, IEEE, Int. Conf. on Universal Personal Communications, Cambridge, MA, 1996.

[44] I. Ziskind and M. Wax, *Maximum Likelihood Localization of Multiple Sources by Alternating Projection*, IEEE Trans. Acoustics, Speech, and Signal Processing, vol. 36, no. 10, Oct. 1988, pp. 1553–1560.